Electrochemical Performance and Structural Interpretation of Sodium Metal Pyrophosphates as a Cathode for Sodium-Ion Batteries

Kwang-Ho Ha

Department of Energy Engineering

(Battery Science and Technology)

Graduate school of UNIST

2015

Electrochemical Performance and Structural Interpretation of Sodium Metal Pyrophosphates as a Cathode for Sodium-Ion Batteries

Kwang-Ho Ha

Department of Energy Engineering

(Battery Science and Technology)
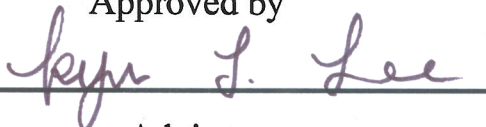
Graduate school of UNIST

Electrochemical Performance and Structural Interpretation of Sodium Metal Pyrophosphates as a Cathode for Sodium-Ion Batteries

A thesis

submitted to the Graduate School of UNIST

in partial fulfillment of the

requirements for the degree of

Master of Science

Kwang-Ho Ha

12. 19. 2014
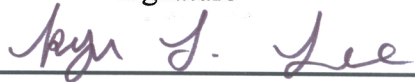
Approved by

_____

Advisor

Kyu Tae Lee

Electrochemical Performance and Structural Interpretation of Sodium Metal Pyrophosphates as a Cathode for Sodium-Ion Batteries

Kwang-Ho Ha

This certifies the thesis of Kwang-Ho Ha is
approved.

12. 19. 2014

signature

Advisor: Kyu Tae Lee

signature

Soojin Park

signature

Nam-Soon Choi

Abstract

Recently, sodium-ion batteries (SIBs) become promising alternatives for lithium-ion batteries (LIBs) due to abundance and cheap cost of sodium resources compared with lithium sources. Like cathode materials for LIBs, various compounds of layered oxides and polyanion materials are synthesized through several methods. However, conventional active materials have difficulties for satisfying both kinetics and safety issues.

Here, new types of polyanion material, sodium metal pyrophosphate, are synthesized having composition of $Na_{3.12}M_{2.44}(P_2O_7)_2$ (M = Fe, $Fe_{0.5}Mn_{0.5}$, Mn, Co). Among them, sodium iron pyrophosphates are made into two ways: stoichiometric and off-stoichiometric ratio. This compounds have triclinic structure having three-dimensional tunnels, with sub-micron- or micron-sized particles. Indeed, the off-stoichiometric sodium iron pyrophosphate, involving continuous solid solution system, shows 85 mA h g^{-1} of reversible capacity with excellent cycleability and kinetics. Inspired by that, compounds containing Mn and Co, which are expected higher redox potentials, are tried. They are also investigated in electrochemical and structural ways.

Contents

List of figures

List of tables

1. Introduction

1.1. Lithium-ion batteries

Since commercialized firstly by SONY in early 1990s, lithium-ion battery (LIB) has been supplied best electrochemical performances toward modern devices such as mobile phones, laptops, MP3 players, or digital cameras with continuous researches.[1-5] And, thanks to a low redox potential of lithium (*ca.* -3.05 V vs. NHE), small ionic radius (*ca.* 0.69 Å), and comparably high capacity and energy density due to the lightest atomic weight of lithium than any other metals (6.941 amu), its application area is expanded to large-scaled machines, not only to conventional portable devices. In particular, a market for electric vehicles (EVs) is keep growing rapidly containing battery electric vehicle (BEV), plug-in hybrid electric vehicle (PHEV), and hybrid electric vehicle (HEV) (Figure 1).[6] This kind of tendency naturally demands more manufacture of lithium-ion battery which should operate them.

However, there are limitations against lithium-ion battery to be used as a promising electrochemical device continuously. Firstly, lithium source is reserved out of balance over the world. Indeed, most lithium source is from South America, such as Bolivia, Chile, Argentina, and Brazil. In addition, the amount of the source itself is also not high compared with other metals. These kinds of issues in rational cost and continuous supply can give people doubts whether lithium-ion battery can be maintained as the best battery device at the near future or not.[7]

As known, LIBs often consist of several main parts: two electrodes called cathode and anode, and electrolytes which can have lithium ion transferred between them (Figure 2), including separator which physically isolates them keeping from internal short-circuit [8]. The basic reaction is arisen from oxidation or reduction of the active material located at both side of the electrodes, withdrawing or depositing lithium ions and electrons. The resultant lithium ion should be compensated by the electrolyte which has lithium-ion conducting ability and they migrate to the other side of electrode. The term of 'discharging' is derived from that kind of process which cathode material is spontaneously reduced and anode should be oxidized with electron transfer from anode to cathode, whereas 'charging' is defined *vice versa*.
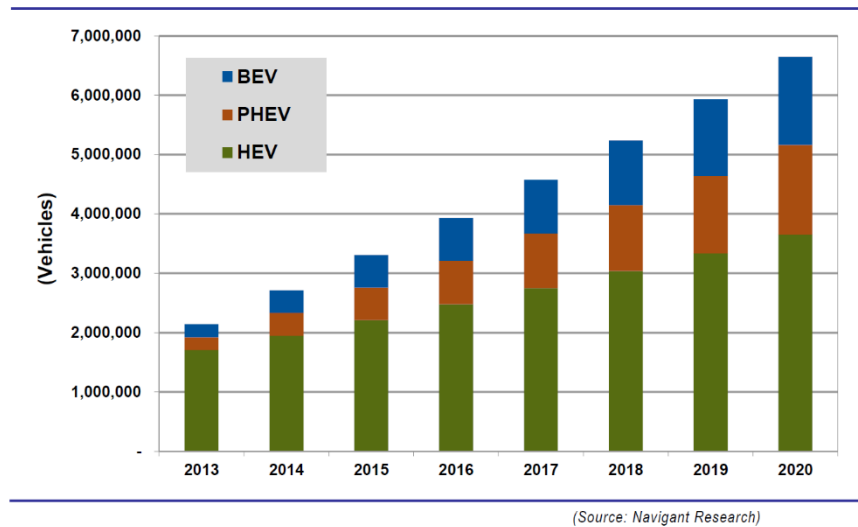
Figure 1. Light duty electric vehicle sales by annual years from 2013 to 2020.
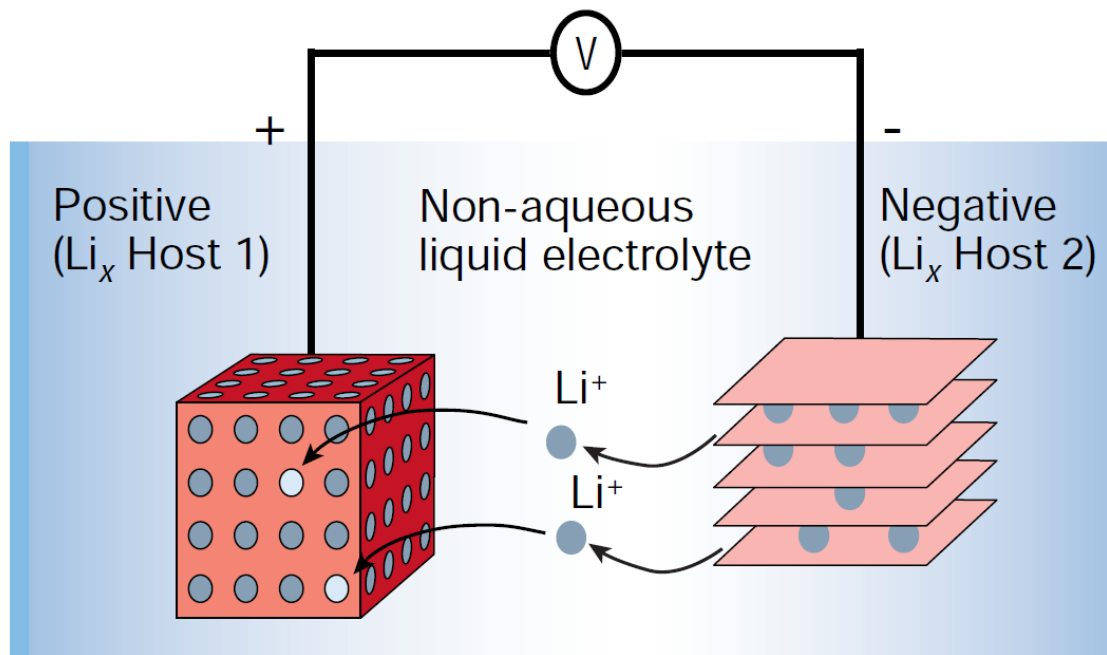
Figure 2. Schematic of a lithium-ion battery (LIB) system composed of two electrodes as lithium hosts with lithium-ion-conducting electrolyte.

1.2. Sodium-ion batteries

Nowadays, sodium-ion battery, often called as SIB or NIB, is being researched as a promising alternative for conventionally used lithium-ion battery.[7, 9-12] Its composition is very same as LIB, which also contains cathode, anode, and electrolyte with separator. The only difference is that two electrodes should host sodium ions, and the electrolyte should have sodium ion conductivity to transfer sodium ion between the electrodes whereas all components mentioned is about lithium-based.

SIBs have several advantages that, firstly, sodium resource itself is very abundant compared to lithium, which shares six largest portion among whole elements in the crust, followed by silicon, aluminum, iron, and calcium (Figure 3).[13] Indeed, reserve of sodium is almost thousand times larger than that of lithium, so its cost competitiveness should be higher, particularly at the future. Also, sodium has still low standard reduction potential of -2.71 V vs. NHE and small ionic radii of 0.98 Å rather than other metals, therefore, SIBs can maintain advantages in energy and power density than alternative batteries composed of other metals despite less energy and power should be ultimately exhibited than the conventional LIBs at the current time, therefore, various researches should be needed to enhance the energy and powder density up to the level of LIBs by improving electrode materials as sodium hosts to be operated at high voltage or showing high capacity. In addition, sodium hosts can be easily synthesized by following synthesis for the traditional lithium hosts because both sodium and lithium are located in 1A group in the periodic table so that they have very similar chemistry upon synthesis or de/intercalation processes.[14, 15] So, a lot of researches upon SIBs are approached by comparing with or inspired by the already known active materials where de/lithiation processes are available.
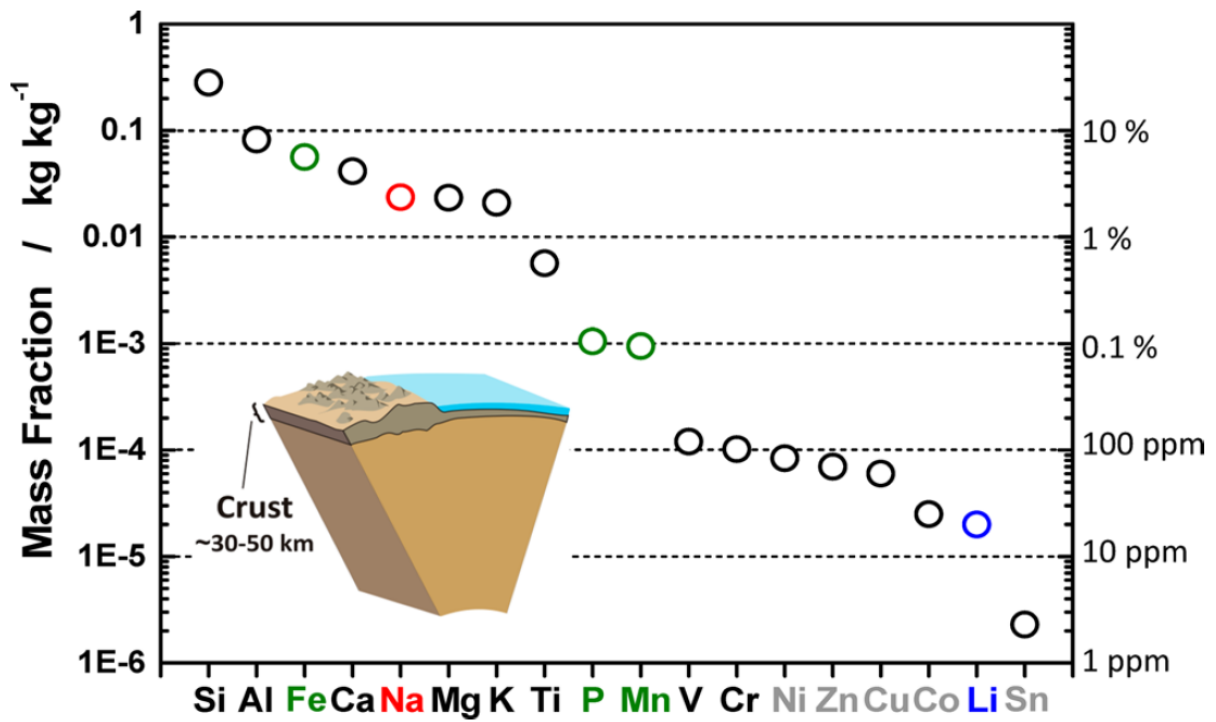
Figure 3. Natural abundance of elements in the crust.

1.3. Cathode materials for lithium- and sodium-ion batteries

Among overall components within alkali ion batteries, cathode material shares quite large percentage of over 30% according to the cost.[16] Cathode material is therefore one of the important components affecting electrochemical performances and cost competitiveness.

Firstly commercialized cathode material was lithium cobalt oxide ($LiCoO_2$) in 1991, as mentioned, which had been already actively reported possibility as the lithium de/intercalation host in 1980s.[17] It has a cubic close-packed structure for oxygen atoms with α-$NaFeO_2$-type structure (Space group : *R-3m*), so lithium ion can be extracted and inserted between CoO_6 layers.[18] It ensures good electrochemical performances with 150 mA h g^{-1} (*ca.* 0.5 Li) of reversible capacity delivered at 4.2 V class, however, the problem toward $LiCoO_2$ has an irreversible reaction of phase transition of $Li_{1-x}CoO_2$ over x > 0.5 so that it cannot be used at that range,[19, 20] and, more seriously, price for cobalt sources is relatively expensive because of their rareness than other transition metals. This should be critical for especially large-scaled devices such as EVs or energy storage system (ESS).

New types of the layered oxide of $LiNiO_2$ and $LiNi_{1-x}Co_xO_2$ have been researched as the alternative to overcome that kind of problem onto $LiCoO_2$.[21-24] Manganese was also introduced to the transition metal sites forming $LiNi_{1-x}Mn_xO_2$.[25-28] In addition, recently, new approaches has been tested electrochemically such as spinel-type lithium manganese oxide ($LiMn_2O_4$),[29-37] their solid solution phases containing cobalt, nickel, and manganese at the same time with varying their compositions within the transition metal sites,[38-45] and lithium layered oxides having lithium ion more than 1, so composing additional phase of Li_2MnO_3 which stabilizes whole structure.[46-58]

Layered oxides as the sodium hosts are also introduced because of the similar chemistry between lithium and sodium, as explained. In fact, sodium layered oxides were reported with lithium or other alkali layered oxides in parallel [59]. Especially, sodium layered oxides are classified into several types such as O3 and P2; the term 'O3' means that sodium possess 'octahedral' sites with 'three' repeating transition metal oxide layers, and 'P2' does it is located at 'prismatic' sites with 'two' repeating unit [60]. Whereas the lithium is positioned at the octahedral sites ordinarily and tetrahedral sites on migrating (REFs), the sodium ion is rather located at the prismatic sites because of the larger ionic size, particularly at the sodium-deficient states.[61-70] However, lots of O3-typed layered oxides are also known such as O3-$NaFeO_2$,[71] O'3-$NaMnO_2$,[72] O'3-$NaNiO_2$,[73] O3-$NaVO_2$,[74] O3-$NaCoO_2$,[75] and O3-$Na[Ni_{1/2}Mn_{1/2}]O_2$.[76]

However, layered oxides have several problems in such as especially safety issues. Although their electrochemical performances are being improved, oxygen gas often evolves at the elevated temperatures.[77] The crucial thing is it can be occurred easily even in our lives in real, therefore, they now face challenges to guarantee safety.

1.4. Phosphate-based cathode materials

A phosphate-based cathode material, olivine-type lithium iron phosphate ($LiFePO_4$), is firstly reported as the lithium de/intercalation host by Goodenough.[78] Unlike $LiMO_2$ (M = Co, Ni, Mn), it does not have any lithium layers, instead, includes two dimensional channels along [010] and [001] directions where the lithium ion can migrate (Figure 4),[18] so its structure is totally different with them (Space group : *Pnma*), however, a research demonstrates that the lithium ion can intercalate through only one dimension in fact.[79] The structure has stronger covalent bonding, between P and O, than conventional layered oxides, so it has an advantage in safety issues, where oxygen gas cannot be evolved because oxygen atoms should keep very powerful interaction with phosphorus. Besides, the iron atom should be partially oxidized thanks to it called 'inductive effect' so that it can deliver its capacity at slightly higher potential.[80]
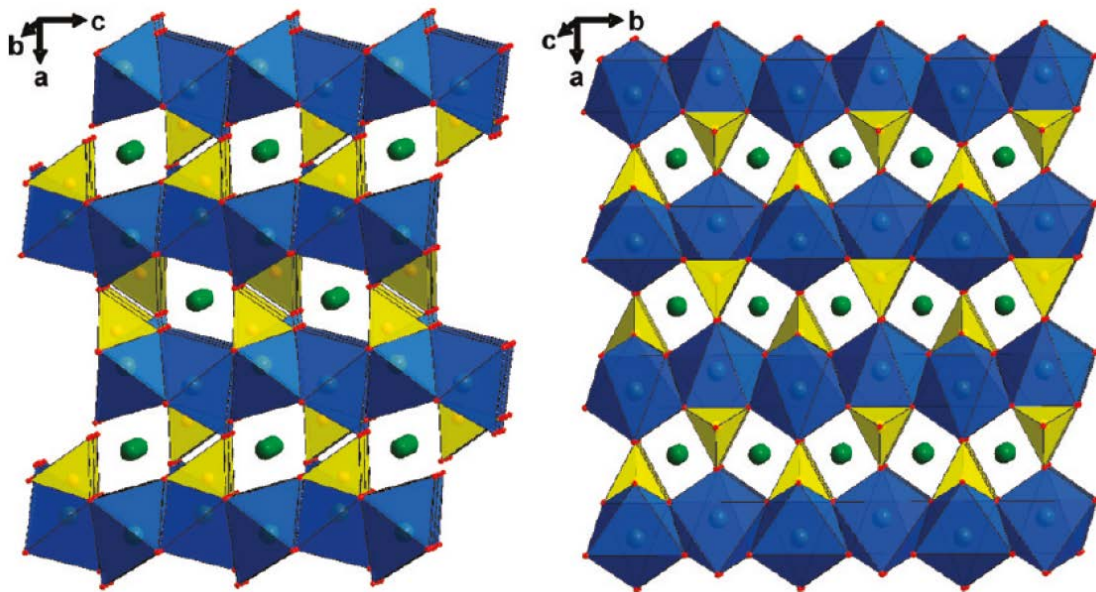
Figure 4. Schematic structure of the olivine-typed $LiFePO_4$ along *b*-and *c*-axes.

Figure 5 shows the typical voltage profile of $LiFePO_4$.[81] As seen, it has a relatively flat plateau at 3.4 V, indicating it undergoes two-phase reaction between lithium-containing $LiFePO_4$ and lithium-deficient $FePO_4$ during the redox reaction. Its theoretical capacity is calculated to about 170 mA h g^{-1} so it should have superior electrochemical performance in capacity than layered $LiCoO_2$ or spinel $LiMn_2O_4$.

Polyanion compounds containing the sodium ion are also synthesized, too. The problem is, sodium iron phosphate, $NaFePO_4$, is existed in maricite in the nature so its synthesis to keep olivine structure is very difficult. Furthermore, this maricite $NaFePO_4$ does not have electrochemical activity on the voltage we uses because different connectivity between iron and sodium blocks pathways for sodium migration.[82] Instead, several groups introduced olivine $NaFePO_4$ during the electrochemical tests where, for example, olivine $LiFePO_4$ is tested with the sodium metal as a counter electrode and the sodium-ion-conducting electrolyte.[83] Or, the olivine structure containing the sodium ion can be made from topological growth process using $NH_4MPO_4 \cdot H_2O$ (M = Mn, $Mn_{0.5}Fe_{0.5}$, $Mn_{0.8}Mg_{0.2}$, $Mn_{0.8}Ca_{0.2}$) that $Na[Mn_{1-x}M_x]PO_4$ (M = Fe, Ca, Mg, $0 \leq x \leq 0.5$) can be grown along (100) plane by cation exchanging from $NH_4MPO_4 \cdot H_2O$ which have same symmetry along (101) plane.[84]

In contrast, polyanion-based materials such as olivine $LiFePO_4$ suffers several problems, and the most ultimate factor is their poor electronic conductivity. This characteristic is arisen directly on the electrochemical tests showing severe capacity fading upon cycles. So, several tests are conducted at very slow C rate and high temperature to overcome this kind of kinetic problem.[80, 85] However, they are not the ultimate solutions which $LiFePO_4$ can be used electrochemically as layered oxides.

Rather, a lot of researches use coating method with conducting material like carbon, or nanosizing synthesis which can decrease diffusion length of the particles.[86, 87] But, it needs additional processes during synthesis so these can be inefficient on manufacturing area in terms of time and cost. Another solution is to make the reaction occurred with single phase. Single phase reaction have the advantage in kinetics because the lithium ion diffusion can be occurred at every dimensions whereas two-phase reaction is found only at the phase boundaries. Indeed, particle size affects to the phase transition so that slope appears at the voltage profile with nano-scaled particles.[88, 89]
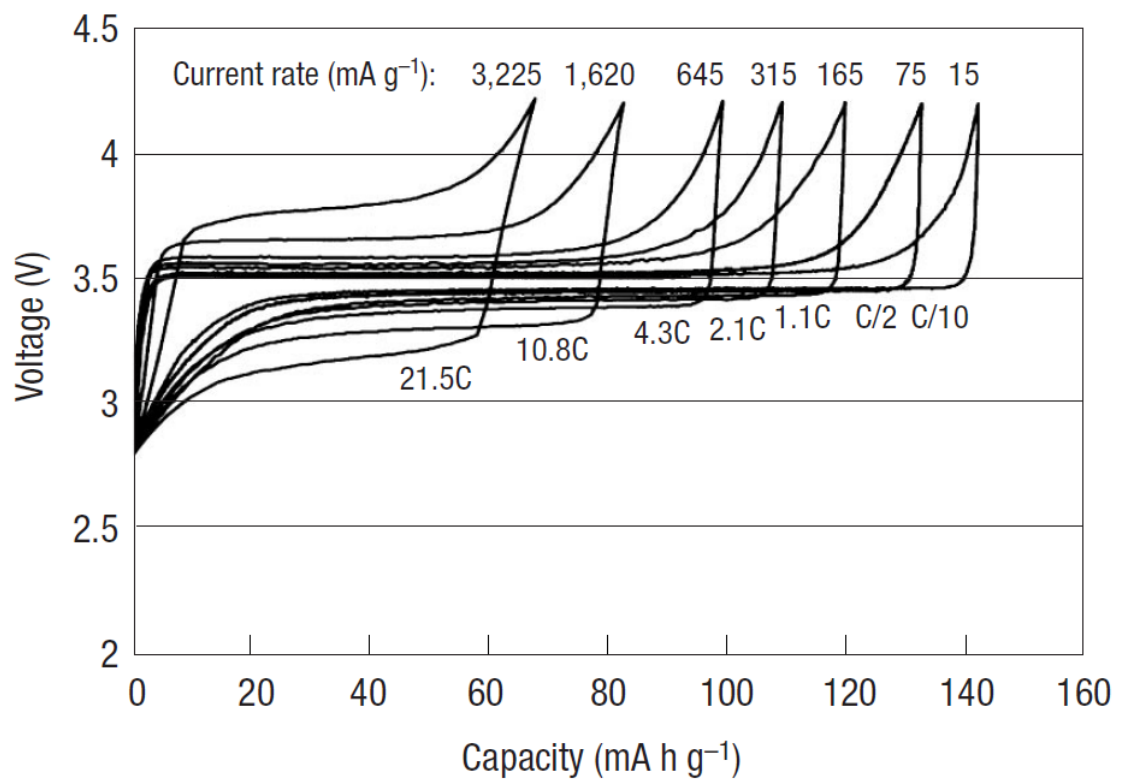
Figure 5. Typical voltage profile of the olivine LiFePO$_4$ at various C rates applied.

1.5. Pyrophosphate-based cathode materials

In 2010, Yamada group reported a new type of phosphate-based cathode material, lithium iron pyrophosphate ($Li_2FeP_2O_7$).[90] Again, its structure is quite different with $LiFePO_4$ having monoclinic phase (Space group : $P2_1/c$) (Figure 6). Also, it naturally shows distinguished voltage profile against $LiFePO_4$. Reversible capacity of 110 mA h g^{-1}, which is corresponding with one electron transfer ($Fe^{2+/3+}$), is exhibited at the Galvanostatic test with 0.05 C rate (Figure 7). More attracted thing is, the capacity fading is not quite serious as $LiFePO_4$ over 30 cycles, and 40% of the original capacity is maintained at 1 C. Considering its particle size is around 1 μm, its kinetics is surprisingly improved compared with that of other phosphate-based materials such as $LiFePO_4$.

Inspired it, a lot of pyrophosphates with different kind of transition metals are synthesized and reported containing manganese and cobalt.[91-94] Also, pyrophosphates which can be used as the sodium de/intercalation hosts are also introduced.[95-103] In this thesis, new types of sodium metal pyrophosphates having composition of triclinic $Na_{3.12}M_{2.44}(P_2O_7)_2$ (M = Fe, $Fe_{0.5}Mn_{0.5}$, Mn, Co) are mentioned and investigated through structural and electrochemical analyses. Firstly, excellent electrochemical performances in terms of capacity and kinetics for sodium iron pyrophosphates with stoichiometric and off-stoichiometric compositions are presented. Also, the electrochemical mechanism is examined in terms of phase transitions. Next, two kinds of possible candidates for alternating the pyrophosphates containing iron atom, $Na_{3.12}Mn_{2.44}(P_2O_7)_2$ and $Na_{3.12}Co_{2.44}(P_2O_7)_2$ are made and evacuated, to get over the limitation in energy density, where high redox potentials are expected than $Na_{3.12}Fe_{2.44}(P_2O_7)_2$ (*ca.* 3.0 V). Although they could not deliver enough amount of reversible capacity at this time, sodium cobalt pyrophosphate show a possibility to be used as a promising cathode material at high voltage, with showing same electrochemical mechanism with that of $Na_{3.12}Fe_{2.44}(P_2O_7)_2$.
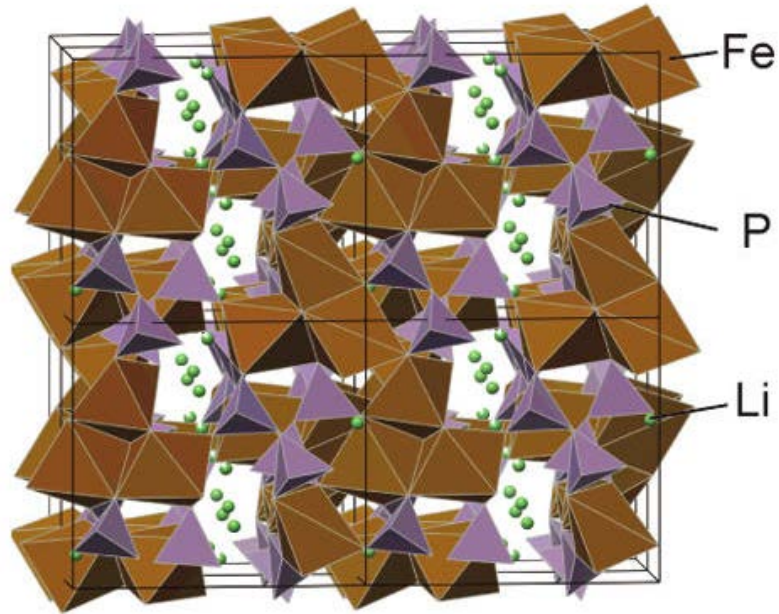
Figure 6. Schematic structure of $Li_2FeP_2O_7$.
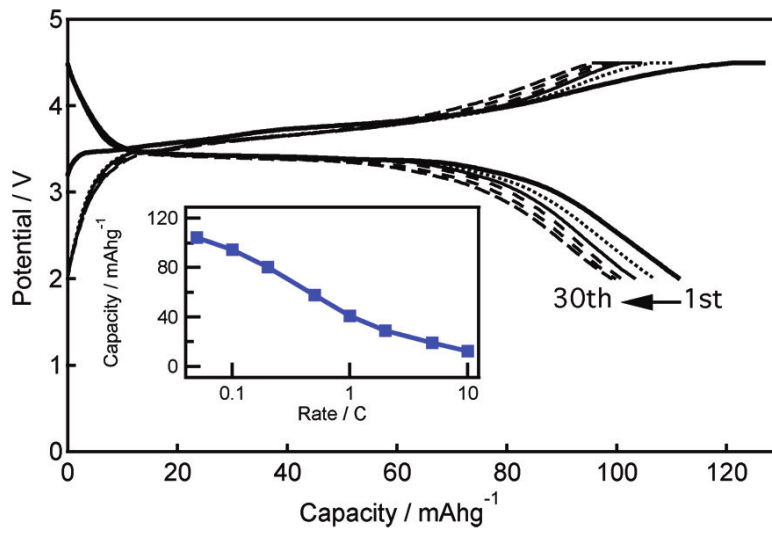
Figure 7. Voltage profile of $Li_2FeP_2O_7$ at 0.05 C rate.

2. Experimental methods

2.1. Synthesis method

Every pyrophosphate compounds was synthesized through solid state method. This method contains only mixing by ball-milling, then heat treatment. Therefore, it has an advantage in simplicity than other synthesis method. Sodium carbonate (Na_2CO_3, $\geq$ 99.5%, Sigma-Aldrich) and ammonium hydrogen phosphate ((NH_4)$_2HPO_4$, 98+%, Sigma-Aldrich) were used to the precursor as sodium and phosphate sources. In transition metal sources, , iron oxalate dihydrate ($FeC_2O_4 \cdot 2H_2O$ 99%, Sigma-Aldrich), manganese acetate tetrahydrate ($Mn(CH_3COO)_2 \cdot 4H_2O$, 99+%, Sigma-Aldrich), and cobalt acetate tetrahydrate ($Co(CH_3COO)_2 \cdot 4H_2O$, $\geq$98%, Sigma-Aldrich) were added for pyrophosphates including cobalt, iron, and manganese in each cases. These were ball-milled by SPEX 8000M Mixer/Mill for 10 minutes with adding small amount of acetone. The slurry was dried then heated at 300 ºC for 6 hours in argon atmosphere. The calcined sample was cooled down to the room temperature, mixed again with high-power ball-milling, then heated at 600 ºC for 12 hours with same condition as the first heat treatment. The final resultant powders were cooled down and collected.

2.2. Structural analysis

For every compounds, X-ray diffraction patterns were achieved by Rigaku D/MAX2500V/PC powder diffractometer with CuKα radiation (λ = 1.5405 Å) from 10 to 80 ˚ in 2 theta, with slow scanning rate of 0.2 ˚ per minute. The patterns of triclinic pyrophosphates ($Na_{3.12}M_{2.44}(P_2O_7)_2$, M = Fe, $Fe_{0.5}Mn_{0.5}$, and Co) were used to understand their lattice environments analyzed by GSAS program. Their morphology containing particle shapes and sizes were confirmed by scanning electron microscopy (SEM) with Quanta 200 field-emission SEM (FE-SEM) and Hitachi S-4800 FE-SEM. For sodium iron pyrophosphate, Varian 720-ES inductively coupled plasma (ICP) spectrometry was used to analyze exact atomic composition in molar ratio during chemical de/sodiation processes. In addition, XPS analysis was also conducted to understand surface environment by Thermo Fischer to compare between stoichiometric and off-stoichiometric sodium iron pyrophosphates.

2.3. Electrochemical measurement

Active material casting process

Each active materials were mixed with carbon black (Super-P), as a conducting material, and polyvinylidene fluoride, as a binder, with composition of 70 : 15 : 15 in weight ratio. The slurry was made with viscosity control by 1-methyl-2-pyrrolidinone (NMP, anhydrous, 99.5%, Sigma-Aldrich), casted on aluminum foil, then dried in an 80 ºC oven.

Galvanostatic cycling and rate tests

Galvanostatic and rate capability tests were performed through 2016 and 2032 coin-type half cells with lithium and sodium as anodes in each one. For sodium cobalt pyrophosphates, 1.3 M $LiPF_6$ in an ethylene carbonate, an ethyl methyl carbonate, and a dimethyl carbonate (3:2:5 v/v/v) solution was used as an electrolyte in the lithium half cells, and 0.8 M $NaPF_6$ in the ethylene carbonate and a propylene carbonate solution (1:1 v/v) with addition of 1 wt.% of tris(trimethylsilyl)phosphide (TMSP), which recently reported as an additive for high-voltage active materials,[104] and 5 wt.% of fluoroethylene carbonate additives in the sodium cells. They were tested with 0.01 C rate in a 30 ºC oven on cycling. In iron and manganese's cases, 0.8 M $NaClO_4$ in the ethylene carbonate and diethyl carbonate (1:1 v/v) electrolyte was chosen. Same operating temperature condition was given with the cobalt compounds, with applying 0.05 C rate during the cycling test. Rate capability was analyzed toward sodium iron pyrophosphate with fixed 0.1 C on charging, then varied current density on discharging.

Electrochemical impedance spectroscopy (EIS) measurement

For two species of sodium cobalt pyrophosphates, electrochemical impedance spectroscopy (EIS) were performed to check charge transfer resistances, in range of 300 kHz to 1mHz, with 5 mV vs. OCV (open-circuit voltage) amplitude. In that analysis, symmetric coin cells were assembled with the exactly same electrodes containing the pyrophosphate, having same weight of the active materials, which were previously electrochemically tested on charging → discharging → charging with applying 0.02 C.

Potentiostatic intermittent titration technique (PITT) measurement

Potentiostatic intermittent titration technique (PITT) was additionally adjusted toward the cobalt pyrophosphates to calculate their diffusion coefficients. Pre-cycling process was carried out like the situation in the preparation of electrodes used in the EIS analyses with applying same *C* rate. Then, the PITT was conducted with 0.42 V of a voltage step until the voltage reached to its cut-off condition (2.7 V vs. Li/Li$^+$ in the lithium's case and 2.4 V vs. Na/Na$^+$ in the sodium's case), where the threshold current density was applied to 0.75 mA g^{-1}.

2.4. Chemical de/sodiation processes

For sodium iron pyrophosphate, its electrochemical mechanism on charging (desodiation) and discharging (sodiation) was confirmed by chemical de/sodiation processes. For easy understanding, the two opposite reactions are explained in Figure 8. On desodiation, nitrosyl tetrafluoroborate (NOBF$_4$, 95%, Sigma-Aldrich) was added in tetrahydrofuran (THF) solvent with the pyrophosphate, sealed in an Iwaki vial. The solution was stirred for 2 hours, then filtered and washed with ethanol. The gained powder of an oxidized pyrophosphate was dried in the vacuum oven. In contrast, sodium iodide (NaI, ≥ 99.5%, Sigma-Aldrich) was selected as a reducing agent during chemical sodiation. THF solvent was also used with 5 hours of stirring. The final reduced powder was achieved through the processes of filtering, washing, and drying step again.
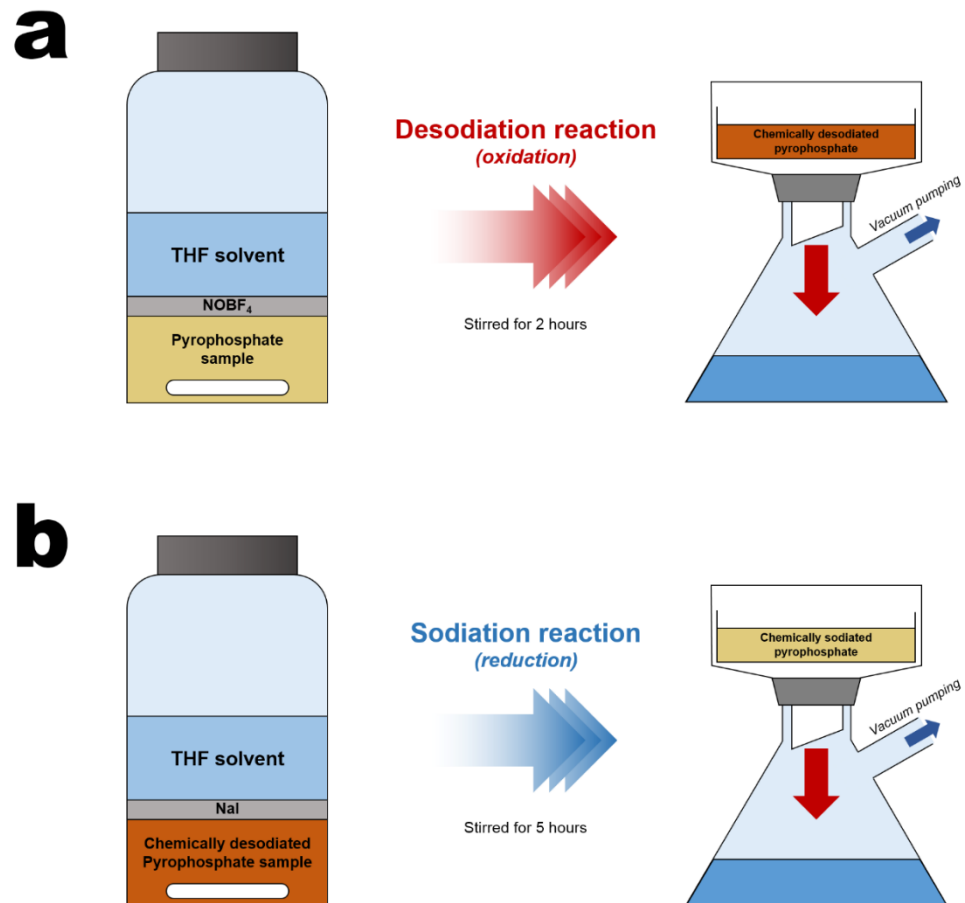
Figure 8. Schematic expression of chemical (a) desodiation and (b) sodiation reaction processes for $Na_{3.12}Fe_{2.44}(P_2O_7)_2$.

3. Result and Discussion

3.1. Sodium iron pyrophosphate

3.1.1. Synthesis and morphological interpretation of sodium iron pyrophosphate

Sodium iron pyrophosphate was firstly reported by Angenault et al. with triclinic structure in single crystal form.[105] They introduced it having the composition of $Na_{3.12}Fe_{2.44}(P_2O_7)_2$, consisting of two types of centrosymmetric crowns, $Fe_2P_4O_{22}$, where every oxygen is corner-sharing each other, and $Fe_2P_4O_{20}$, which an edge-shared part is observed with conventional corner-sharing sites (Figure 9). Furthermore, these mainly crowns consist of two FeO_6 octahedral model (blue polyhedron) and P_2O_7 group (yellow polyhedron), which contains two PO_4 tetrahedral models with corner sharing each other.

Powder X-ray diffraction pattern of the synthesized powder, using sodium carbonate, iron oxalate dihydrate, and ammonium hydrogen phosphate as precursors, was firstly gained in a microcrystalline form (Figure 10). The pattern shows high crystallinity, well matched with a powder diffraction file (PDF) which is already known. According to the result of the Rietveld refinement toward it (Figure 11), it is belonging to a triclinic group with lattice parameters of a = 6.4046(8) Å, b = 9.3908(11) Å, c = 10.9729(13) Å, α = 64.4874(13), β = 85.9939(15), and γ = 73.1075(14). Its unit cell, gained from the refinement, is well agreed with the former reported one that it consists of $Fe_2P_4O_{22}$ and $Fe_2P_4O_{20}$ crowns with sodium sites (Figure 12). According to it, three-dimensional pathways which sodium ion can be de/intercalated exist along [100]. [010], and [101] directions.
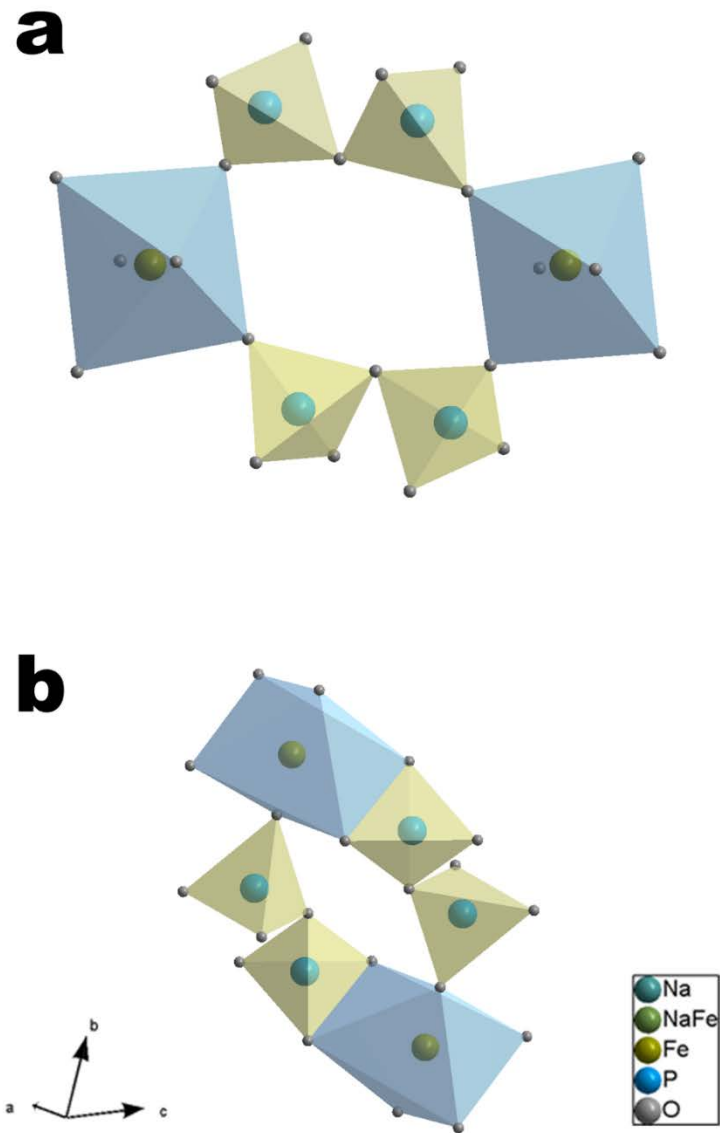
Figure 9. Two centrosymmetric crowns of (a) $Fe_2P_4O_{22}$ and (b) $Fe_2P_4O_{20}$ compositing triclinic $Na_{3.12}Fe_{2.44}(P_2O_7)_2$.
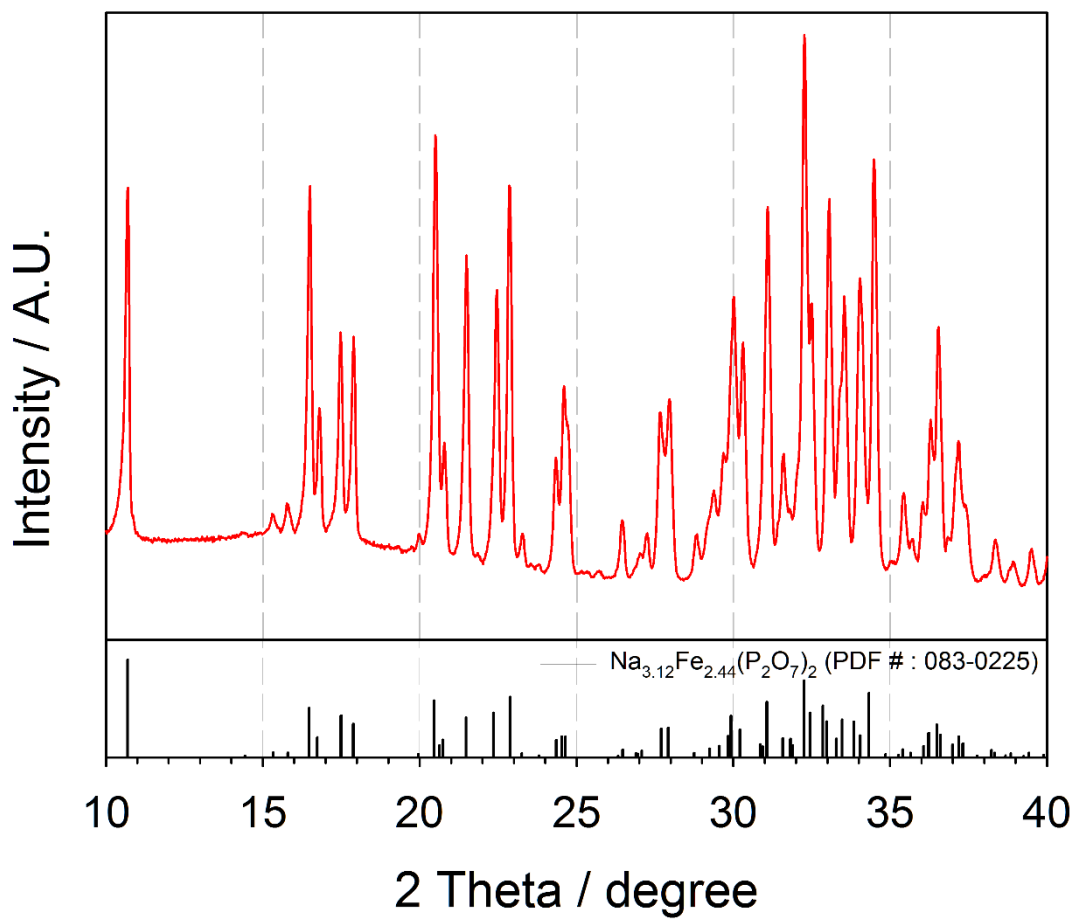
Figure 10. Powder X-ray diffraction pattern of microcrystalline $Na_{3.12}Fe_{2.44}(P_2O_7)_2$ compared with powder diffraction file (PDF # : 083-0225).
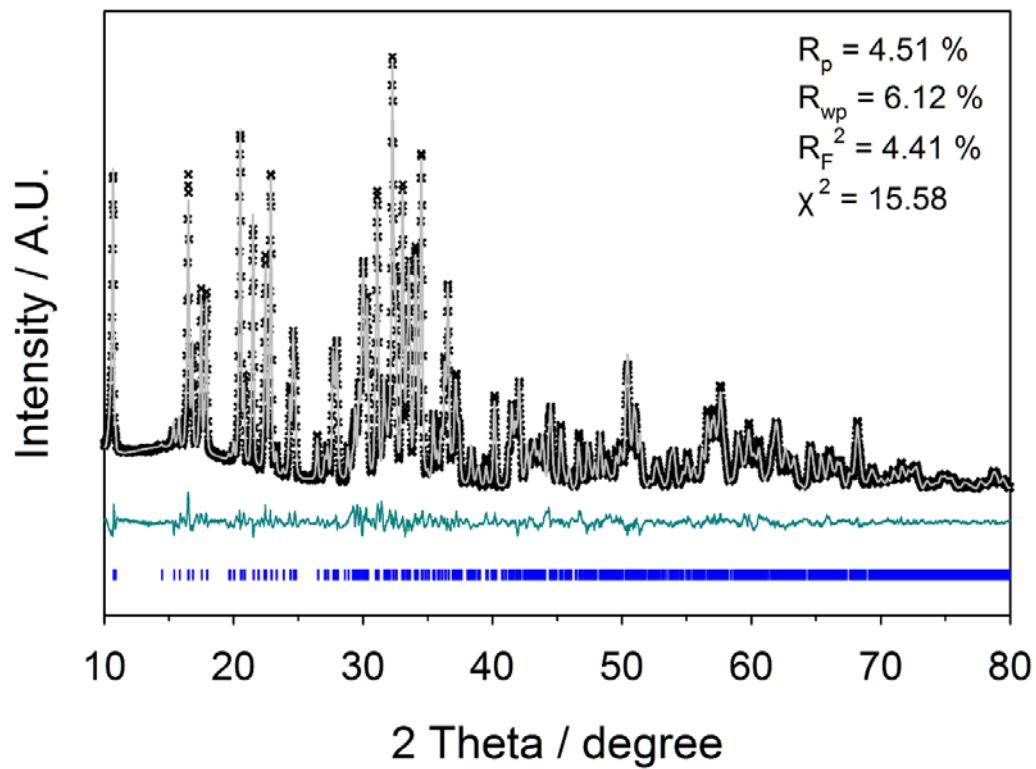
Figure 11. Rietveld refinement data of $Na_{3.12}Fe_{2.44}(P_2O_7)_2$ with (inset) agreement factors achieved by GSAS program.
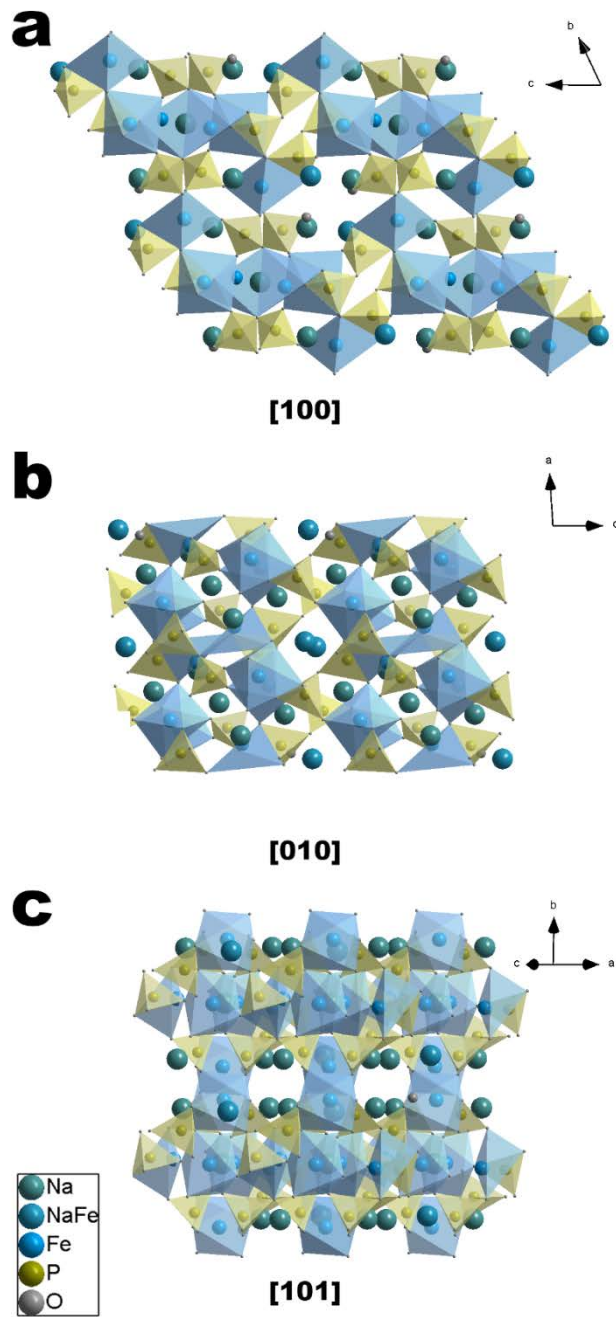
Figure 12. Structure model of $Na_{3.12}Fe_{2.44}(P_2O_7)_2$ view along (a) [100], (b) [010], and
(c) [101] directions.

Detail crystal information upon the refinement is shown in Table 1, exhibiting four sodium and iron sites are present. Among them, Na(3) and Fe(4) sites have partial occupancy factors although they possesses different sites in coordinates. This phenomenon is attributed from that Na(3) and Fe(4) cannot coexist in the same cell because the distance between these sites is too close. This characteristics is already proved by Angenault et al., suggesting the relationship between occupation factor between Na(3), Na(4), Fe(3), and Fe(4) which are partially occupied, and comparing $Na_{3.12}Fe_{2.44}(P_2O_7)_2$ with $Na_4P_2O_7 - Mg_2P_2O_7$ binary system.[105-107]

Table 1. Crystallographic information for each atomic sites of $Na_{3.12}Fe_{2.44}(P_2O_7)_2$.

Atom	Position			Occupancy	Multiplicity	Uiso
	a	b	c			
Na(1)	0.2188(12)	0.8445(9)	0.6012(8)	1	2	0.0240(33)
Na(2)	0.3997(13)	0.1523(10)	0.8409(8)	1	2	0.0369(33)
Na(3)	0.5	0.5	0.5	0.882	1	0.0172(44)
Na(4)	-0.0249(8)	0.1748(6)	0.0269(5)	0.677	2	0.1073(19)
Fe(1)	-0.0249(8)	0.1748(6)	0.0269(5)	0.323	2	0.0173(19)
Fe(2)	0.3502(5)	0.5050(5)	0.23523(33)	1	2	0.0112(11)
Fe(3)	0.2738(6)	0.1036(4)	0.28281(32)	1	2	0.0175(13)
Fe(4)	0.856(5)	0.4689(33)	0.3992(30)	0.118	2	0.0292(12)
P(1)	-0.0698(11)	0.1709(9)	0.7194(7)	1	2	0.0276(23)
P(2)	0.2872(10)	0.1947(8)	0.5352(6)	1	2	0.0218(23)
P(3)	0.5690(11)	0.7061(8)	-0.0455(6)	1	2	0.0359(23)
P(4)	0.8654(10)	0.4609(8)	0.1885(7)	1	2	0.02265(24)
O(1)	0.0923(20)	0.2779(16)	0.5930(15)	1	2	0.07949
O(2)	0.7608(21)	0.5429(17)	0.0308(11)	1	2	0.04099
O(3)	0.8850(18)	0.0565(13)	0.6693(10)	1	2	0.0329
O(4)	0.7122(19)	0.3151(15)	0.6981(11)	1	2	0.0329
O(5)	0.0706(20)	0.0880(14)	0.8599(12)	1	2	0.03917
O(6)	0.4405(18)	0.4405(18)	0.6497(11)	1	2	0.0183
O(7)	0.2046(19)	0.1063(14)	0.4593(11)	1	2	0.03487
O(8)	0.3649(20)	0.3337(14)	0.4506(11)	1	2	0.03487
O(9)	0.6553(18)	0.8568(14)	-0.0550(10)	1	2	0.02317
O(10)	0.5413(17)	0.7132(13)	0.8020(10)	1	2	0.01784
O(11)	0.3576(17)	0.7049(12)	0.0416(10)	1	2	0.01664
O(12)	0.0257(17)	0.5734(14)	0.1820(11)	1	2	0.01455
O(13)	0.9707(19)	0.2971(17)	0.2001(12)	1	2	0.05598
O(14)	0.6779(18)	0.4838(14)	0.2937(10)	1	2	0.01261

Its morphology was confirmed *via* its SEM images as shown in Figure 13. Irregular particles are observed in submicron size, which ranges from hundreds of nanometers to a few micrometers. So, it is confirmed that this iron pyrophosphate is synthesized to very bulk size through the solid state method.
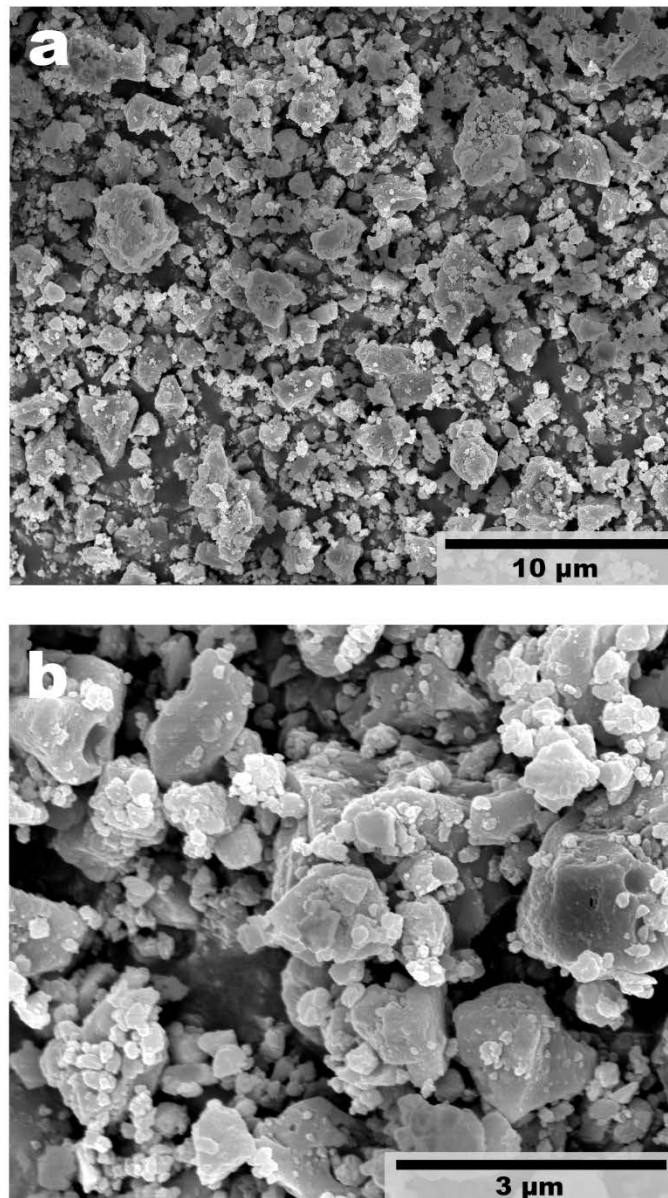
Figure 13. SEM images of $Na_{3.12}Fe_{2.44}(P_2O_7)_2$.

3.1.2. Electrochemical performances of sodium iron pyrophosphate

First, half cells in the coin type were assembled for the Galvanostatic electrochemical tests with $Na_{3.12}Fe_{2.44}(P_2O_7)_2$ as the cathode material and sodium metal as the anode. Theoretically and mathematically, $Na_{3.12}Fe_{2.44}(P_2O_7)_2$ can be oxidized with releasing 2.44 of electrons, following redox reaction from Fe^{2+} to Fe^{3+}. Then, its calculated specific capacity would be 117.6 mA h g^{-1} which is the higher value than that of the motivated pyrophosphate of $Li_2FeP_2O_7$, with 110 mA h g^{-1}, which only one-electron transfer can be possible at maximum. Indeed, on 1st charging and discharging process, $Na_{3.12}Fe_{2.44}(P_2O_7)_2$ delivered about 85 mA h g^{-1} of reversible capacity which is corresponded with the amount of 1.76 of electron transferred (Figure 14). The problem is that a large irreversible capacity is exhibited during the 1st charging. Considering the amount of reversible capacity, this kind of excess capacity should be from side reactions, including formation of solid-electrolyte interface (SEI) layer due to reaction with the electrode and electrolyte on the electrode surface, except for the expected reaction of the redox reaction between Fe^{2+} and Fe^{3+}.
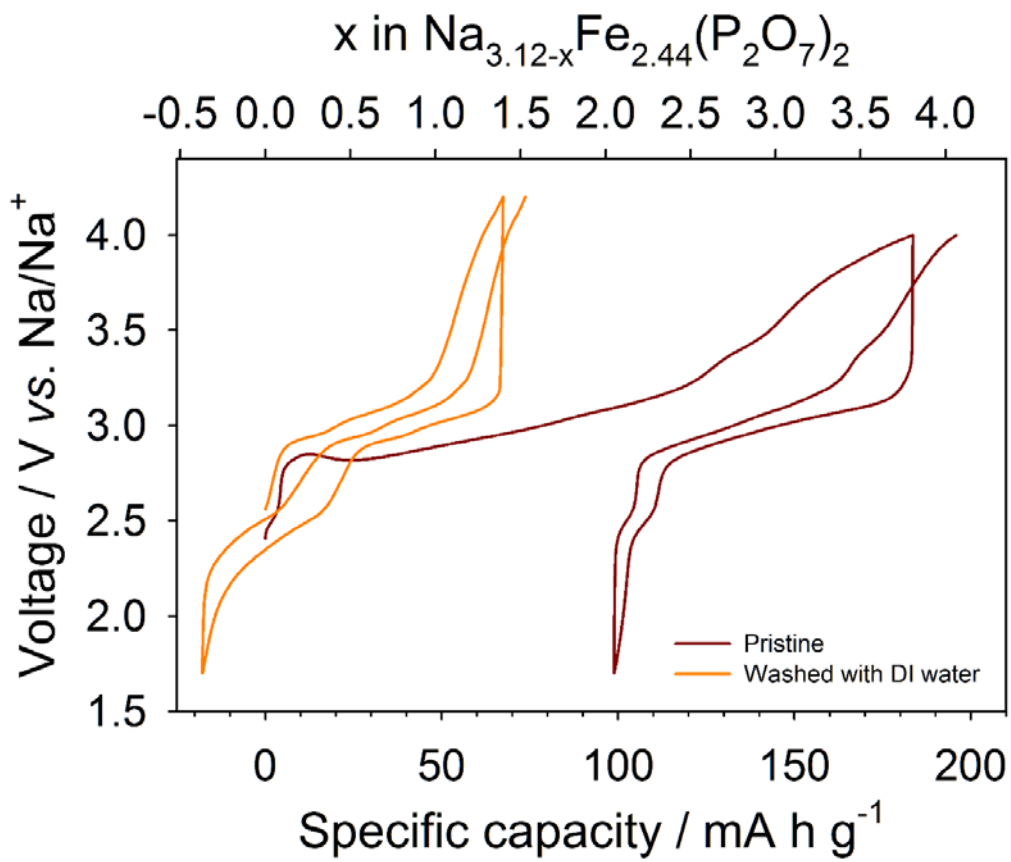
Figure 14. Voltage profile of $Na_{3.12}Fe_{2.44}(P_2O_7)_2$ before and after washed with DI water.

25

To find the cause, X-ray photoelectron spectroscopy (XPS) analysis was carried out to understand the surface environment of the active material, $Na_{3.12}Fe_{2.44}(P_2O_7)_2$ (Figure 15). Unfortunately, peaks indexed as sodium carbonate are presented in Na1s and C1s definitely, as well as peaks for $Na_{3.12}Fe_{2.44}(P_2O_7)_2$ is found. Also, the peak of Na_2CO_3 is clearly eliminated by additional etching process for 2650 s so that Na_2CO_3 is existed only at the surface of $Na_{3.12}Fe_{2.44}(P_2O_7)_2$ particles. Particularly, there should have been no peaks for C1s in case of the theoretically ideal form of the pyrophosphate because the compound does not have carbon. However, peaks denoting Na_2CO_3 are presented with the peaks affected by carbon itself in form of such as hydrocarbons (shown in red and green lines). In O1s, Na Auger peak is displayed at the higher energy before and after etching, and, it is impossible to distinguish two compound of $Na_{3.12}Fe_{2.44}(P_2O_7)_2$ and $NaCO_3$ at the lower energy because they show too similar binding energy. In addition, there are shifts in Fe2p peaks of the compound to the lower energy after etching. Considering Fe^{3+} has slightly higher binding energy than Fe^{2+}, is also demonstrates that oxidized state of iron-based compound exists at the surface. (Figure 16) Any additional impurities are not observed that, for example, only pyrophosphate peak is showed in P2p. (Figure 15c) Na_2CO_3 can be existed due to the decomposition of the electrolyte or contact between the compound and the air, particularly carbon dioxide. This kind of extraordinary situation would be often found in conventional active materials such as $LiCoO_2$.[108] When $Na_{3.12}Fe_{2.44}(P_2O_7)_2$ reacts with CO_2, partially oxidized pyrophosphate is formed like $Na_{3.12-\alpha}Fe^{II}_{2.44-\alpha/2}Fe^{III}_{\alpha/2}(P_2O_7)_2$ with a specific amount of $\alpha/2$ Na_2CO_3. It is believed that it affects to the electrolyte and system, and ultimately forms the solid-electrolyte interface (SEI) layer which increases irreversible capacity dramatically.
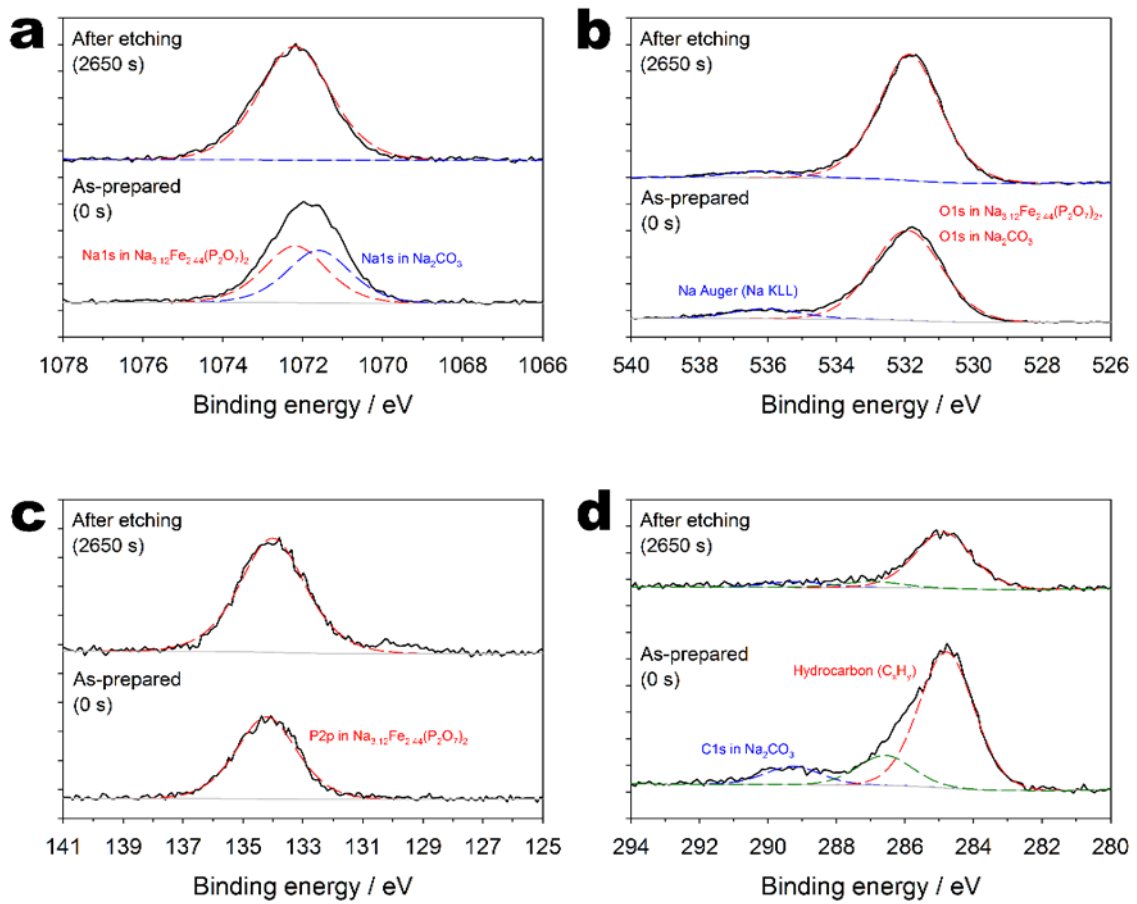
Figure 15. XPS profile of $Na_{3.12}Fe_{2.44}(P_2O_7)_2$ in (a) Na1s, (b) O1s, (c) P2p, and (d) C1s.
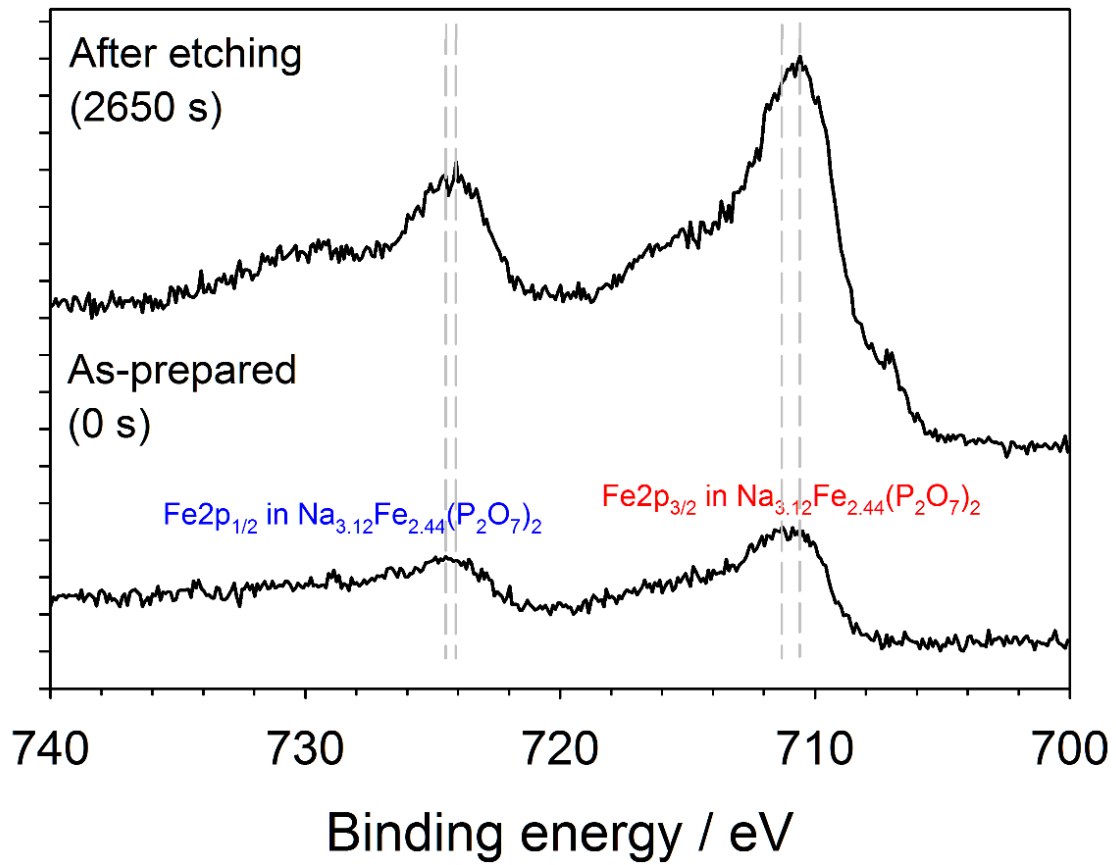
Figure 16. XPS profile of $Na_{3.12}Fe_{2.44}(P_2O_7)_2$ in Fe2p.

Washing the final product of $Na_{3.12}Fe_{2.44}(P_2O_7)_2$ with deionized water was considered as the next step to vanish Na_2CO_3 in advance and inhibit the irreversible reaction upon the charging process. After washing it, the reversibility is quite improved (orange curve in Figure 14) compared with the pristine one. Instead, coulombic efficiency exceeds 100% due to the larger the discharging capacity than the charging one because the partially oxidized compound of the iron pyrophosphate is further reduced at the 1st discharging process.

3.1.3. Off-stoichiometric sodium iron pyrophosphate

Another strategy to inhibit the formation of Na_2CO_3 and the irreversible unexpected reactions on the charging, without extra treatments such as washing process, was fulfilled as an off-stoichiometric synthesis of the sodium iron pyrophosphate. Same synthesis method and conditions are applied to the off-stoichiometric one, except its composition to $Na_{3.42}Fe_{2.44}(P_2O_7)_{2.05}$, with adding small additional amount of sodium and phosphate precursors.

The powder X-ray diffraction pattern of the off-stoichiometric sodium iron pyrophosphate shows exactly same peaks with the conventional ones of $Na_{3.12}Fe_{2.44}(P_2O_7)_2$ and small additional impurity ones of maricite $NaFePO_4$ (Figure 17). However, it doesn't make sense because $Na_{3.42}Fe_{2.44}(P_2O_7)_{2.05}$ can never consist of $Na_{3.12}Fe_{2.44}(P_2O_7)_2$ and $NaFePO_4$ in mathematics. By the way, the specific situation of continuous solid solution system was already informed for $Na_{3.12}Fe_{2.44}(P_2O_7)_2$, taking the example of the binary system between $Na_4P_2O_7$ and $Mg_2P_2O_7$, where the sodium iron pyrophosphate can be existed in the continuous form of $Na_{4-\alpha}Fe_{2+\alpha/2}(P_2O_7)_2$ ($2/3 \le \alpha \le 1$) which α means the occupation factor of the Na(3) site.[105] Therefore, overall composition of the sodium iron pyrophosphate can be determined along how much the Na(3) site is occupied. As explained before, the reason why the Na(3) site is partially occupied is that the distance between the Na(3) and Fe(4) site is comparably close. Adjusting this factor, the off-stoichiometric sodium iron pyrophosphate synthesized is composed of $NaFePO_4$ with $Na_{3.32}Fe_{2.34}(P_2O_7)_2$ ($\alpha = 0.68$) mathematically.
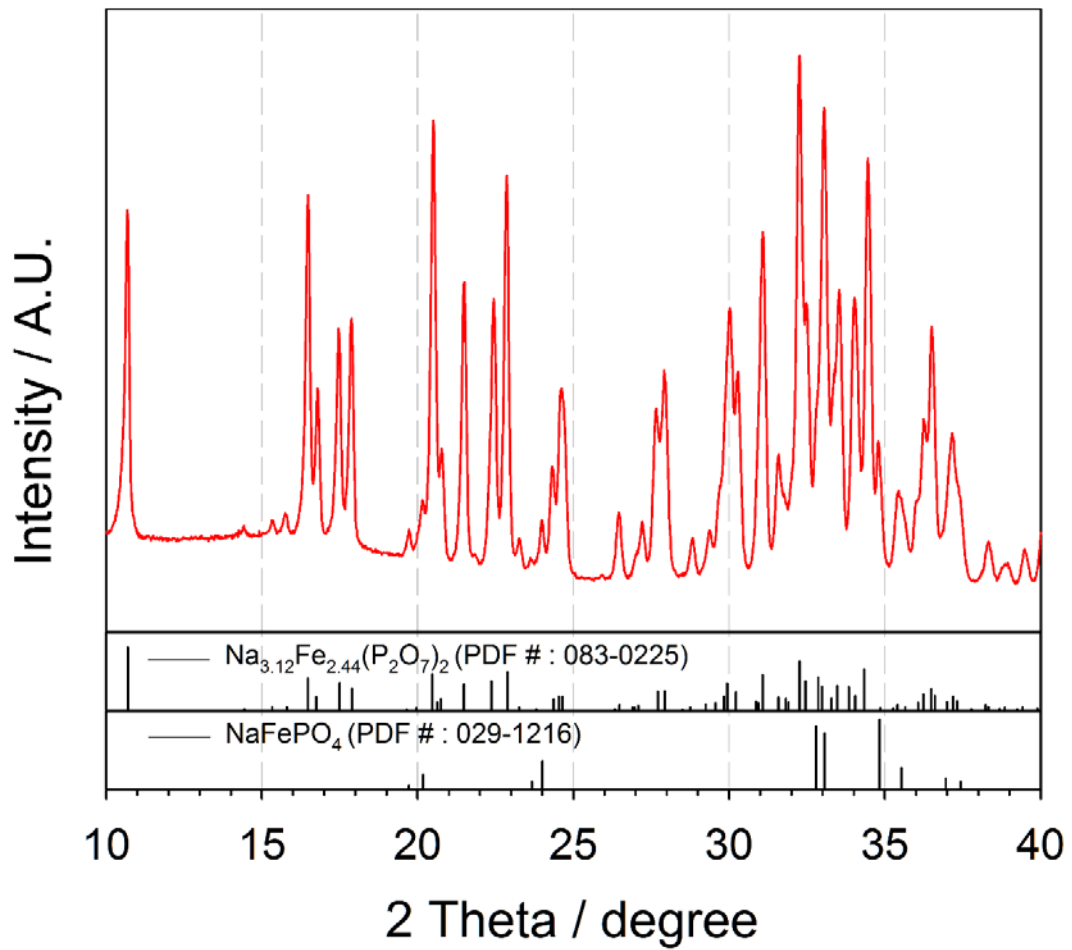
Figure 17. Powder X-ray diffraction pattern of the off-stoichiometric sodium iron pyrophosphate with the composition of $Na_{3.42}Fe_{2.44}(P_2O_7)_{2.05}$ with the consistent PDFs.

To check no existence of Na_2CO_3, the XPS peaks were achieved again in Figure 18. Consequentially, despite the peaks of Na_2CO_3 are detected in C1s (Figure. 18d), diminished intensity related with the off-stoichiometric sodium metal pyrophosphate is observed in Na1s before and after etching the off-stoichiometric powder. In addition, shift is also decreased in Fe2p compared with the data from $Na_{3.12}Fe_{2.44}(P_2O_7)_2$. (Figure. 19) Therefore, the strategy should have the positive effect of less surface oxidation by CO_2 rather than the original stoichiometric one. In addition, the stoichiometric $Na_{3.12}Fe_{2.44}(P_2O_7)_2$ and the off-stoichiometric $Na_{3.32}Fe_{2.34}(P_2O_7)_2$ have different Fe/Na peak area ratio according to the XPS depth profiles, indicating that $Na_{3.12}Fe_{2.44}(P_2O_7)_2$ should have naturally the larger ratio than $Na_{3.32}Fe_{2.34}(P_2O_7)_2$ (Figure 20). Also, it proves that the both compounds have very homogeneous environment at bulk region as etching continues.
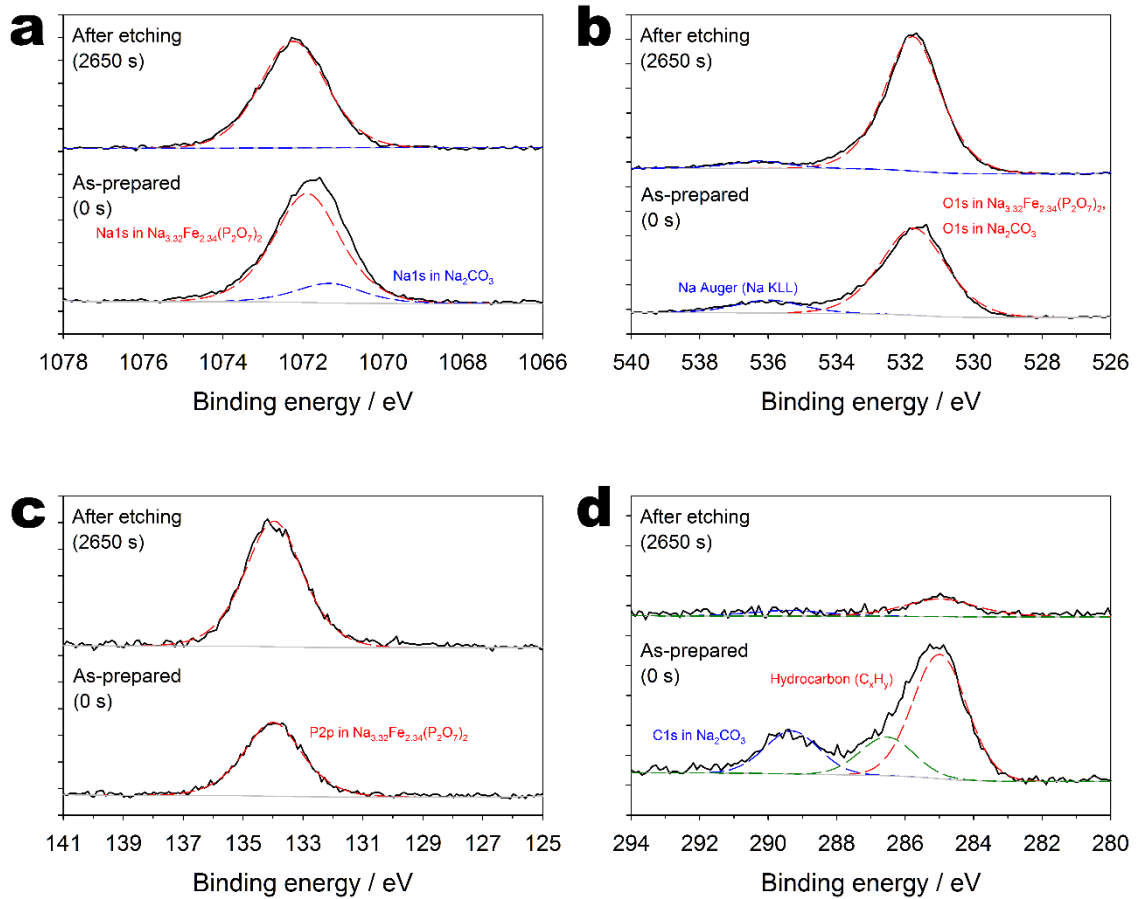
Figure 18. XPS profiles of the off-stoichiometric sodium iron pyrophosphate with the composition of $Na_{3.42}Fe_{2.44}(P_2O_7)_{2.05}$ in in (a) Na1s, (b) O1s, (c) P2p, and (d) C1s.

After etching
(2650 s)

As-prepared
(0 s)

Fe2p$_{3/2}$ in Na$_{3.32}$Fe$_{2.34}$(P$_2$O$_7$)$_2$

Fe2p$_{1/2}$ in Na$_{3.32}$Fe$_{2.34}$(P$_2$O$_7$)$_2$

740   730   720   710   700

Binding energy / eV
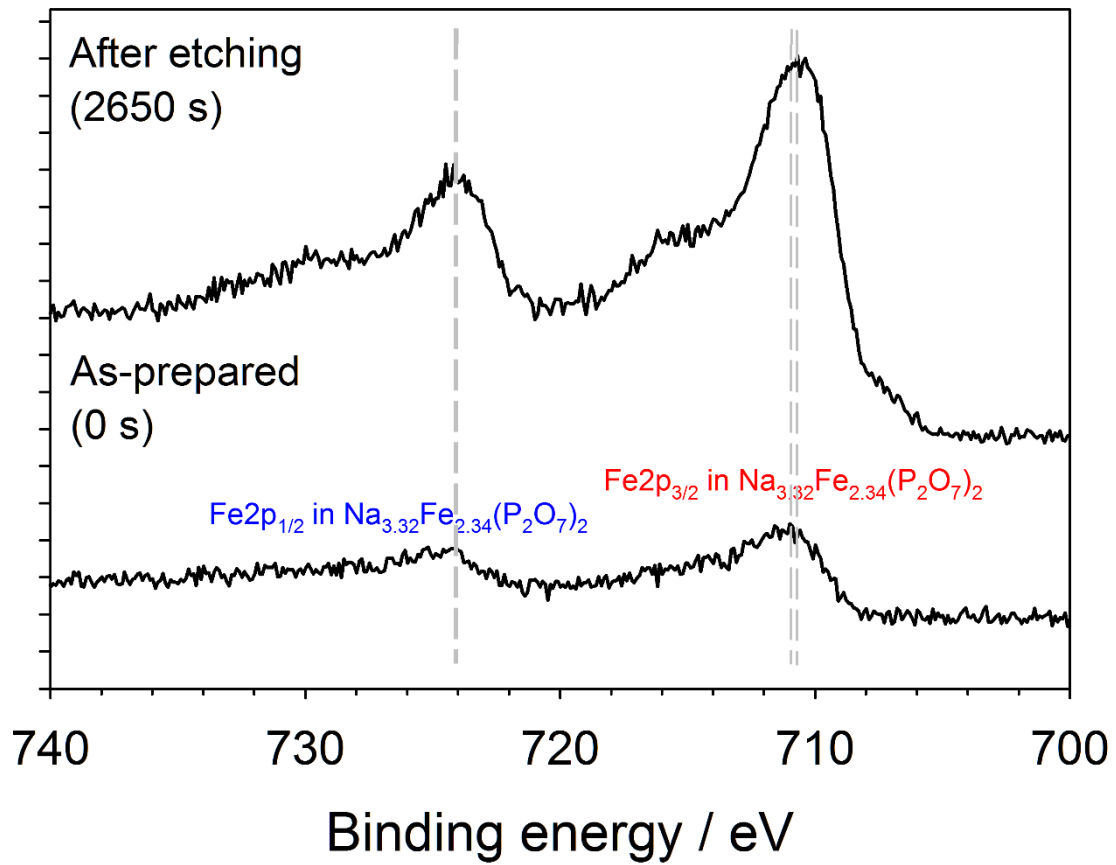
Figure 19. XPS profiles of the off-stoichiometric sodium iron pyrophosphate with the
composition of Na$_{3.42}$Fe$_{2.44}$(P$_2$O$_7$)$_{2.05}$ in Fe2p.
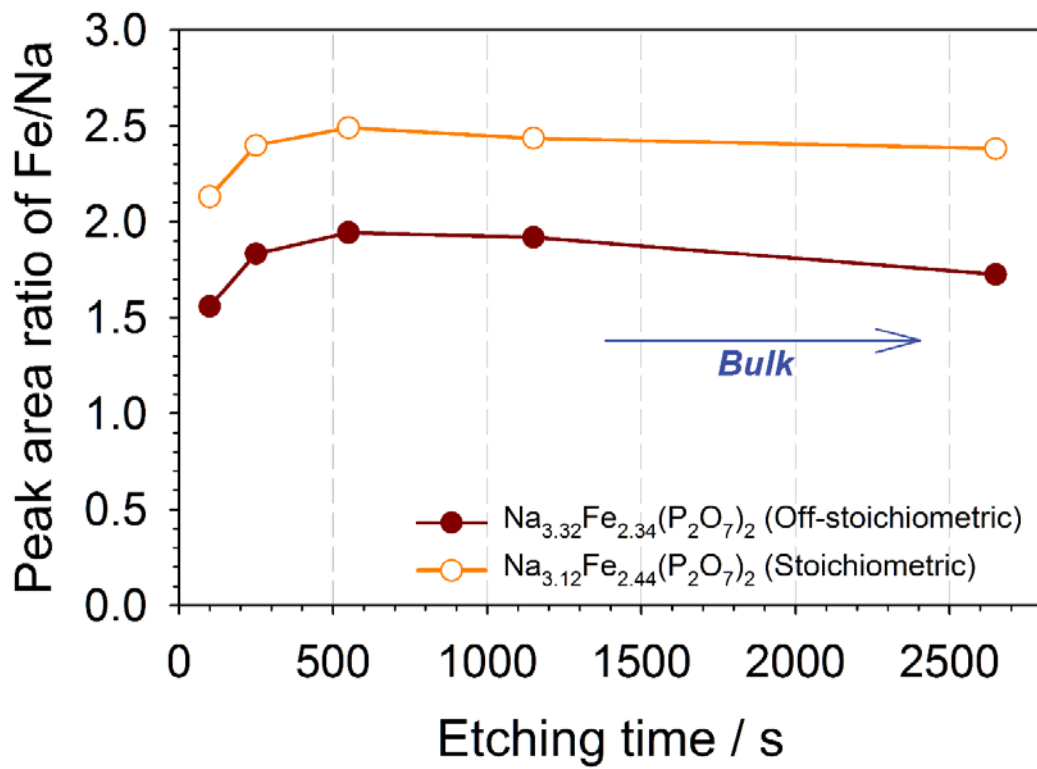
Figure 20. Comparison of the XPS depth profiles between the stoichiometric $Na_{3.12}Fe_{2.44}(P_2O_7)_2$ and the off-stoichiometric $Na_{3.32}Fe_{2.34}(P_2O_7)_2$.

The-off stoichiometric $Na_{3.32}Fe_{2.34}(P_2O_7)_2$ was tested electrochemically with the same condition as the stoichiometric $Na_{3.12}Fe_{2.44}(P_2O_7)_2$ (Figure 21). As a result, $Na_{3.32}Fe_{2.34}(P_2O_7)_2$ delivered 85 mA h g^{-1} of the initial reversible capacity without any irreversible capacity during charging unlike the test with $Na_{3.12}Fe_{2.44}(P_2O_7)_2$ thanks to the advance suppression of the formation of Na_2CO_3. In addition, this amount of capacity seldom shows fading over 60 cycles even at 0.2 *C* rate, exhibiting about 99% of coulombic efficiency (Figure 22). Considering its theoretically capacity is 110 mA h g^{-1}, where 2.34 of sodium ion can be totally transferred through an electron transfer by an iron atom, its cycling performance is quite promising as a bulk-scaled phosphate-based active material. By the way, the maricite impurity of $NaFePO_4$ is not included on calculating it because it has no electrochemical activity in the nature. Furthermore, the off-stoichiometric pyrophosphate shows excellent rate capability up to 10 *C* rate on discharging with retention of about 72% of its reversible capacity at 0.1 *C* rate (Figure 23). This kind of case is quite rare that a submicron- or micron-sized polyanion-based material exhibits very good electronic conductivity without any additional treatments such as carbon coating or nanosizing during the synthesis processes. This tendency occurs due to the large channel size of the final product along [100] direction, and relatively weak bonding between sodium and oxygen which results an irregular environment is formed upon two sodium sites, Na(1) and Na(2), with coordinated to eight and seven oxygen atoms, and whose strength is weaker than that between iron and oxygen, or phosphorus and oxygen.
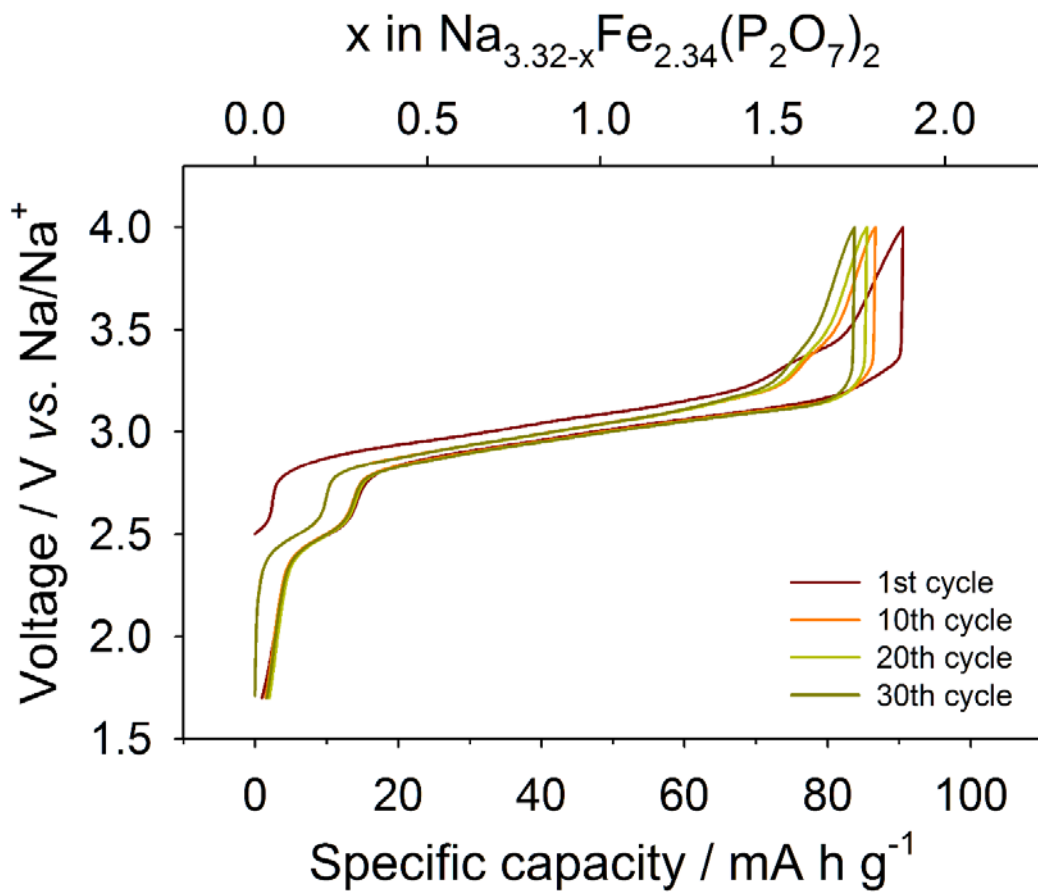
Figure 21. Voltage profile of the off-stoichiometric $Na_{3.32}Fe_{2.34}(P_2O_7)_2$ on the 1st, 10th, 20th, and 30th cycle
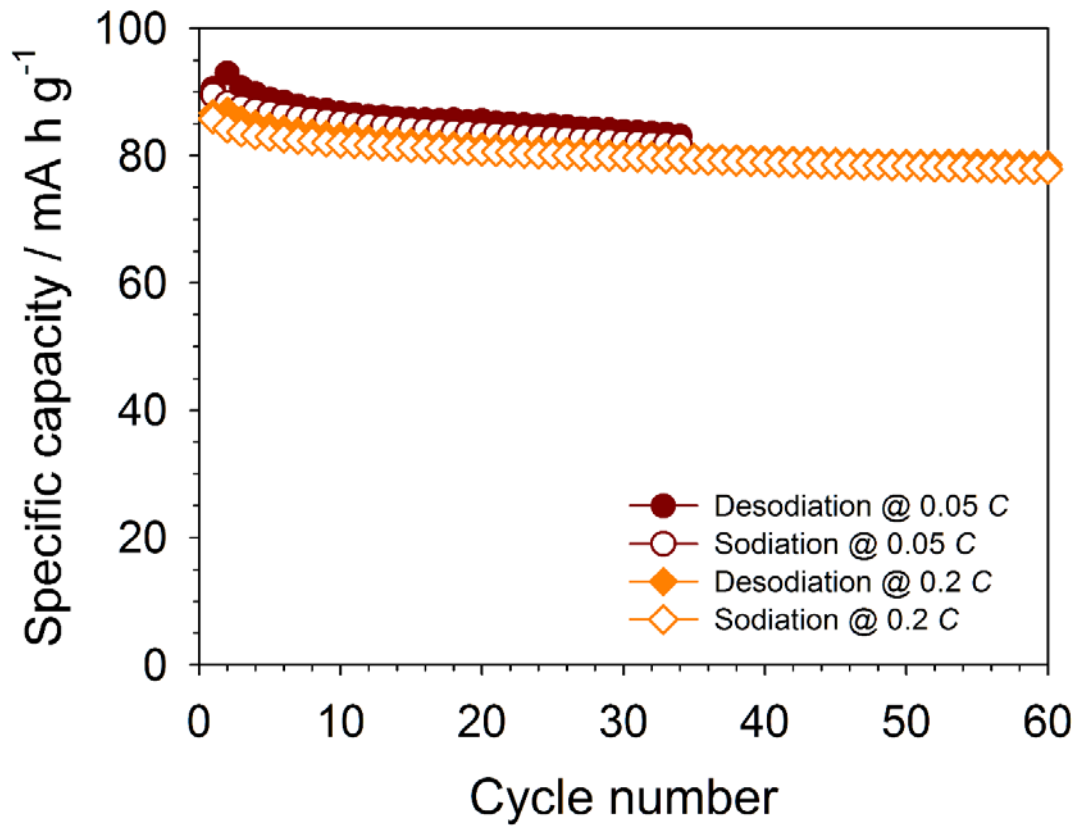
Figure 22. Cycleability of the off-stoichiometric $Na_{3.32}Fe_{2.34}(P_2O_7)_2$ at 0.05 and 0.2 C rates.
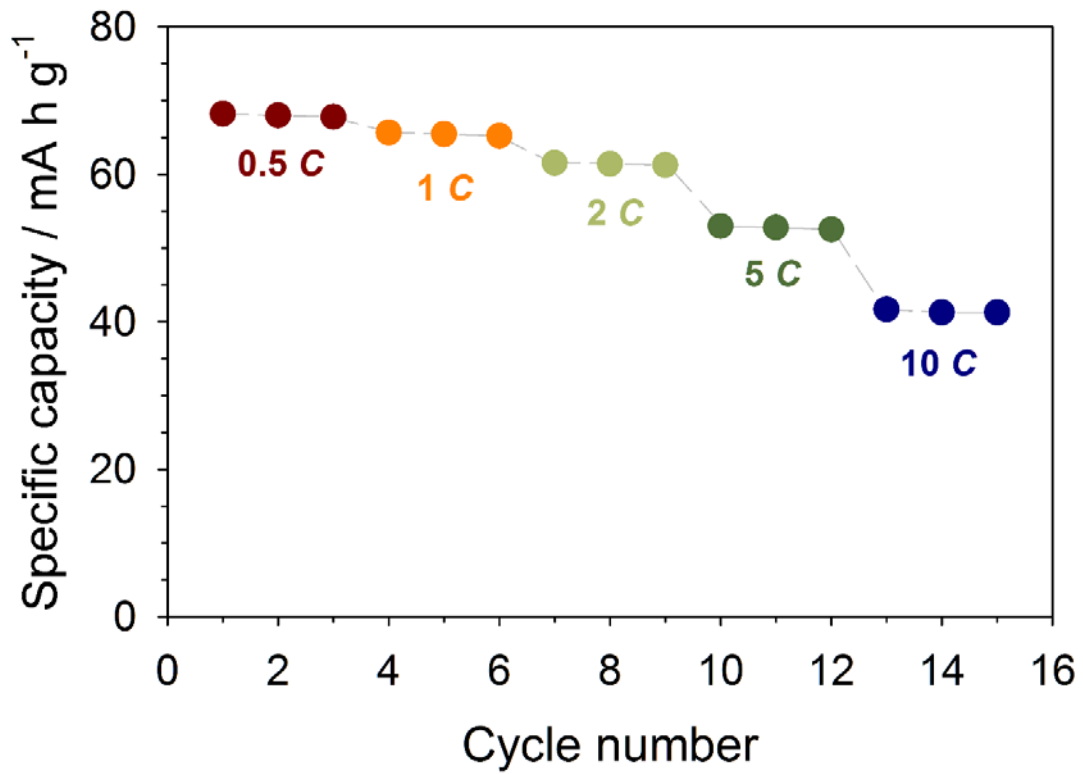
Figure 23. Rate capability of the off-stoichiometric $Na_{3.32}Fe_{2.34}(P_2O_7)_2$ with varying the C rates on discharging (sodiation).

3.1.4. Electrochemical mechanism for sodium iron pyrophosphate

The electrochemical mechanism for sodium iron pyrophosphates were analyzed in terms of its structure and phase transition. At the voltage profile, two distinct plateaus are shown in Figure 14 and 19, with different potentials of about 2.5 and 3.0 V vs. Na/Na^+. It means there are two distinct redox reactions on charging and discharging, and can be explained by the structural environment of them. As seen in Table 1, there are four sites for iron atoms, as redox centers, and Fe(3) site exists with five neighboring oxygen atoms although others do with six-coordinating.[105] Considering this kind of different environmental systems, Fe(3) should have distinguished in the potential.

Phase transition of the sodium iron pyrophosphate during the electrochemical reaction was analyzed through chemical de/sodiation processes. Sodium iron pyrophosphates having equivalent amount of sodium, when its SOC (state of charge) is 50%, 100%, and DOD (degree of discharge) is 50%, and DOD 100%, was ready with controlling the molar ratio of the oxidizing agent of $NOBF_4$ (or reducing agent of NaI). Molar compositions toward the final products were confirmed ICP (Figure 24), and it exhibits that the stoichiometry with the sodium atom is well matched with the empirically predicted one, when fixing the amount of iron atom to 2.44. Figure 25 shows corresponding powder XRD patterns for each sodium iron pyrophosphates, and indicates that it goes through single phase reaction without any appearances for additional phases except for shifts in the peaks. In addition, very tiny volume change on charging is calculated through Rietveld refinements. The partially sodiated sodium iron pysophosphate (SOC 50%) has the lattice parameters of a = 6.35862(27) Å, b = 9.4253(4) Å, c = 11.0016(5) Å, α = 63.6517(22), β = 84.8881(27), and γ = 73.1909(25) whereas the fully sodiated one has a = 6.32887(34) Å, b = 9.3980(5) Å, c = 11.0270(5) Å, α = 63.0667(23), β = 83.8493(30), and γ = 72.6569(29). The detail information upon the refinement is shown in Figure 26 and Table 2 to 3. The change in volume is about 1.9% at its maximum, so small amount is observed compared with other phosphate materials as sodium hosts.[84, 109]
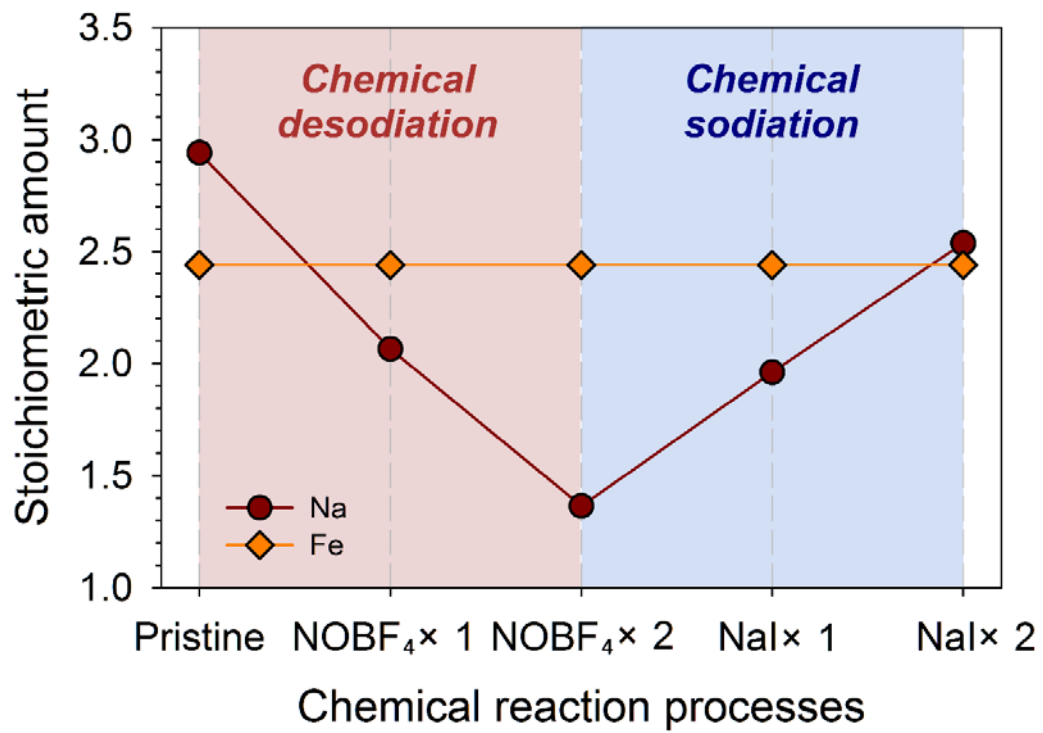
Figure 24. Stoichiometric amount changes in sodium atoms along chemical de/sodiation processes.
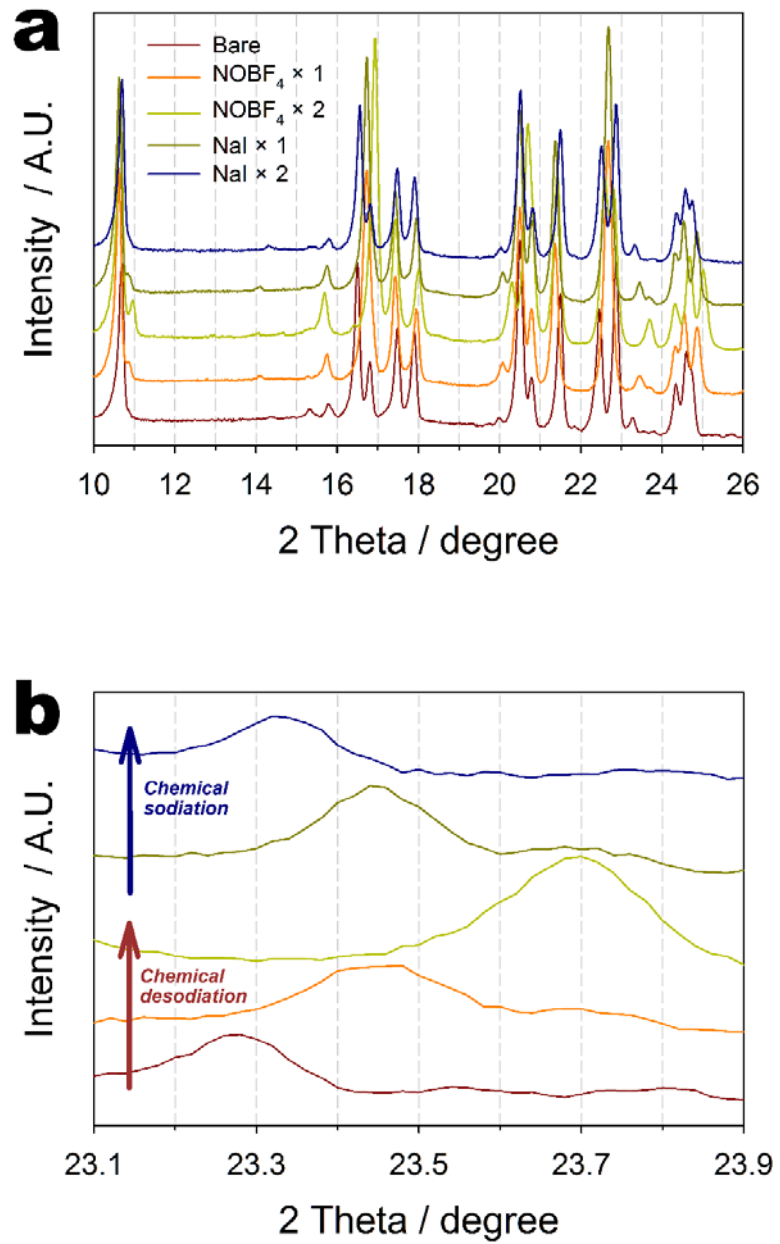
Figure 25. Powder XRD patterns of the sodium iron pyrophosphates after chemical de/sodiation processes along (a) 10 to 26° and (b) magnified ranges.
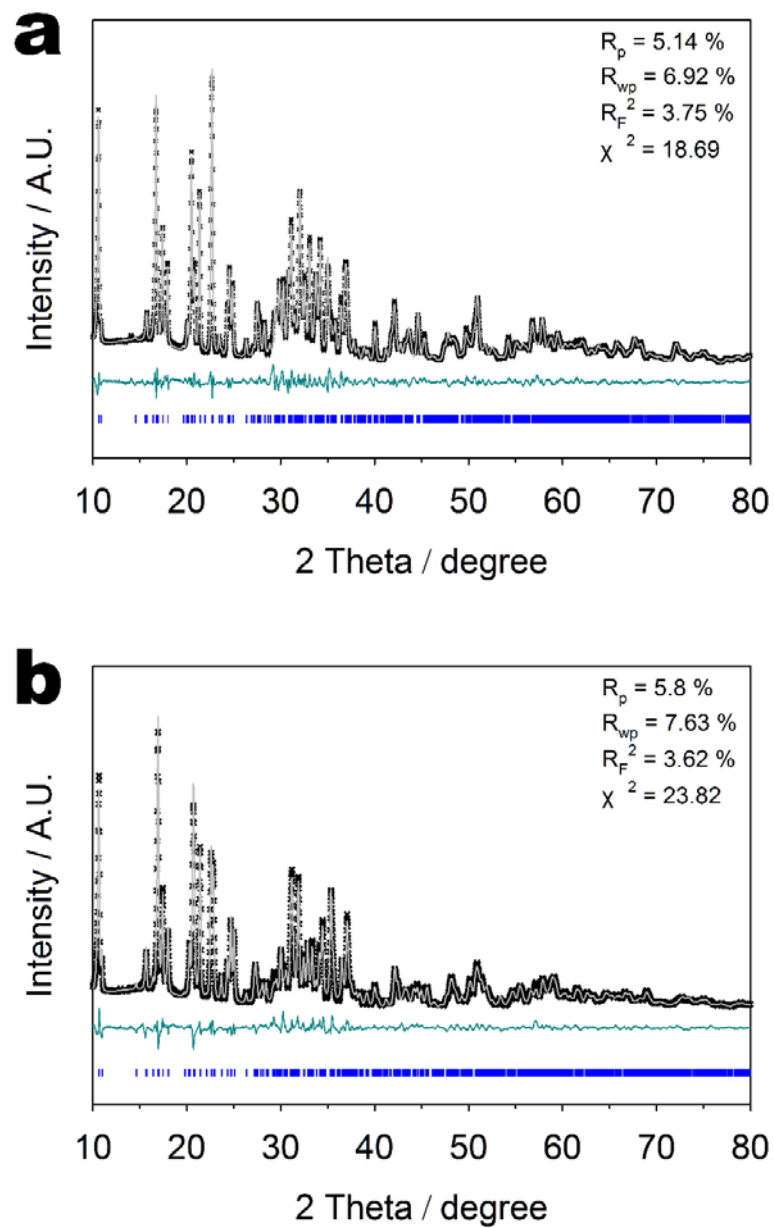
Figure 26. Rietveld refinement data of the chemically desodiated sodium iron
pyrophosphates with theoretically equivalent amount at (a) SOC 50%
and (b) SOC 100% (fully charged).

43

Table 2. Crystallographic information for each atomic sites of the partially desodiated sodium iron pyrophosphate with theoretically equivalent amount at SOC 50%.

Atom	Position			Occupancy	Multiplicity	Uiso
	a	b	c			
Na(1)	0.2398(22)	0.8252(17)	0.5993(14)	0.767(15)	2	0.011(4)
Na(2)	0.357(4)	0.1206(25)	0.8763(22)	0.479(13)	2	0.011(4)
Na(3)	0.5	0.5	0.5	0.631(22)	1	0.011(4)
Na(4)	-0.0284(12)	0.1819(9)	0.0177(7)	0.677	2	0.013(2)
Fe(1)	-0.0284(12)	0.1819(9)	0.0177(7)	0.323	2	0.013(2)
Fe(2)	0.3519(8)	0.4946(6)	0.2386(5)	1	2	0.02197
Fe(3)	0.2711(8)	0.1058(6)	0.2834(6)	1	2	0.02197
Fe(4)	0.700(6)	0.460(5)	0.456(4)	0.118	2	0.02197
P(1)	-0.0796(16)	0.1808(13)	0.7148(9)	1	2	0.01895
P(2)	0.2867(14)	0.1875(11)	0.5304(8)	1	2	0.01895
P(3)	0.5824(14)	0.7032(11)	-0.0406(8)	1	2	0.01895
P(4)	0.8909(13)	0.4675(12)	0.1766(10)	1	2	0.01895
O(1)	0.0681(25)	0.2545(19)	0.6129(17)	1	2	0.025
O(2)	0.7244(29)	0.5428(23)	0.0344(15)	1	2	0.025
O(3)	0.8492(24)	0.0514(18)	0.6749(16)	1	2	0.025
O(4)	0.7180(29)	0.3252(23)	0.6918(16)	1	2	0.025
O(5)	0.0401(25)	0.0857(21)	0.8569(17)	1	2	0.025
O(6)	0.3988(24)	0.0903(20)	0.6672(17)	1	2	0.025
O(7)	0.1962(24)	0.0962(18)	0.4665(15)	1	2	0.025
O(8)	0.3541(24)	0.3461(20)	0.4509(18)	1	2	0.025
O(9)	0.6971(24)	0.8875(18)	-0.0907(14)	1	2	0.025
O(10)	0.5625(28)	0.7296(20)	0.8059(15)	1	2	0.025
O(11)	0.3761(25)	0.7115(19)	0.0446(14)	1	2	0.025
O(12)	0.0309(26)	0.5448(18)	0.1961(15)	1	2	0.025
O(13)	0.9546(25)	0.2967(20)	0.1843(17)	1	2	0.025
O(14)	0.6881(26)	0.4737(20)	0.2803(15)	1	2	0.025

Table 3. Crystallographic information for each atomic sites of the fully desodiated sodium iron pyrophosphate with theoretically equivalent amount at SOC 100%.

Atom	Position			Occupancy	Multiplicity	Uiso
	a	b	c			
Na(1)	0.236(6)	0.839(5)	0.5933(35)	0.328(18)	2	0.012(7)
Na(2)	0.510(7)	0.100(5)	0.891(4)	0.289(17)	2	0.012(7)
Na(3)	0.5	0.5	0.5	0.242(29)	1	0.012(7)
Na(4)	-0.0150(15)	0.1711(11)	0.0244(9)	0.677	2	0.011(3)
Fe(1)	-0.0150(15)	0.1711(11)	0.0244(9)	0.323	2	0.011(3)
Fe(2)	0.3588(9)	0.4959(8)	0.2439(6)	1	2	0.01326
Fe(3)	0.2751(11)	0.0986(7)	0.2902(6)	1	2	0.01326
Fe(4)	0.573(7)	0.452(6)	0.514(6)	0.118	2	0.01326
P(1)	-0.0758(17)	0.1639(13)	0.7140(11)	1	2	0.1712
P(2)	0.2698(16)	0.1950(12)	0.5279(9)	1	2	0.1712
P(3)	0.5974(17)	0.7018(13)	-0.0371(11)	1	2	0.1712
P(4)	0.8659(18)	0.4500(14)	0.1940(12)	1	2	0.1712
O(1)	0.1512(29)	0.2713(21)	0.6160(18)	1	2	0.02164
O(2)	0.7571(32)	0.5504(24)	0.0415(17)	1	2	0.01764
O(3)	0.8818(35)	0.0561(25)	0.6827(20)	1	2	0.6206
O(4)	0.7227(31)	0.3203(24)	0.6761(17)	1	2	0.01761
O(5)	0.0603(26)	0.1295(25)	0.8536(21)	1	2	0.04141
O(6)	0.416(4)	0.0488(30)	0.6465(19)	1	2	0.0669
O(7)	0.1836(30)	0.1235(23)	0.4626(18)	1	2	0.0439
O(8)	0.3679(24)	0.3650(19)	0.4431(15)	1	2	0.00137
O(9)	0.6990(30)	0.8663(22)	-0.0866(17)	1	2	0.3409
O(10)	0.561(4)	0.7164(26)	0.8173(23)	1	2	0.05612
O(11)	0.3199(32)	0.7022(22)	0.0413(17)	1	2	0.04795
O(12)	0.071(4)	0.5358(25)	0.2047(19)	1	2	0.04714
O(13)	1.0156(27)	0.3155(20)	0.1820(17)	1	2	0.00342
O(14)	0.6906(33)	0.4416(21)	0.2861(18)	1	2	0.02641

3.2. Sodium manganese pyrophosphate

3.2.1. Synthesis and structural differences with addition of manganese precursor to sodium iron pyrophosphate

Sodium manganese pyrophosphate is also synthesized with the triclinic structure form from three precursors of sodium carbonate, manganese acetate tetrahydrate, and ammonium hydrogen pyrophosphate, which have an overall composition of $Na_{3.12}Mn_{2.44}(P_2O_7)_2$, same as the sodium iron pyrophosphate's case. Figure 27 shows the powder XRD patterns of several pyrophosphates where they have different species or compositions of transition metals in their units. The XRD patterns of $Na_{3.12}Mn_{2.44}(P_2O_7)_2$ exist with slightly left shifted compared with those of $Na_{3.12}Fe_{2.44}(P_2O_7)_2$ synthesized also with the triclinic phase. This phenomenon follows Bragg's law well which denotes the relationship between angle between an incident and a scattered plane (θ) and the distance between lattices, as d-spacing value, (d) as below:

$$2\ d \sin \theta = n\ \lambda$$

where n is an interger and λ is wavelength of the incident X-ray beam. In detail, the d-spacing value should be larger in the case of $Na_{3.12}Mn_{2.44}(P_2O_7)_2$ rather than $Na_{3.12}Fe_{2.44}(P_2O_7)_2$ naturally because the ionic size of Mn^{2+} is larger than that of Fe^{2+} due to less amount electrons and consequent stronger interaction between the nuclei and electrons. This tendency is often discovered in a lot of active materials consisting solid solution system on the transition metal sites.[110, 111] Additionally, peaks of $Na_{3.12}Fe_{1.22}Mn_{1.22}(P_2O_7)_2$ normally exist between those of $Na_{3.12}Fe_{2.44}(P_2O_7)_2$ and $Na_{3.12}Mn_{2.44}(P_2O_7)_2$ by this rule, forming the solid solution phase between manganese and iron.
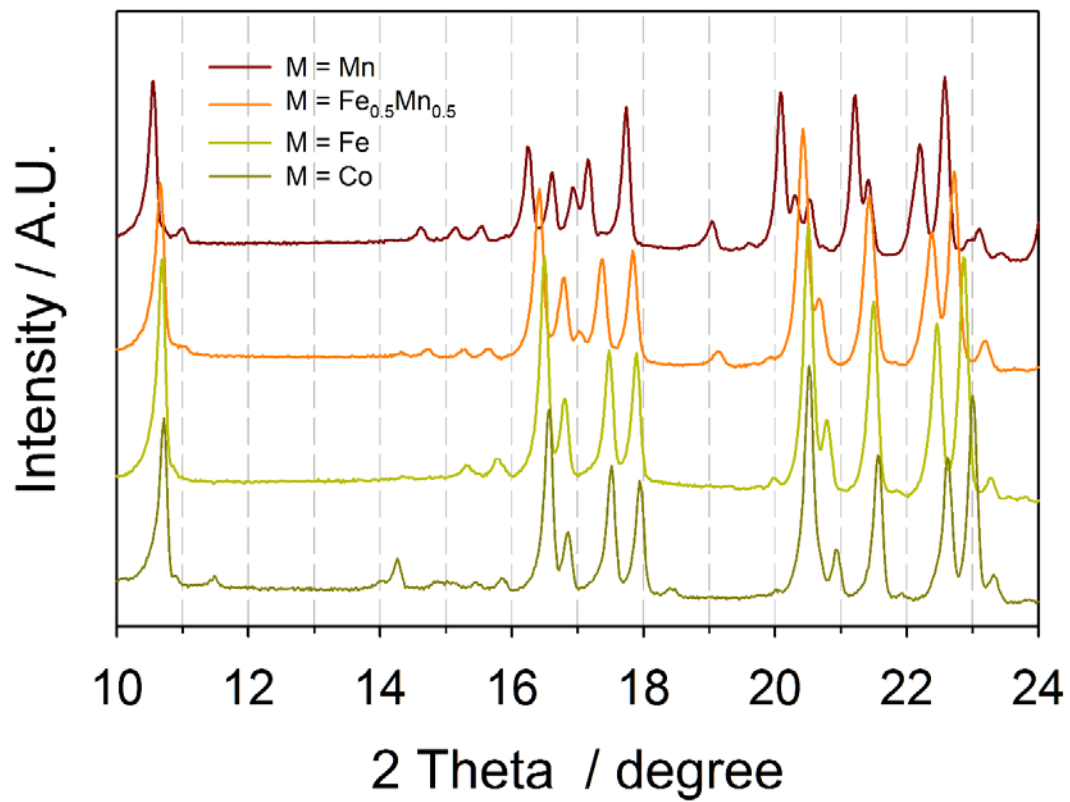
Figure 27. Powder XRD patterns of the triclinic $Na_{3.12}M_{2.44}(P_2O_7)_2$ along the transition metals and compositions.

The intermediate structure between $Na_{3.12}Fe_{2.44}(P_2O_7)_2$ and $Na_{3.12}Mn_{2.44}(P_2O_7)_2$, with the composition of $Na_{3.12}Fe_{1.22}Mn_{1.22}(P_2O_7)_2$, is analyzed through Rietveld refinement to understand the structural changes by inserting manganese atoms on traditional iron sites (Figure 28a). Its lattice parameters are slightly changed to a = 6.4653(5) Å, b = 9.4305(8) Å, c = 11.0295(10) Å, α = 64.360(4), β = 85.811(5), and γ = 72.955(5), which is more elongated to all axes rather than those in $Na_{3.12}Fe_{2.44}(P_2O_7)_2$, suggesting that the larger ionic size of manganese affects to the triclinic structure directly. Furthermore, the parameters of $Na_{3.12}Mn_{2.44}(P_2O_7)_2$ are predicted by CRYSFIRE as a = 6.532 Å, b = 9.526 Å, c = 11.089 Å, α = 64.4160, β = 85.9592, and γ = 73.4145, which are more increased values.

Its structure is displayed in Figure 28b geometrically. Compared with Figure 12a, it has a slightly distorted unit due to the manganese atoms, however, the overall structure is very similar with $Na_{3.12}Fe_{2.44}(P_2O_7)_2$. This situation is also followed in Table 4 that there is no change in sites except certain part of iron sites is substituted by manganese atoms. Basically, occupancy factor for the transition metal sites is divided equally for manganese and iron because they have the exact molar ratio of 0.5 : 0.5 during the synthesis, and M(1) site equals with Na(4) site in coordination as the iron's case, so three atoms are co-existed in that point. M(4) site still keeps small distance with Na(3) site so that manganese and iron atoms cannot be occupied by half, rather, Na(3), Fe(4), and Mn(4) sites are located partially at this time.
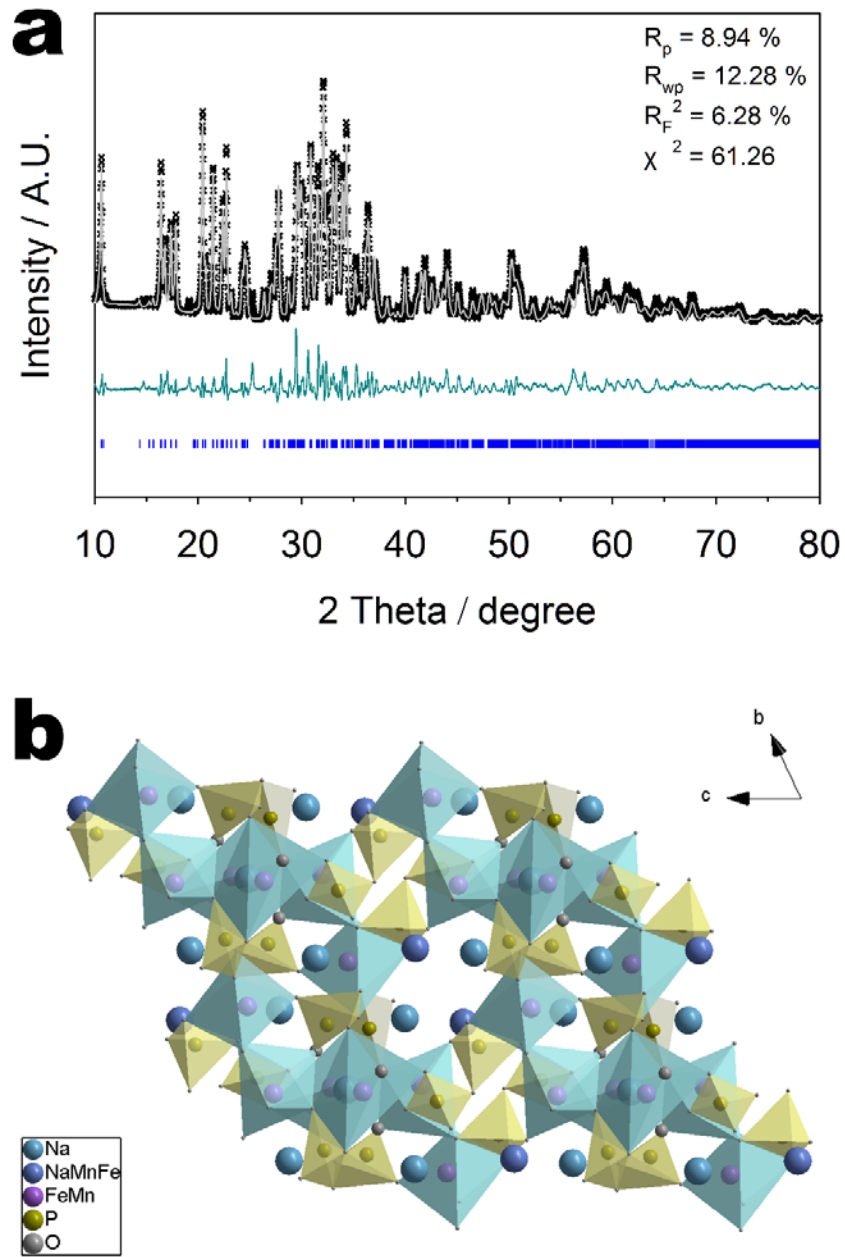
Figure 28. (a) Rietveld refinement data of $Na_{3.12}Fe_{1.22}Mn_{1.22}(P_2O_7)_2$ and (b) its structure viewed along [100] direction.

Table 4. Crystallographic information for each atomic sites of $Na_{3.12}Fe_{1.22}Mn_{1.22}(P_2O_7)_2$.

Atom	Position			Occupancy	Multiplicity	Uiso
	a	b	c			
Na(1)	0.2153(33)	0.8751(28)	0.6060(23)	1	2	0.0115(44)
Na(2)	0.4227(31)	0.1580(26)	0.8236(22)	1	2	0.0115(44)
Na(3)	0.5	0.5	0.5	0.882	1	0.0115(44)
Na(4)	-0.0185(24)	0.1751(21)	0.0240(16)	0.677	2	0.0106(58)
Fe(1)	-0.0185(24)	0.1751(21)	0.0240(16)	0.1615	2	0.0106(58)
Fe(2)	0.3436(16)	0.5230(12)	0.2318(9)	0.5	2	0.00961
Fe(3)	0.2878(15)	0.1072(12)	0.2850(10)	0.5	2	0.00961
Fe(4)	0.948(14)	0.493(11)	0.450(8)	0.059	2	0.00961
Mn(1)	-0.0185(24)	0.1751(21)	0.0240(16)	0.1615	2	0.0106(58)
Mn(2)	0.3436(16)	0.5230(12)	0.2318(9)	0.5	2	0.0121(57)
Mn(3)	0.2878(15)	0.1072(12)	0.2850(10)	0.5	2	0.0121(57)
Mn(4)	0.948(14)	0.493(11)	0.450(8)	0.059	2	0.0121(57)
P(1)	-0.1435(33)	0.2103(28)	0.6789(24)	1	2	0.04696
P(2)	0.2759(30)	0.1900(25)	0.5379(21)	1	2	0.04696
P(3)	0.5426(35)	0.7074(27)	-0.0373(22)	1	2	0.04933
P(4)	0.8534(32)	0.4468(24)	0.2011(24)	1	2	0.05598
O(1)	0.077(8)	0.195(6)	0.607(5)	1	2	0.1312
O(2)	0.796(5)	0.486(4)	0.0600(33)	1	2	0.00752
O(3)	0.959(7)	0.035(6)	0.0714(4)	1	2	0.0891
O(4)	0.702(6)	0.413(4)	0.652(4)	1	2	0.04643
O(5)	-0.024(6)	0.075(5)	0.81414(35)	1	2	0.05314
O(6)	0.409(5)	0.157(4)	0.6617(32)	1	2	0.01763
O(7)	0.224(5)	0.062(2)	0.4740(30)	1	2	0.02041
O(8)	0.387(5)	0.318(4)	0.4567(30)	1	2	0.00497
O(9)	0.646(5)	0.823(4)	-0.0382(30)	1	2	0.00949
O(10)	0.570(5)	0.727(4)	0.8048(33)	1	2	0.04297
O(11)	0.348(6)	0.7330(35)	0.0531(33)	1	2	0.06398

O(12)	0.004(7)	0.592(5)	0.193(4)	1	2	0.09761
O(13)	0.941(6)	0.317(5)	0.197(4)	1	2	0.0699
O(14)	0.666(6)	0.409(4)	0.324(4)	1	2	0.07759

3.2.2. Differences in electrochemical performances with addition of manganese precursor to sodium iron pyrophosphate

Figure 29 shows the voltage profiles of $Na_{3.12}Fe_{1.22}Mn_{1.22}(P_2O_7)_2$ and $Na_{3.12}Mn_{2.44}(P_2O_7)_2$. Considering those compounds have theoretically larger redox potential ($Mn^{2+/3+}$) unlike $Na_{3.12}Fe_{2.44}(P_2O_7)_2$, their cut-off voltages was also modified to 4.5 V vs. Na/Na$^+$ in especially $Na_{3.12}Mn_{2.44}(P_2O_7)_2$. $Na_{3.12}Fe_{1.22}Mn_{1.22}(P_2O_7)_2$ exhibits less than 45 mA h g^{-1} with still two plateaus at 2.5 and 3.0 V vs. Na/Na$^+$ (Figure 27a). It means that these two equilibrium potentials are still from four iron sites, exhibiting reversible capacity which is almost half of that of the sodium iron pyrophosphate (Figure 30). The fact that manganese cannot act as the redox center is more critical upon $Na_{3.12}Mn_{2.44}(P_2O_7)_2$ (Figure 27b). It delivers less than 10 mA h g^{-1} of reversible capacity up to 4.5 V vs. Na/Na$^+$ with no specific plateau in contrast to other pyrophosphates including iron. It indicates that it is not only the problem of electrolyte with operated by that high voltage, but that of manganese itself. Several cases of phosphate-based active materials which have manganese as in the transition metal site suffers very poor cycling performances due to the electrochemical activity of manganese.[91]
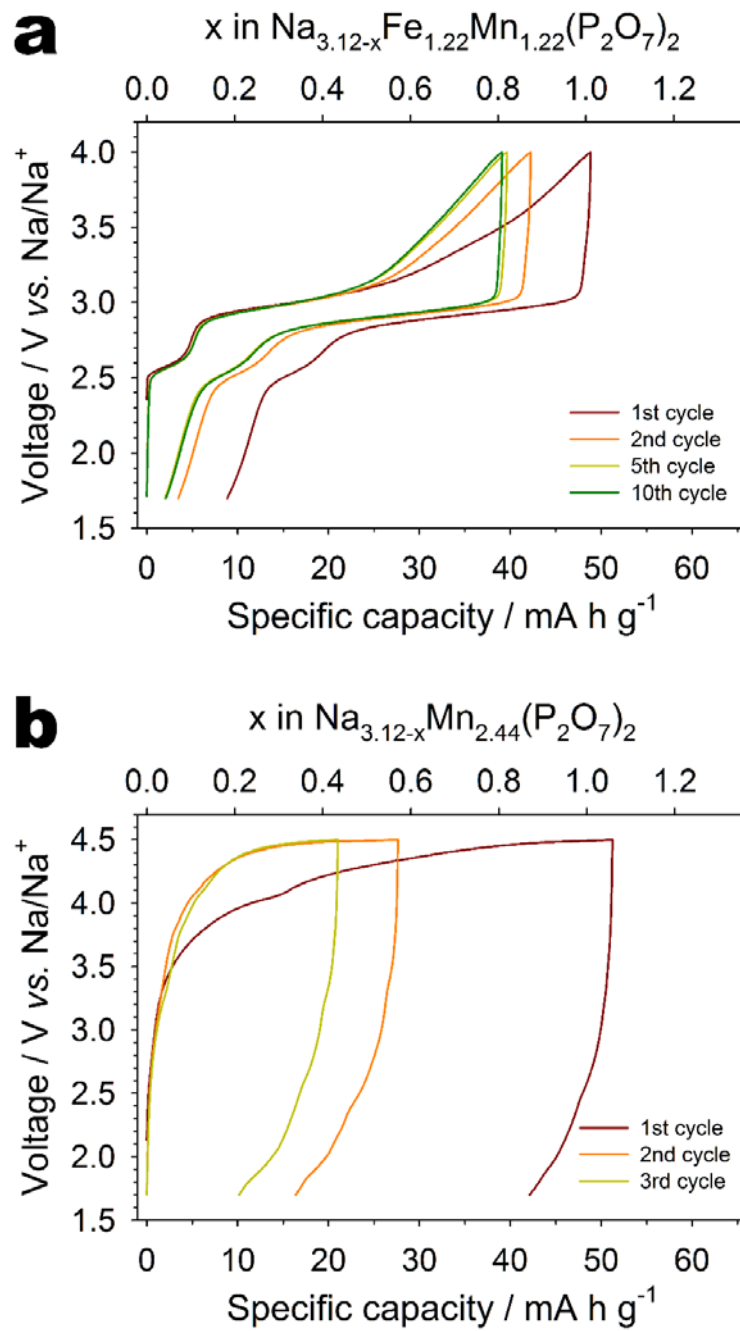
Figure 29. Voltage profiles of $Na_{3.12}Fe_{1.22}Mn_{1.22}(P_2O_7)_2$ and $Na_{3.12}Mn_{2.44}(P_2O_7)_2$.
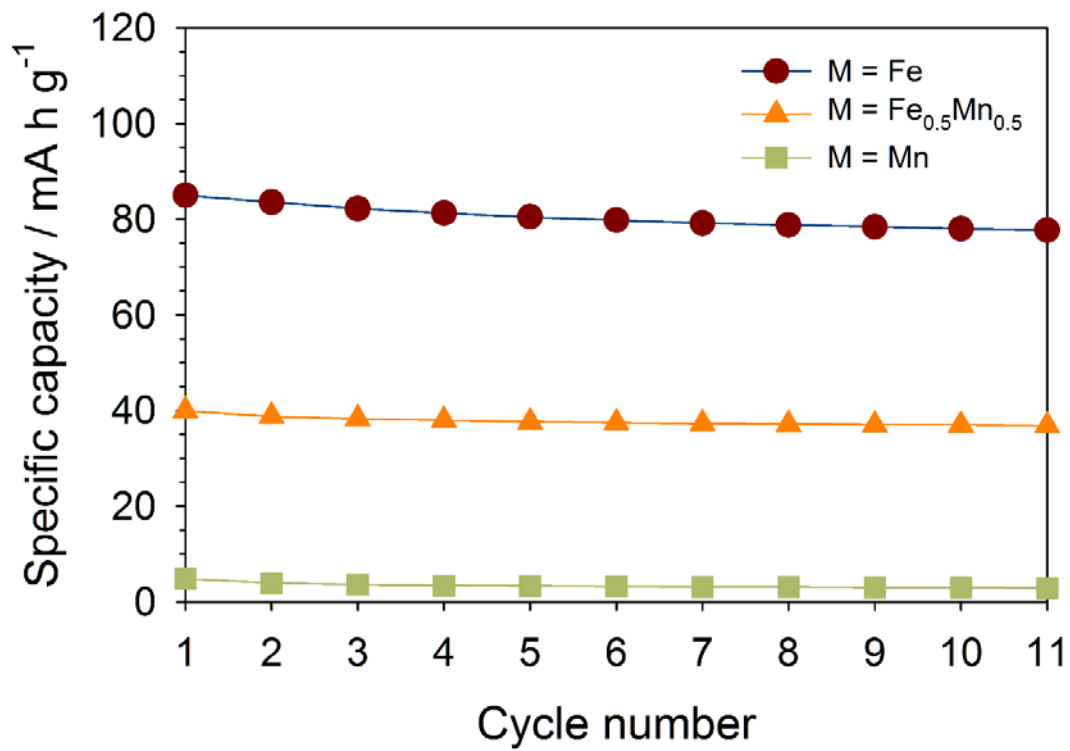
Figure 30. Sodiation capacity of $Na_{3.12}M_{2.44}(P_2O_7)_2$ (M = Fe, $Fe_{0.5}Mn_{0.5}$, and Mn) along cycles.

3.3. Sodium cobalt pyrophosphate

3.3.1. Synthesis and structural examination toward triclinic and orthorhombic sodium cobalt pyrophosphate

Sodium cobalt pyrophosphate has three distinct kinds of types of triclinic (*P-1*), orthorhombic *(Pna2$_1$)*, and tetragonal (*P4$_2$/mmm*) structures naturally.[112] Among them, sodium cobalt pyrophosphate having the triclinic structure as the most stabilized phase in thermodynamics, which has its composition of $Na_{3.12}Co_{2.44}(P_2O_7)_2$, was firstly experimented as the active material for sodium ion batteries. Also, for comparison, an orthorhombic type of the cobalt pyrophosphate, $Na_2CoP_2O_7$, was also synthesized and electrochemically tested which was already reported.[96, 97]

They are synthesized with sodium carbonate, cobalt acetate tetrahydrate, and ammonium hydrogen phosphate by solid state method, as mentioned, with amounts meeting their stoichiometry. The final products were analyzed by the XRD to know whether they are well synthesized or not, and be ready for Rietveld refinement to calculate their lattice parameters. Again, Figure 27 shows again exactly same patterns with triclinic $Na_{3.12}Fe_{2.44}(P_2O_7)_2$ and $Na_{3.12}Mn_{2.44}(P_2O_7)_2$, with just peak shifts to higher 2 theta values by Bragg's law, therefore, $Na_{3.12}Co_{2.44}(P_2O_7)_2$ is also belonging to the solid solution system with the other synthesized ones. Unlike $Na_2CoP_2O_7$ is stabilized in orthorhombic structure in thermodynamics, $Na_{3.12}Co_{2.44}(P_2O_7)_2$ exists in triclinic structure as the final product, therefore, their structural environments should be distinguished each other. XRD peaks of the orthorhombic type of $Na_2CoP_2O_7$ also seems to be well-synthesized, compared with the known pattern (PDF # : 80-2410) (Figure 31).
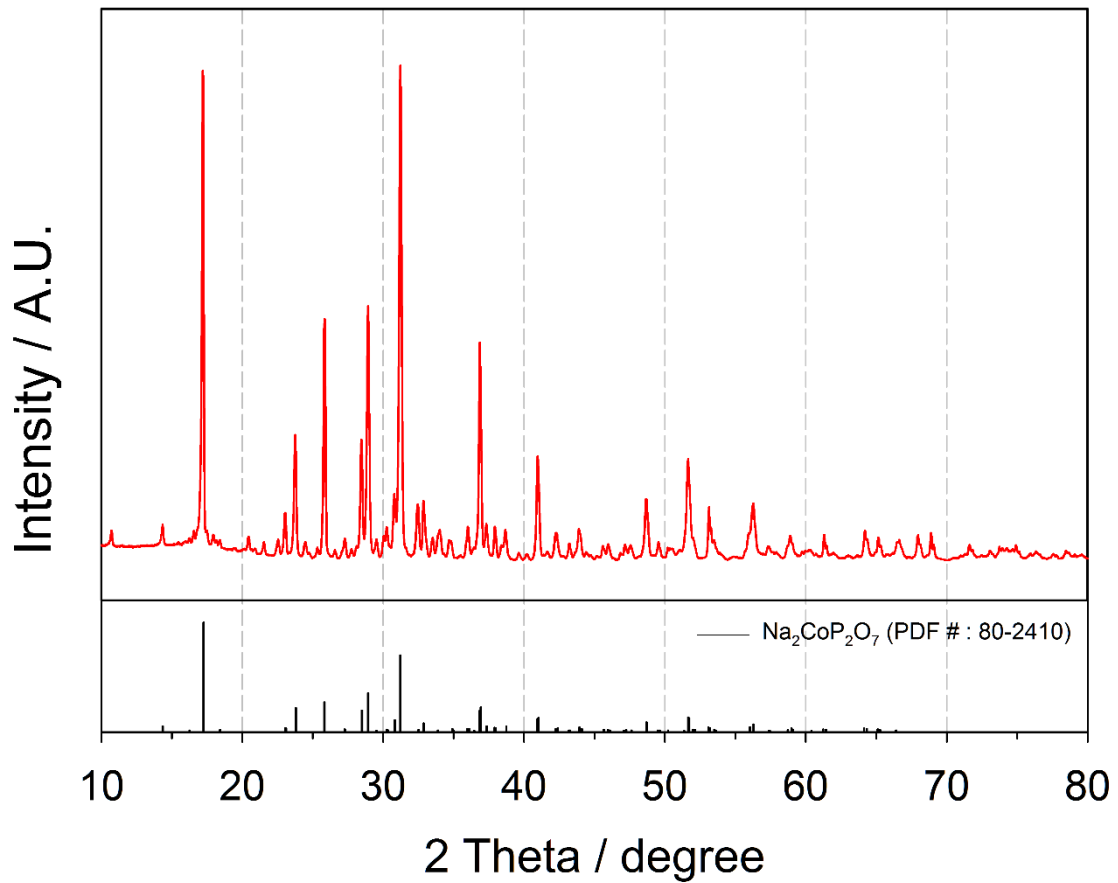
Figure 31. Powder XRD pattern of the orthorhombic $Na_2CoP_2O_7$ with the consistent PDF.

Rietveld refinement on the triclinic $Na_{3.12}Co_{2.44}(P_2O_7)_2$ with the XRD pattern tells that it has somewhat distorted structure than that of $Na_{3.12}Fe_{2.44}(P_2O_7)_2$ with smaller ionic size of the transition metal (Figure 32). However, the basic structure is maintained composed of the two centrosymmetric crowns of $Co_2P_4O_{22}$ and $Co_2P_4O_{20}$. Its lattice parameters are a = 6.3711(20) Å, b = 9.3451(29) Å, c = 10.9311(34) Å, α = 64.4872(15), β = 86.0195(18), and γ = 73.4348(17), contracted along all axes than that of $Na_{3.12}Fe_{2.44}(P_2O_7)_2$. Though, still it has huge sodium ion channels enough to be intercalated as about 4.90 Å at their maxima along [100] direction. This channel size is comparable with that of several solid electrolytes such as β''-alumina. The story of partial occupation factor of Na(3) is continued to $Na_{3.12}Co_{2.44}(P_2O_7)_2$ because still the distance between Na(3) and Co(4) sites is quite small as 1.2222(4) Å (Table 5).

The structure of orthorhombic $Na_2CoP_2O_7$ is also drawn like Figure 33. It has interlayers whose gap is about 3.02 Å between each cobalt pyrophosphate structure, along *ac* plane as known with stacking ABAB... type.[96, 97] Also, an additional channel where sodium ion can de/intercalate is found along [010] direction with size of about 3.57 Å. Totally, three channels are available for de/sodiation processes in geometry, however, it cannot be certain that all three-dimensional channels are used like that the olivine $LiFePO_4$ can has only one pathway for lithium ion migration despite it really has two-dimensional channels [79].

SEM images upon two species of sodium cobalt pyrophosphate are driven in Figure 34. Their morphologies is not much different, which both have submicron- or micron-scaled particles with no specific shapes. This characteristics is maintained as the particles of $Na_{3.12}Fe_{2.44}(P_2O_7)_2$ synthesized with same method.

a

R_p = 6.14 %

R_{wp} = 8.47 %

R_F^2 = 4.39 %

χ^2 = 16.16

Intensity / A.U.

2 Theta / degree

b

Na
NaCo
Co
P
O
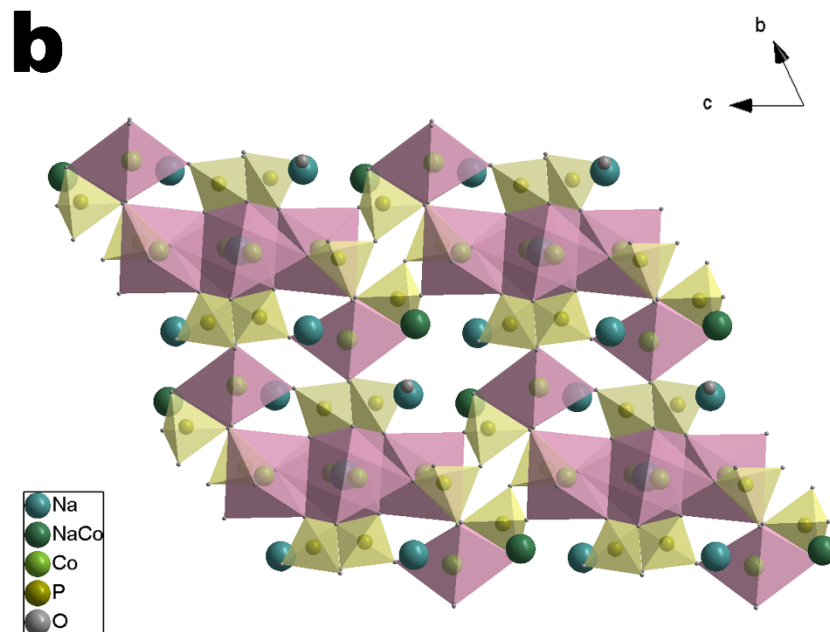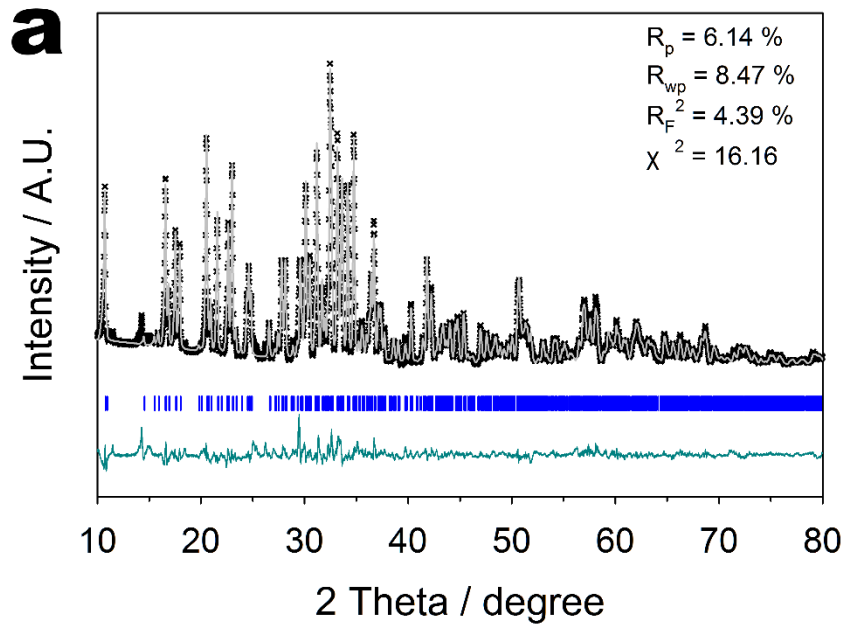
Figure 32. Rietveld refinement data of (a) $Na_{3.12}Co_{2.44}(P_2O_7)_2$ and (b) its structure viewed along [100] direction.

Table 5. Crystallographic information for each atomic sites of $Na_{3.12}Co_{2.44}(P_2O_7)_2$.

Atom	Position			Occupancy	Multiplicity	Uiso
	a	b	c			
Na(1)	0.2046	0.8538	0.6061	1	2	0.0099
Na(2)	0.4153	0.1380	0.8377	1	2	0.0404
Na(3)	0.5000	0.5000	0.5000	0.882	1	0.0225
Na(4)	-0.0197	0.1761	0.0296	0.677	2	0.0054
Co(1)	-0.0197	0.1761	0.0296	0.323	2	0.0054
Co(2)	0.3529	0.5055	0.2315	1	2	0.0127
Co(3)	0.2762	0.1038	0.2818	1	2	0.0229
Co(4)	0.6883	0.4884	0.4616	0.118	2	0.0142
P(1)	-0.0765	0.1776	0.7159	1	2	0.0459
P(2)	0.2851	0.2025	0.5363	1	2	0.0056
P(3)	0.5585	0.7123	-0.0492	1	2	0.0148
P(4)	0.8749	0.4674	0.1826	1	2	0.0376
O(1)	0.0802	0.2819	0.6034	1	2	0.0650
O(2)	0.7669	0.5441	0.0339	1	2	0.0214
O(3)	0.8877	0.0622	0.6672	1	2	0.0648
O(4)	0.7059	0.3127	0.6966	1	2	0.0260
O(5)	0.0469	0.1006	0.8478	1	2	0.0311
O(6)	0.4342	0.0816	0.6596	1	2	0.0222
O(7)	0.2045	0.1139	0.4678	1	2	0.1193
O(8)	0.3697	0.3292	0.4450	1	2	0.0076
O(9)	0.6476	0.8672	-0.0550	1	2	0.0771
O(10)	0.5490	0.7074	0.8131	1	2	0.0152
O(11)	0.3746	0.6955	0.0341	1	2	0.0153
O(12)	0.0356	0.5438	0.1892	1	2	0.0889
O(13)	0.9809	0.2811	0.2017	1	2	0.0904
O(14)	0.6776	0.4778	0.2817	1	2	0.0165
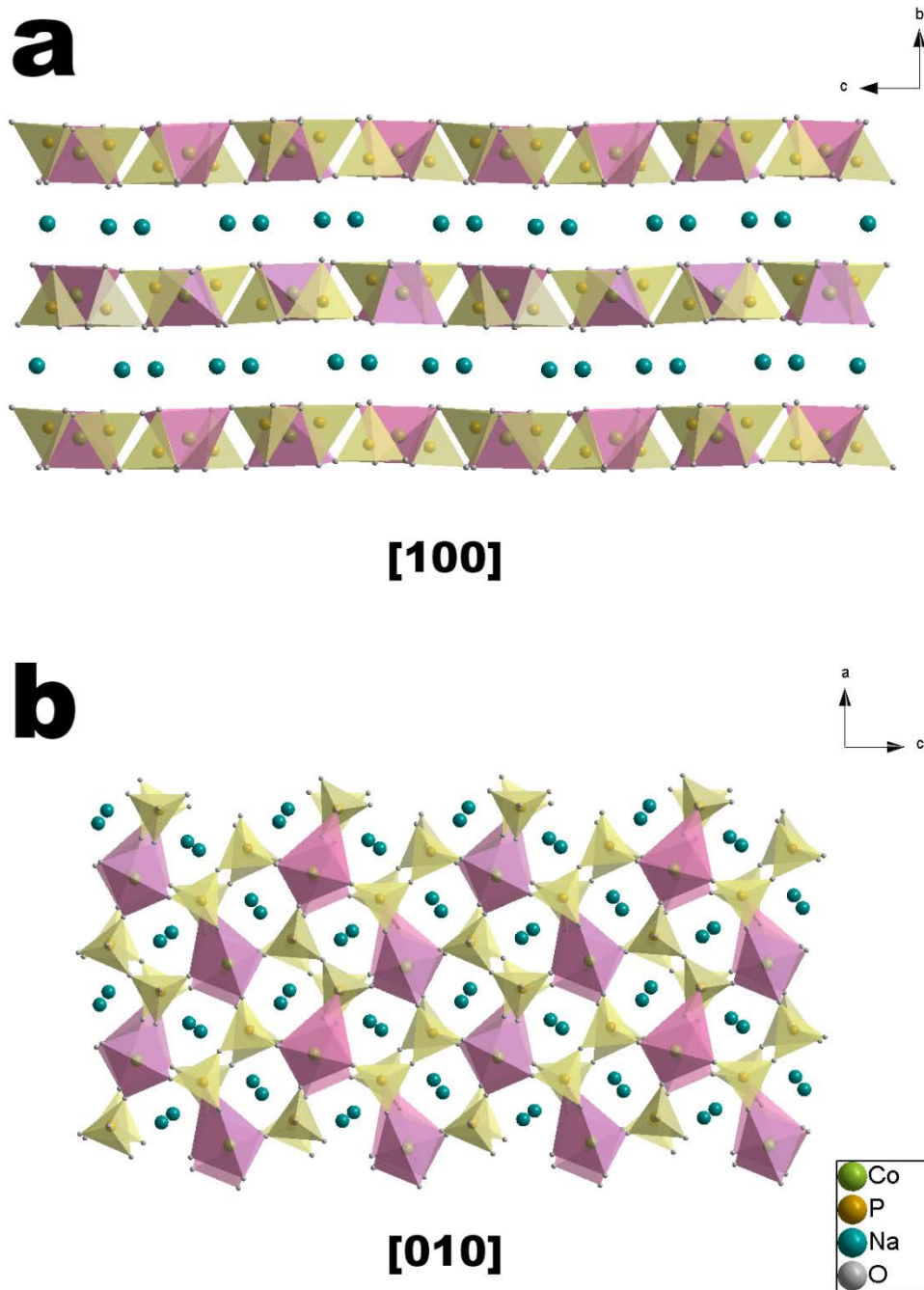
Figure 33. Structure model of the orthorhombic $Na_2CoP_2O_7$ view along (a) [100] and (b) [010] directions.
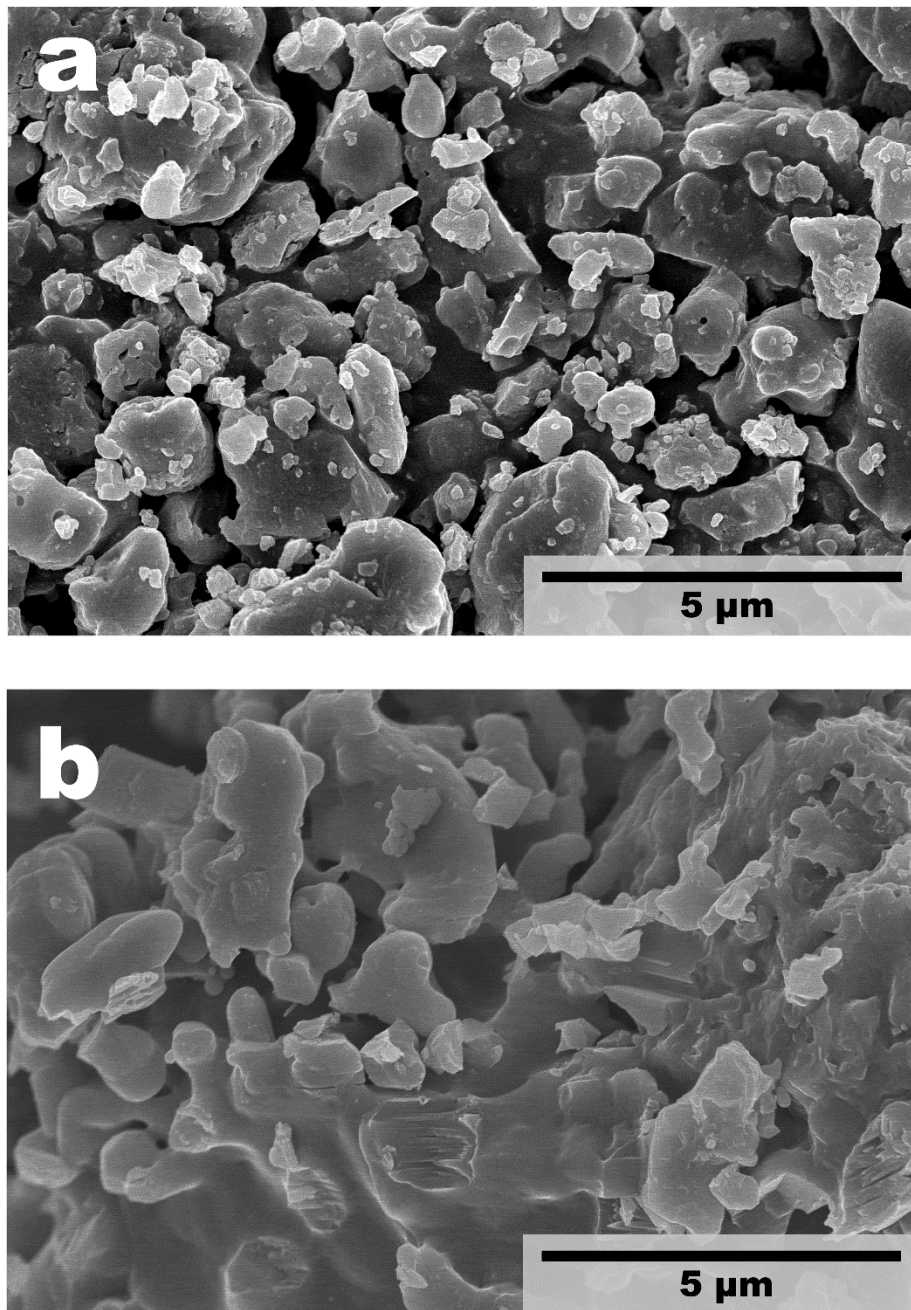
Figure 34. SEM images of (a) $Na_{3.12}Co_{2.44}(P_2O_7)_2$ and (b) $Na_2CoP_2O_7$.

3.3.2. Electrochemical performances for sodium cobalt pyrophosphates

Figure 35 shows the voltage profiles of the triclinic $Na_{3.12}Co_{2.44}(P_2O_7)_2$ and orthorhombic $Na_2CoP_2O_7$ at the 1st and 2nd cycle tested by the half cells with the sodium metal as the counter electrode. As expected, they have a quite large equilibrium potential over 4.3 V vs. Na/Na$^+$ mainly although they exhibit small amount of reversible capacity of about 0.7 Na in $Na_{3.12}Co_{2.44}(P_2O_7)_2$ and less than 0.1 Na in $Na_2CoP_2O_7$. This is more certain as seen in Figure 36 of dQ/dV plots. In addition, there are additional redox potential existed at 3.9 ~ 4.0 V vs. Na/Na$^+$. The capacity delivered at that range is attributed to the different coordination environment of Co(3) site with other three cobalt sites, Co(1), Co(2), and Co(4), as well as that in sodium iron pyrophosphates.[95, 105]

Additionally, lithium half cells were also assembled toward those two species of sodium cobalt pyrophosphate to check possibility to be used as lithium de/intercalation hosts at this time (Figure 37). However, it overall shows worse result than those in the sodium cells that they deliver similar or less reversible capacity with larger polarizations. It denotes that these two compounds have advantages as sodium hosts rather than lithium hosts. Plus, dQ/dV plots surely indicate that Co(3) site can rarely be acted as the redox center at this time (Figure 38), unlike the situation in sodium cells, considering discharging occurred at about 4.5 V vs. Li/Li$^+$. This might be caused by the different ionic radii between sodium and lithium ion and the special environment of Co(3) site, with distinct activation energies for migration.

As though they have small amount of reversible capacity compared with their theoretical capacity (2.4 Na should be transferred in $Na_{3.12}Co_{2.44}(P_2O_7)_2$ at its maximum, and 1 Na in $Na_2CoP_2O_7$), the profiles themselves are not so bad than the case in sodium manganese pyrophosphate because they show exact plateaus and electrochemical mechanisms which are similarly expected with sodium iron pyrophosphates. Therefore, it should need several improvements to overcome the limitation of cut-off voltage such as additional and continuous researches on such as electrolytes to be used at high-voltage to eliminate the side reactions at the high voltage ranges over 4.5 V vs. Na/Na$^+$ or 4.8 V vs. Li/Li$^+$.
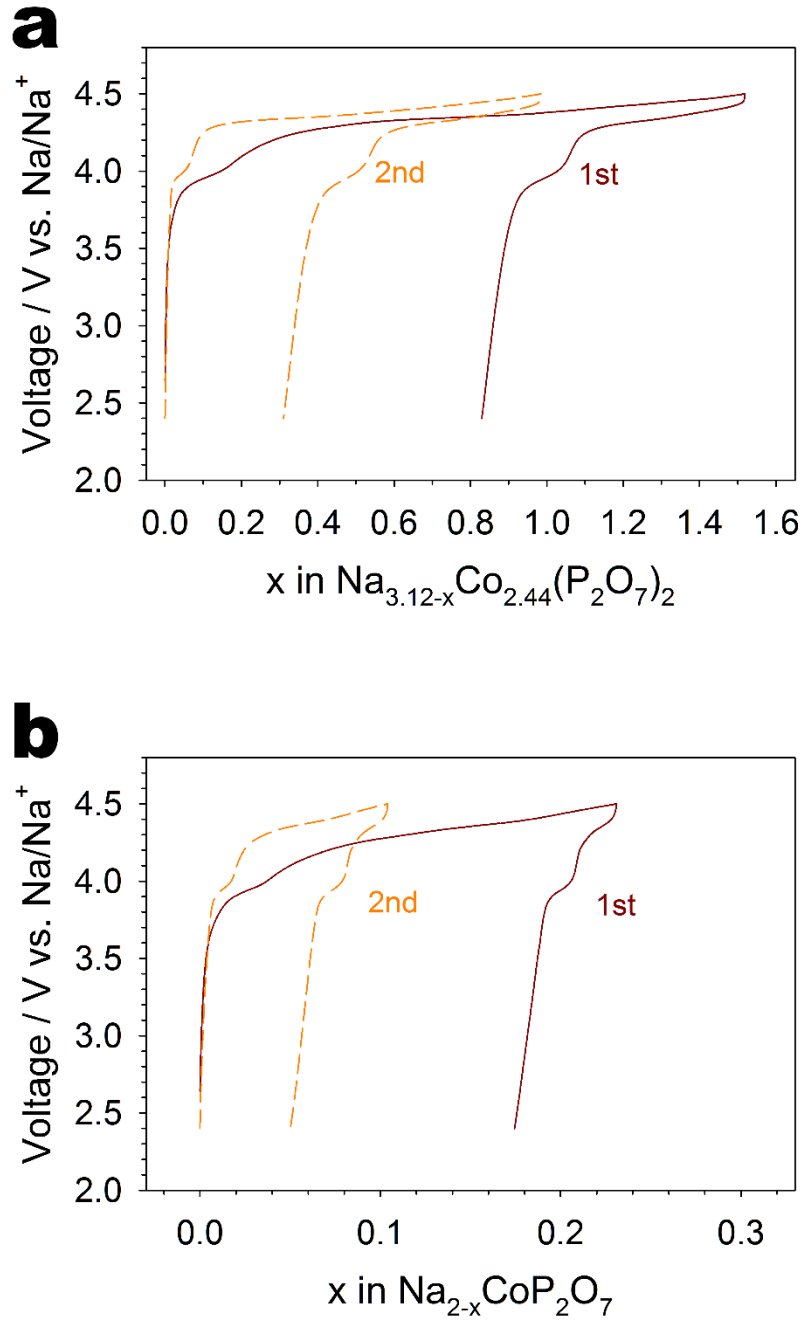
Figure 35. Voltage profile of (a) $Na_{3.12}Co_{2.44}(P_2O_7)_2$ and (b) $Na_2CoP_2O_7$ tested in the sodium half cells.

a

b
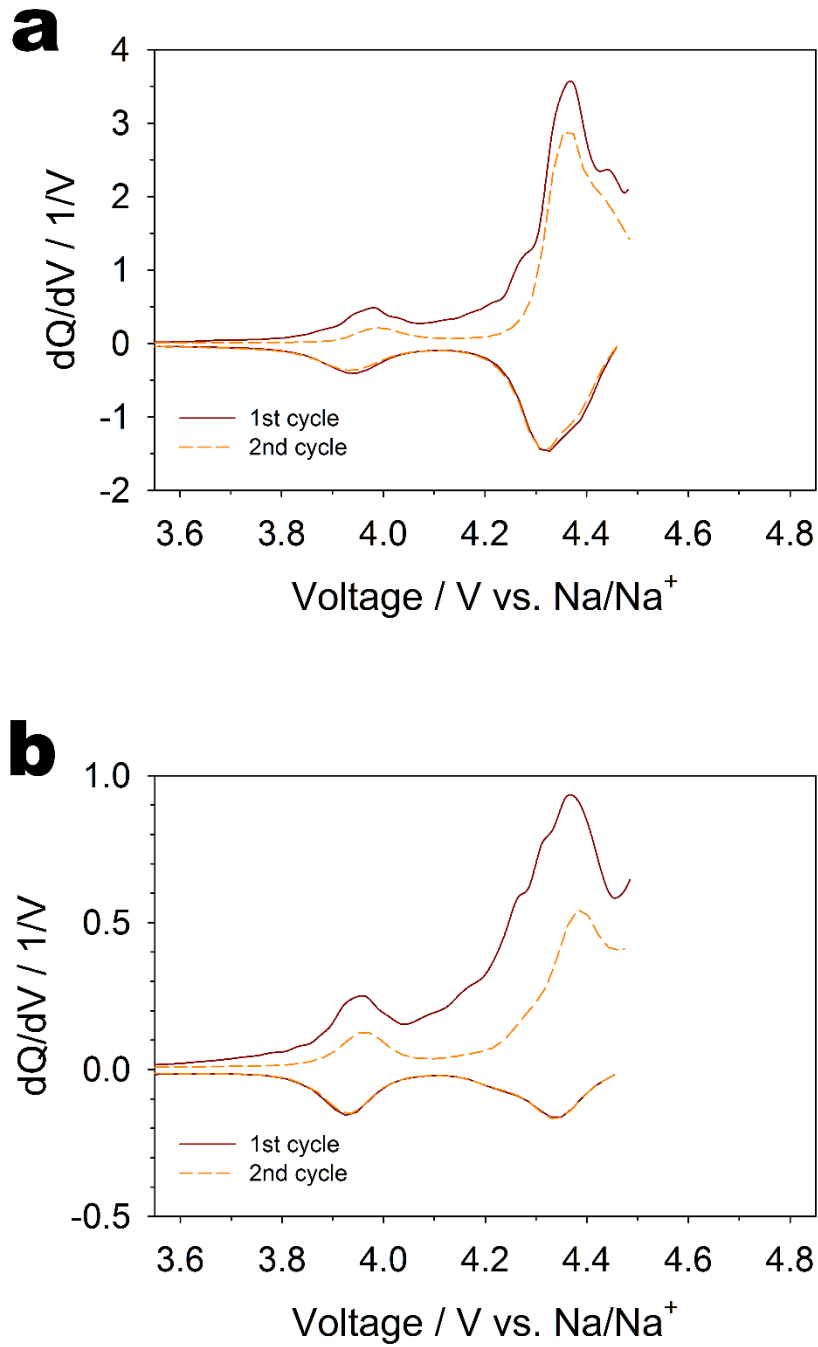
Figure 36. dQ/dV plots of (a) $Na_{3.12}Co_{2.44}(P_2O_7)_2$ and (b) $Na_2CoP_2O_7$
tested with the sodium half cells.

64
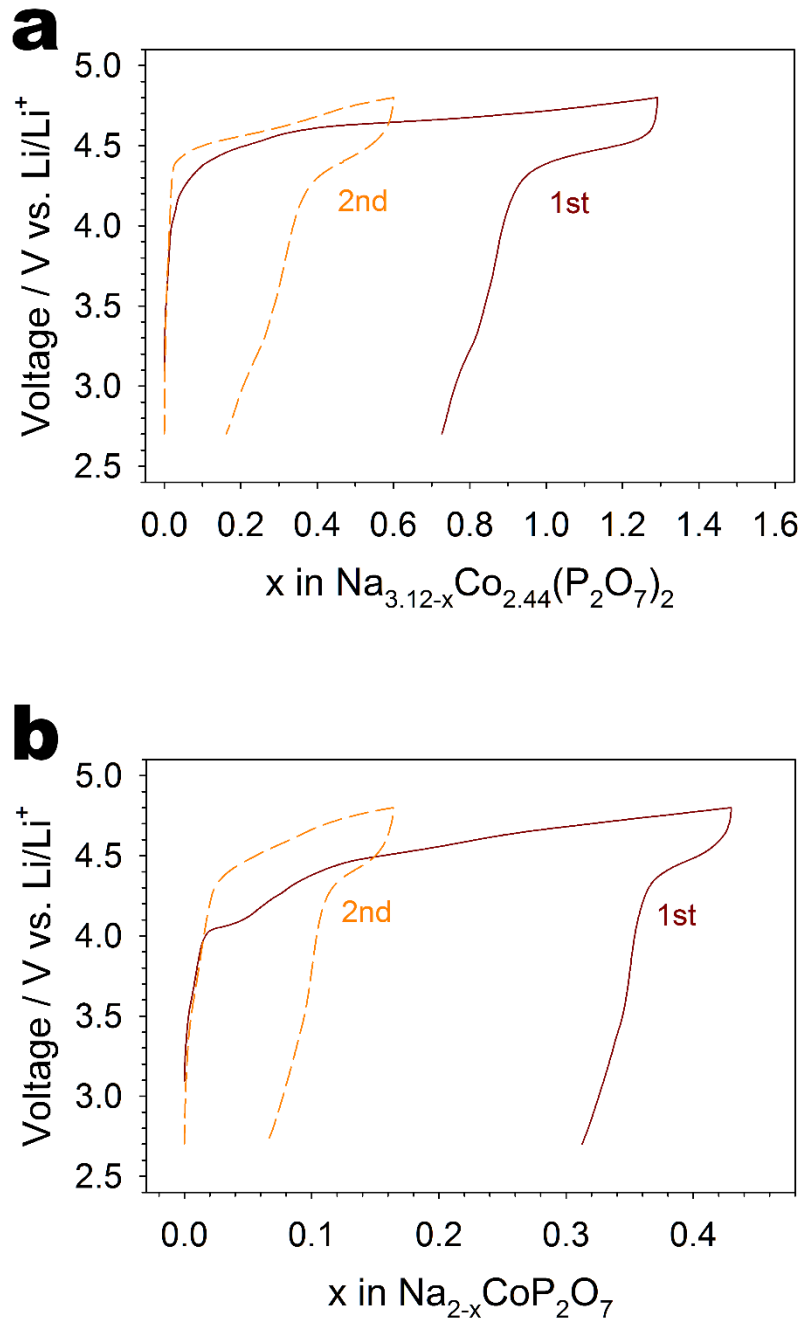
Figure 37. Voltage profiles of (a) $Na_{3.12}Co_{2.44}(P_2O_7)_2$ and (b) $Na_2CoP_2O_7$ tested in the lithium half cells.
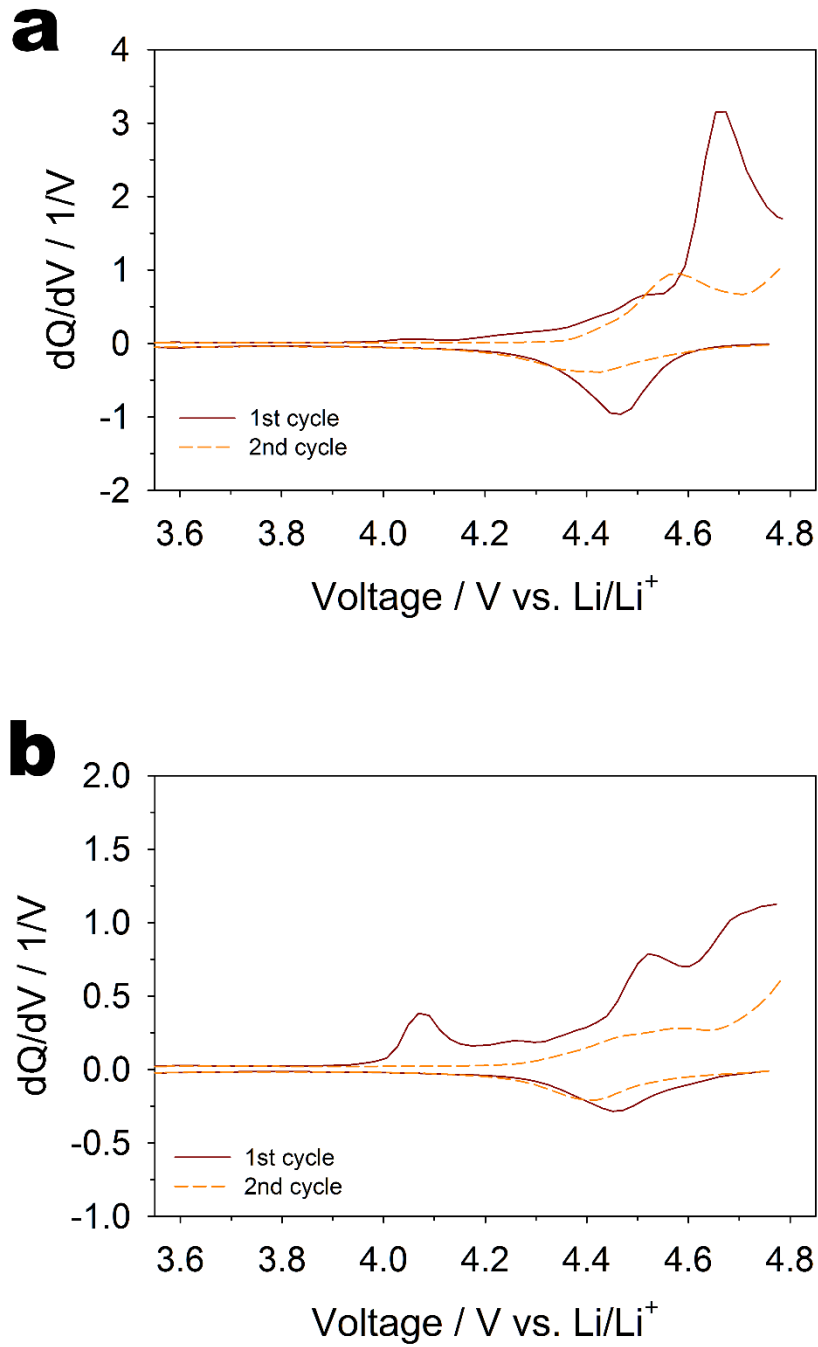
Figure 38. dQ/dV plots of (a) $Na_{3.12}Co_{2.44}(P_2O_7)_2$ and (b) $Na_2CoP_2O_7$ tested in the lithium half cells.

3.3.3. Evaluation in mass and charge transfer for sodium cobalt pyrophosphates

More details about these two sodium cobalt pyrophosphates were analyzed. First, diffusion abilities were estimated between the sodium cobalt pyrophosphates by achieving data of diffusion coefficients. Potentiostatic intermittent titration technique (PITT) was introduced to calculate solid-state mass transfer diffusion coefficients at each five voltage steps of these compounds. And, Cottrell equation is adapted as below:

$$i = (2\ n\ F\ A\ D\ \Delta C\ /\ a)\ \exp\left[(-\pi^2\ D\ /\ a^2)\ t\right]$$

where i is current, t is applied time, n is number of electron transferred, F is Faraday constant, A is surface area, D is the diffusion coefficient, and ΔC is concentration variation of the active material at each steps. Diffusion coefficient is easily calculated at finite diffusion, thus, at long time applied, because semi-finite diffusion region at short time is affected by surface roughness of the material particle seriously.[113] Considering it, the logarithm term of the current (ln (i)) should have a linear relationship corresponded with time, having a slope of $-\pi^2\ D\ /\ a^2$. Therefore, the diffusion coefficients can be estimated with calibrating the slopes.

Figure 39 shows the mentioned t vs. ln (i) plots of the both compounds given by the PITT test. Slopes are achieved and displayed as gray dashed lines at every voltage steps in the figure. The diffusion coefficients are naturally decreased on charging because of the repulsive force between sodium or lithium ions already inserted would be increased, and minimized at the redox potential.[114] Figure 40 finally exhibits calculated diffusion coefficients, and the value of $Na_2CoP_2O_7$ is slightly larger than that of $Na_{3.12}Co_{2.44}(P_2O_7)_2$ at the main redox potential unlike their voltage profiles.
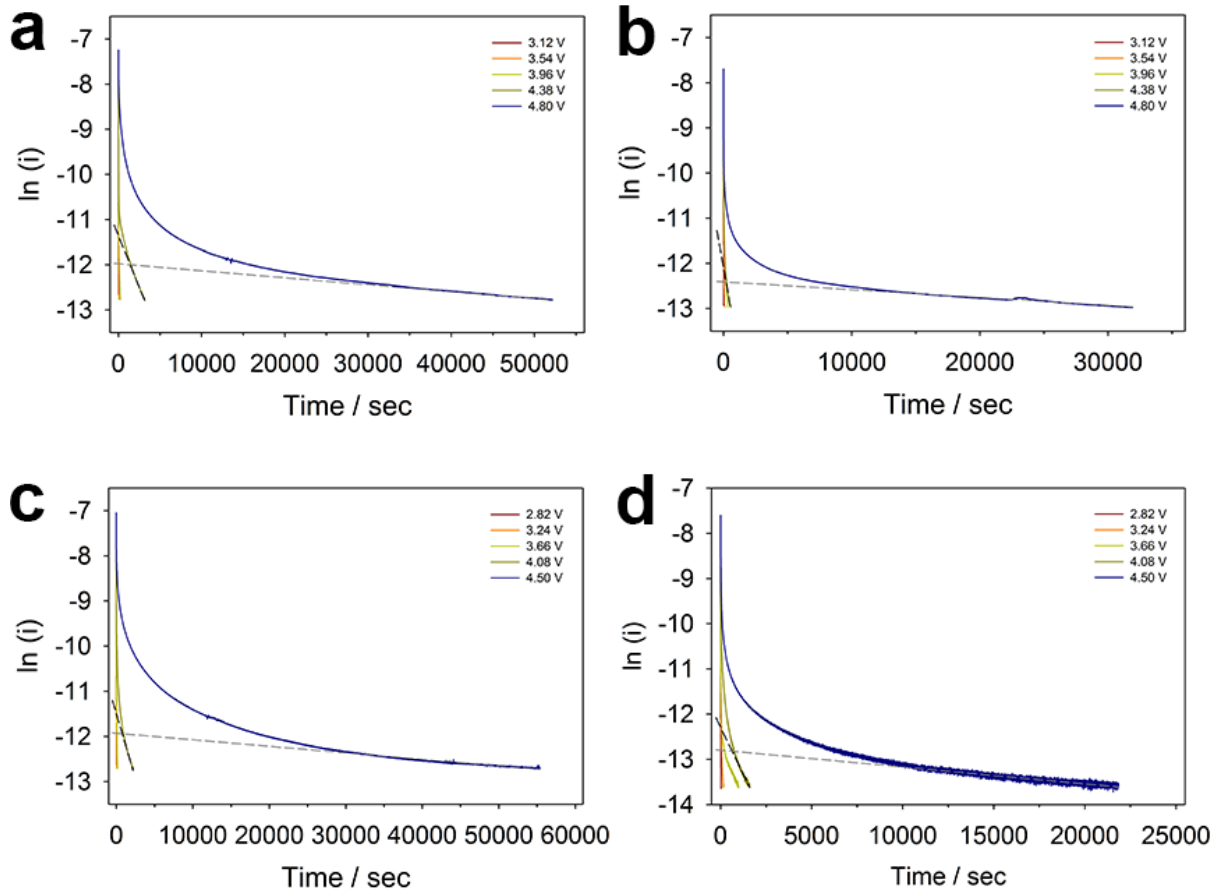
Figure 39. *t* vs. ln (*i*) plots of (a and c) $Na_{3.12}Co_{2.44}(P_2O_7)_2$ and (b and d) $Na_2CoP_2O_7$ tested with (a and b) lithium and (c and d) sodium half cells.
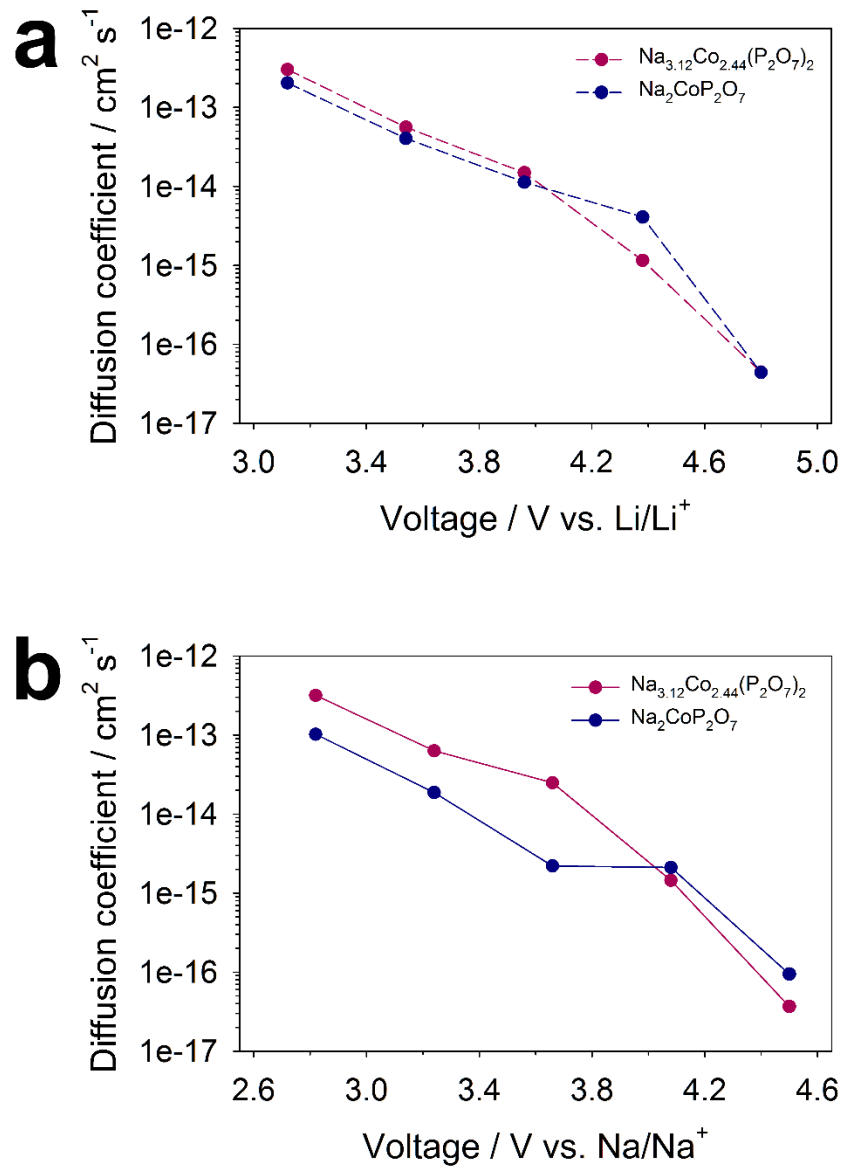
Figure 40. Diffusion coefficients at every voltage steps tested with (a) lithium and (b) sodium half cells.

Next, charge transfer resistances were compared between those materials to understand the difference in terms of kinetics including polarization. Figure 41 shows the Nyquist plots for each compounds achieved with lithium and sodium half cells. Weight term is additionally multiplied to the impedance term to calibrate side effects from gravimetric difference then to make parallel. The tendency is exactly matched with the Galvanostatic tests given in Figure 35 and 37 that $Na_{3.12}Co_{2.44}(P_2O_7)_2$ tested with the sodium half cell delivers the least charge transfer resistance. In detail, $Na_{3.12}Co_{2.44}(P_2O_7)_2$ always exhibit less resistances than $Na_2CoP_2O_7$ in both sodium and lithium half cell tests. In addition, the resistances gained from the sodium half cell tests are smaller than those from the lithium's cases, indicating that the both pyrophosphates are more favorable as sodium hosts rather than lithium hosts in kinetics with smaller polarization.
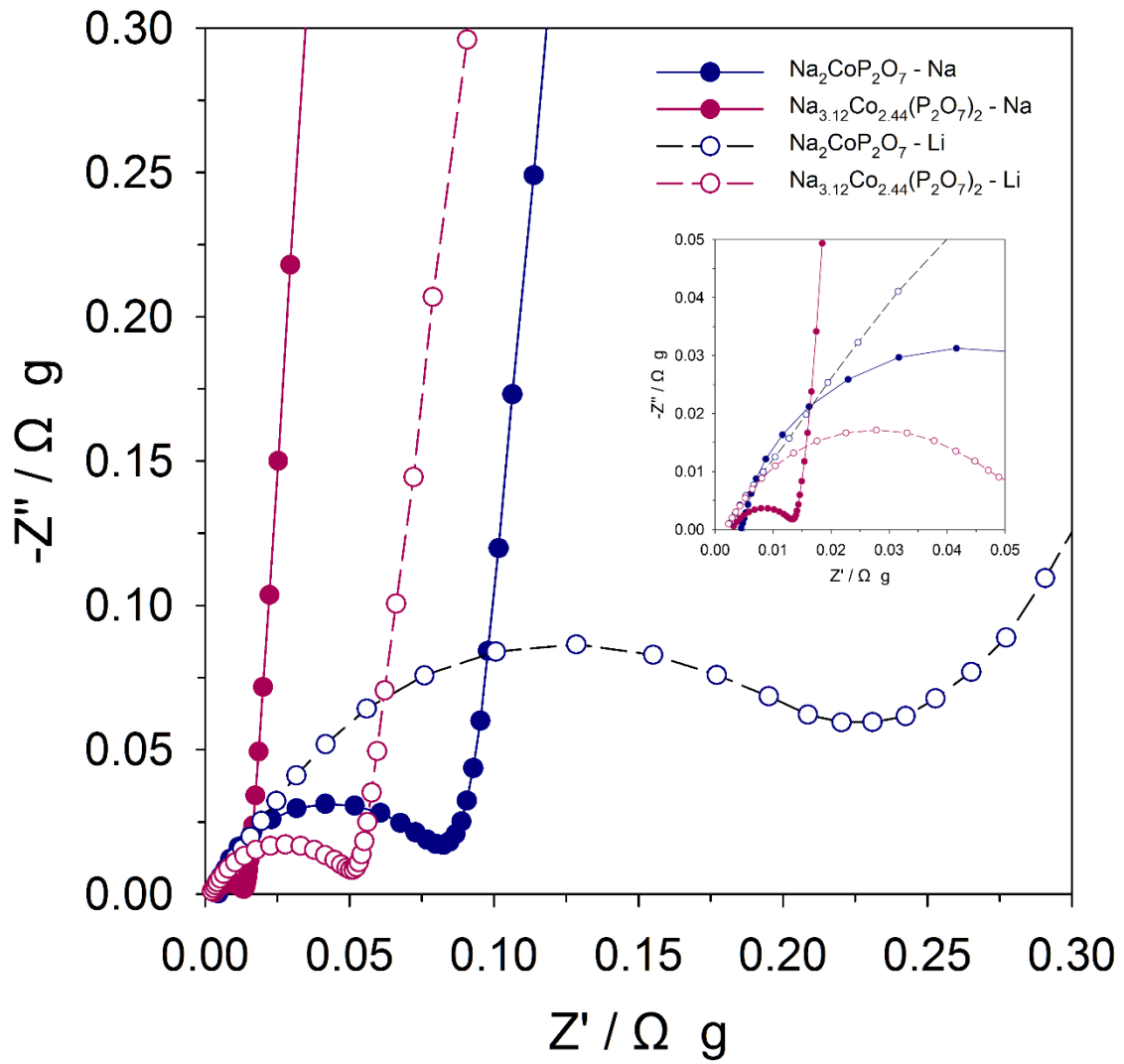
Figure 41. Nyquist plots of $Na_{3.12}Co_{2.44}(P_2O_7)_2$ (violet) and $Na_2CoP_2O_7$ (blue) tested with the sodium and lithium half cells with (inset) scale-magnified one.

4. Conclusion

New type of sodium metal pyrophosphates with composition of $Na_{3.12}M_{2.44}(P_2O_7)_2$ where M is possessed by iron, manganese, or cobalt are synthesized by solid state method and analyzed structurally and electrochemically. Sub-micron- or micron-scaled sodium iron pyrophosphate is synthesized without impurity on the powder XRD, in triclinic structure, matched well with conventionally reported peak pattern. Its structure has de/intercalation pathway candidates in three dimensions which sodium ion can be migrated. However, it has Na_2CO_3 on its surface due to the unexpected oxidation reaction with CO_2 in the air. This characteristics results a large irreversible capacity might exhibited by the side reaction between the electrode and electrolyte on the 1st charging. This problem is solved through washing the final product with water to dissolve it, or off-stoichiometric synthesis without any additional processes. The powder XRD peak of the latter one is mixed to $Na_{3.12}Fe_{2.44}(P_2O_7)_2$ and small amount of maricite $NaFePO_4$. The real composition of this off-stoichiometric compound is calculated to $Na_{3.32}Fe_{2.34}(P_2O_7)_2$ introducing the continuous solid solution system. Na_2CO_3 is rarely discovered through this off-stoichiometric compound, and naturally the reversibility in capacity would be certainly improved with delivering 85 mA h g^{-1}. Furthermore, its cycleability and rate capability is excellent up to 10 C rate which indicates that this pyrophosphate has superior kinetic properties without any additional treatments such as carbon coating or nanosizing during the synthesis. In addition, sodium iron pyrophosphate goes through single phase reaction during a cycle confirmed by chemical de/sodiation processes.

To complement the characteristic toward the sodium iron pyrophosphate in voltage term and to maximize the advantage in cost competitiveness, alternative redox couples are tried with substituting transition metal. First, sodium manganese pyrophosphate ($Na_{3.12}Mn_{2.44}(P_2O_7)_2$) and the intermediate type between iron and manganese ($Na_{3.12}Fe_{1.22}Mn_{1.22}(P_2O_7)_2$) is made, having solid solution system with the conventional $Na_{3.12}Fe_{2.44}(P_2O_7)_2$. However, it exhibits less than 10 mA h g^{-1} of reversible capacity with very poor electronic conductivity and electrochemical activity of Mn itself at that voltage ranges.

Next, sodium cobalt pyrophosphate, $Na_{3.12}Co_{2.44}(P_2O_7)_2$ with same triclinic structure is made as well as conventionally reported orthorhombic type of another pyrophosphate with $Na_2CoP_2O_7$. They have totally different structure, but are synthesized having similar particle size. Both exhibit small amount of reversible capacity but exactly two plateaus like the sodium iron pyrophosphate. Among them, $Na_{3.12}Co_{2.44}(P_2O_7)_2$ tested with the sodium half cell shows the least polarization, and this phenomenon is proved by achieving each charge transfer resistances.

Of course, the best choice for the active material is which delivers excellent reversible capacity, cycleability, and rate capability in kinetics with safety. Sodium iron pyrophosphate gets over the limitations for conventional polyanion-based active materials having bad kinetics, and other pyrophosphates also give possibility exhibiting high energy density using high redox potential in particularly cobalt's cases. Therefore, continuous researches should be needed to have those kind of conditions to be used as a complete cathode material for SIBs in the future.

References

1. Poizot, P.; Laruelle, S.; Grugeon, S.; Dupont, L.; Tarascon, J. M., Nano-sized transition-metal oxides as negative-electrode materials for lithium-ion batteries. *Nature* **2000,** *407* (6803), 496-499.

2. Whittingham, M. S., Lithium batteries and cathode materials. *Chem. Rev.* **2004,** *104* (10), 4271-4301.

3. Wang, Y.; Cao, G., Developments in nanostructured cathode materials for high-performance lithium-ion batteries. *Adv. Mater.* **2008,** *20* (12), 2251-2269.

4. Goodenough, J. B.; Kim, Y., Challenges for Rechargeable Li Batteries. *Chem. Mater.* **2010,** *22* (3), 587-603.

5. Ellis, B. L.; Makahnouk, W. R. M.; Rowan-Weetaluktuk, W. N.; Ryan, D. H.; Nazar, L. F., Crystal Structure and Electrochemical Properties of A(2)MPO(4)F Fluorophosphates (A = Na, Li; M = Fe, Mn, Co, Ni). *Chem. Mater.* **2010,** *22* (3), 1059-1070.

6. Hurst, D.; Gartner, J., *Executive Summary: Electric Vehicle Market Forecasts*. Navigant Consulting, Inc.: 1320 Pearl Street, Suite 300, Boulder, CO 8002 USA, 2013.

7. Slater, M. D.; Kim, D.; Lee, E.; Johnson, C. S., Sodium-Ion Batteries. *Adv. Funct. Mater.* **2013,** *23* (8), 947-958.

8. Tarascon, J. M.; Armand, M., Issues and challenges facing rechargeable lithium batteries. *Nature* **2001,** *414* (6861), 359-367.

9. Senguttuvan, P.; Rousse, G.; Seznec, V.; Tarascon, J. M.; Palacin, M. R., Na2Ti3O7: Lowest Voltage Ever Reported Oxide Insertion Electrode for Sodium Ion Batteries. *Chem. Mater.* **2011,** *23* (18), 4109-4111.

10. Chevrier, V. L.; Ceder, G., Challenges for Na-ion Negative Electrodes. *J. Electrochem. Soc.* **2011,** *158* (9), A1011-A1014.

11. Komaba, S.; Murata, W.; Ishikawa, T.; Yabuuchi, N.; Ozeki, T.; Nakayama, T.; Ogata, A.; Gotoh, K.; Fujiwara, K., Electrochemical Na Insertion and Solid Electrolyte Interphase for Hard-Carbon Electrodes and Application to Na-Ion Batteries. *Adv. Funct. Mater.* **2011,** *21* (20), 3859-3867.

12. Ellis, B. L.; Nazar, L. F., Sodium and sodium-ion energy storage batteries. *Curr. Opin. Solid State Mater. Sci.* **2012,** *16* (4), 168-177.

13. Carmichael, R. S., *Practical Handbook of Physical Properties of Rocks and Minerals*. CRC Press: 1988.

14. Palomares, V.; Serras, P.; Villaluenga, I.; Hueso, K. B.; Carretero-Gonzalez, J.; Rojo, T., Na-ion batteries, recent advances and present challenges to become low cost energy storage systems. *Energy Environ. Sci.* **2012,** *5* (3), 5884-5901.

15. Hong, S. Y.; Kim, Y.; Park, Y.; Choi, A.; Choi, N. S.; Lee, K. T., Charge carriers in rechargeable batteries: Na ions vs. Li ions. *Energy Environ. Sci.* **2013,** *6* (7), 2067-2081.

16. Kim, Y.; Ha, K.-H.; Oh, S. M.; Lee, K. T., High-Capacity Anode Materials for Sodium-Ion Batteries. *Chemistry-a European Journal* **2014,** *20* (38), 11980-11992.

17. Mizushima, K.; Jones, P. C.; Wiseman, P. J.; Goodenough, J. B., LIXCOO2 "(OLESS-THANXLESS-THAN-OR-EQUAL-TO1) - A NEW CATHODE MATERIAL FOR BATTERIES OF HIGH-ENERGY DENSITY. *Mater. Res. Bull.* **1980,** *15* (6), 783-789.

18. Ellis, B. L.; Lee, K. T.; Nazar, L. F., Positive Electrode Materials for Li-Ion and Li-Batteries†. *Chem. Mater.* **2010,** *22* (3), 691-714.

19. Reimers, J. N.; Dahn, J. R., ELECTROCHEMICAL AND INSITU X-RAY-DIFFRACTION STUDIES OF LITHIUM INTERCALATION IN LIXCOO2. *J. Electrochem. Soc.* **1992,** *139* (8), 2091-2097.

20. Ohzuku, T.; Ueda, A., SOLID-STATE REDOX REACTIONS OF LICOO2 (R(3)OVER-BAR-M) FOR 4 VOLT SECONDARY LITHIUM CELLS. *J. Electrochem. Soc.* **1994,** *141* (11), 2972-2977.

21. Dahn, J. R.; Vonsacken, U.; Michal, C. A., STRUCTURE AND ELECTROCHEMISTRY OF LI1+/-YNIO2 AND A NEW LI2NIO2 PHASE WITH THE NI(OH)2 STRUCTURE. *Solid State Ion.* **1990,** *44* (1-2), 87-97.

22. Dahn, J. R.; Vonsacken, U.; Juzkow, M. W.; Aljanaby, H., RECHARGEABLE LINIO2 CARBON CELLS. *J. Electrochem. Soc.* **1991,** *138* (8), 2207-2211.

23. Li, W.; Reimers, J. N.; Dahn, J. R., IN-SITU X-RAY-DIFFRACTION AND ELECTROCHEMICAL STUDIES OF LI-1-XNIO2. *Solid State Ion.* **1993,** *67* (1-2), 123-130.

24. Ohzuku, T.; Ueda, A.; Nagayama, M.; Iwakoshi, Y.; Komori, H., COMPARATIVE-STUDY OF LICOO2, LINI1/2CO1/2O2 AND LINIO2 FOR 4-VOLT SECONDARY LITHIUM CELLS. *Electrochim. Acta* **1993,** *38* (9), 1159-1167.

25. Kang, S. H.; Kim, J.; Stoll, M. E.; Abraham, D.; Sun, Y. K.; Amine, K., Layered Li(Ni0.5-xMn0.5-xM '(2x))O-2 (M ' = Co, Al, Ti; x = 0, 0.025) cathode materials for Li-ion rechargeable batteries. *J. Power Sources* **2002,** *112* (1), 41-48.

26. Kang, S. H.; Belharouak, I.; Sun, Y. K.; Amine, K., Effect of fluorine on the electrochemical properties of layered Li(Ni0.5Mn0.5)O-2 cathode materials. *J. Power Sources* **2005,** *146* (1-2), 650-653.

27. Kang, K. S.; Meng, Y. S.; Breger, J.; Grey, C. P.; Ceder, G., Electrodes with high power and high capacity for rechargeable lithium batteries. *Science* **2006,** *311* (5763), 977-980.

28. Breger, J.; Meng, Y. S.; Hinuma, Y.; Kumar, S.; Kang, K.; Shao-Horn, Y.; Ceder, G.; Grey, C. P., Effect of high voltage on the structure and electrochemistry of LiNi0.5Mn0.5O2: A joint experimental and theoretical study. *Chem. Mater.* **2006,** *18* (20), 4768-4781.

29. Thackeray, M. M.; Johnson, P. J.; Depicciotto, L. A.; Bruce, P. G.; Goodenough, J. B., ELECTROCHEMICAL EXTRACTION OF LITHIUM FROM LIMN2O4. *Mater. Res. Bull.* **1984,** *19* (2), 179-187.

30. Tarascon, J. M.; Wang, E.; Shokoohi, F. K.; McKinnon, W. R.; Colson, S., THE SPINEL PHASE OF LIMN2O4 AS A CATHODE IN SECONDARY LITHIUM CELLS. *J. Electrochem. Soc.* **1991,** *138* (10), 2859-2864.

31. Jang, D. H.; Shin, Y. J.; Oh, S. M., Dissolution of spinel oxides and capacity losses in 4V Li/LixMn2O4 coils. *J. Electrochem. Soc.* **1996,** *143* (7), 2204-2211.

32. Liu, W.; Farrington, G. C.; Chaput, F.; Dunn, B., Synthesis and electrochemical studies of spinel phase LiMn2O4 cathode materials prepared by the Pechini process. *J. Electrochem. Soc.* **1996,** *143* (3), 879-884.

33. Zhong, Q. M.; Bonakdarpour, A.; Zhang, M. J.; Gao, Y.; Dahn, J. R., Synthesis and electrochemistry of LiNixMn2-xO4. *J. Electrochem. Soc.* **1997,** *144* (1), 205-213.

34. Park, S. C.; Kim, Y. M.; Kang, Y. M.; Kim, K. T.; Lee, P. S.; Lee, J. Y., Improvement of the rate capability of LiMn2O4 by surface coating with LiCoO2. *J. Power Sources* **2001,** *103* (1), 86-92.

35. Choi, W.; Manthiram, A., Factors controlling the fluorine content and the electrochemical performance of spinel oxyfluoride cathodes. *J. Electrochem. Soc.* **2007,** *154* (8), A792-A797.

36. Hosono, E.; Kudo, T.; Honma, I.; Matsuda, H.; Zhou, H., Synthesis of Single Crystalline Spinel LiMn2O4 Nanowires for a Lithium Ion Battery with High Power Density. *Nano Lett.* **2009,** *9* (3), 1045-1051.

37. Woo, S. H.; Lim, H.-W.; Jeon, S.; Travis, J. J.; George, S. M.; Lee, S.-H.; Jo, Y. N.; Song, J. H.; Jung, Y. S.; Hong, S. Y.; Choi, N.-S.; Lee, K. T., Ion-Exchangeable Functional Binders and Separator for High Temperature Performance of Li1.1Mn1.86Mg0.04O4 Spinel Electrodes in Lithium Ion Batteries. *J. Electrochem. Soc.* **2013,** *160* (11), A2234-A2243.

38. Yoshio, M.; Noguchi, H.; Itoh, J.; Okada, M.; Mouri, T., Preparation and properties of LiCoyMnxNi1-x-yO2 as a cathode for lithium ion batteries. *J. Power Sources* **2000,** *90* (2), 176-181.

39. Ohzuku, T.; Makimura, Y., Layered lithium insertion material of LiCo1/3Ni1/3Mn1/3O2 for lithium-ion batteries. *Chem. Lett.* **2001,** (7), 642-643.

40. Zhang, L.; Wang, X.; Muta, T.; Li, D.; Noguchi, H.; Yoshio, M.; Ma, R.; Takada, K.; Sasaki, T., The effects of extra Li content, synthesis method, sintering temperature on synthesis and electrochemistry of layered LiNi1/3Mn1/3Co1/O-3(2). *J. Power Sources* **2006,** *162* (1), 629-635.

41. Lee, K. S.; Myung, S. T.; Amine, K.; Yashiro, H.; Sun, Y. K., Structural and electrochemical properties of layered Li Ni1-2xCoxMnx O-2 (x=0.1-0.3) positive electrode materials for Li-ion batteries. *J. Electrochem. Soc.* **2007,** *154* (10), A971-A977.

42. Yabuuchi, N.; Makimura, Y.; Ohzuku, T., Solid-state chemistry and electrochemistry of LiCo1/3Ni1/3Mn1/3O2 for advanced lithium-ion batteries III. Rechargeable capacity and cycleability. *J. Electrochem. Soc.* **2007,** *154* (4), A314-A321.

43. Eom, J.; Kim, M. G.; Cho, J., Storage characteristics of LiNi0.8Co0.1+xMn0.1-xO2 (x=0, 0.03, and 0.06) cathode materials for lithium batteries. *J. Electrochem. Soc.* **2008,** *155* (3), A239-A245.

44. Noh, H.-J.; Youn, S.; Yoon, C. S.; Sun, Y.-K., Comparison of the structural and electrochemical properties of layered Li NixCoyMnz O-2 (x=1/3, 0.5, 0.6, 0.7, 0.8 and 0.85) cathode material for lithium-ion batteries. *J. Power Sources* **2013,** *233*, 121-130.

45. Jung, S.-K.; Gwon, H.; Hong, J.; Park, K.-Y.; Seo, D.-H.; Kim, H.; Hyun, J.; Yang, W.; Kang, K., Understanding the Degradation Mechanisms of LiNi0.5Co0.2Mn0.3O2 Cathode Material in Lithium Ion Batteries. *Adv. Energy Mater.* **2014,** *4* (1).

46. Lu, Z. H.; MacNeil, D. D.; Dahn, J. R., Layered cathode materials Li NixLi(1/3-2x/3)Mn(2/3-x/3) O-2 for lithium-ion batteries. *Electrochem. Solid State Lett.* **2001,** *4* (11), A191-A194.

47. Lu, Z. H.; Dahn, J. R., Understanding the anomalous capacity of Li/Li NixLi(1/3-2x/3)Mn(2/3-x/3 O-2 cells using in situ X-ray diffraction and electrochemical studies. *J. Electrochem. Soc.* **2002,** *149* (7), A815-A822.

48. Johnson, C. S.; Kim, J. S.; Lefief, C.; Li, N.; Vaughey, J. T.; Thackeray, M. M., The significance of the Li2MnO3 component in 'composite' xLi(2)MnO(3) center dot (1-x)LiMn0.5Ni0.5O2 electrodes. *Electrochem. Commun.* **2004,** *6* (10), 1085-1091.

49. Johnson, C. S.; Li, N.; Vaughey, J. T.; Hackney, S. A.; Thackeray, M. M., Lithium-manganese oxide electrodes with layered-spinel composite structures xLi(2)MnO(3)center dot(1-x)Li1+yMn2-yO4 (0 < x < 1, 0 <= y <= 0.33) for lithium batteries. *Electrochem. Commun.* **2005,** *7* (5), 528-536.

50. Thackeray, M. M.; Kang, S.-H.; Johnson, C. S.; Vaughey, J. T.; Benedek, R.; Hackney, S. A., Li2MnO3-stabilized LiMO2 (M = Mn, Ni, Co) electrodes for lithium-ion batteries. *J. Mater. Chem.* **2007,** *17* (30), 3112-3125.

51. Johnson, C. S.; Li, N.; Lefief, C.; Vaughey, J. T.; Thackeray, M. M., Synthesis, Characterization and Electrochemistry of Lithium Battery Electrodes: xLi(2)MnO(3)center dot(1-x)LiMn0.333Ni0.333Co0.333O2 (0 <= x <= 0.7). *Chem. Mater.* **2008,** *20* (19), 6095-6106.

52. Wu, Y.; Murugan, A. V.; Manthiram, A., Surface modification of high capacity layered Li Li(0.2)Mn(0.54)Ni(0.13)Co(0.13) O(2) cathodes by AlPO(4). *J. Electrochem. Soc.* **2008,** *155* (9), A635-A641.

53. Gao, J.; Kim, J.; Manthiram, A., High capacity Li Li0.2Mn0.54Ni0.13Co0.13 O-2-V2O5 composite cathodes with low irreversible capacity loss for lithium ion batteries. *Electrochem. Commun.* **2009,** *11* (1), 84-86.

54. Lim, J.-H.; Bang, H.; Lee, K.-S.; Amine, K.; Sun, Y.-K., Electrochemical characterization of Li2MnO3-Li Ni1/3Co1/3Mn1/3 O-2-LiNiO2 cathode synthesized via co-precipitation for lithium secondary batteries. *J. Power Sources* **2009,** *189* (1), 571-575.

55. Deng, Z. Q.; Manthiram, A., Influence of Cationic Substitutions on the Oxygen Loss and Reversible Capacity of Lithium-Rich Layered Oxide Cathodes. *J. Phy. Chem. C* **2011,** *115* (14), 7097-7103.

56. Amalraj, F.; Kovacheva, D.; Talianker, M.; Zeiri, L.; Grinblat, J.; Leifer, N.; Goobes, G.; Markovsky, B.; Aurbach, D., Integrated Materials xLi(2)MnO(3)center dot(1-x) LiMn1/3Ni1/3Co1/3O2 (x=0.3, 0.5, 0.7) Synthesized. *J. Electrochem. Soc.* **2010,** *157* (10), A1121-A1130.

57. Jarvis, K. A.; Deng, Z.; Allard, L. F.; Manthiram, A.; Ferreira, P. J., Atomic Structure of a Lithium-Rich Layered Oxide Material for Lithium-Ion Batteries: Evidence of a Solid Solution. *Chem. Mater.* **2011,** *23* (16), 3614-3621.

58. Yabuuchi, N.; Yoshii, K.; Myung, S.-T.; Nakai, I.; Komaba, S., Detailed Studies of a High-Capacity Electrode Material for Rechargeable Batteries, Li2MnO3-LiCo1/3Ni1/3Mn1/3O2. *J. Am. Chem. Soc.* **2011,** *133* (12), 4404-4419.

59. Delmas, C.; Menil, F.; Leflem, G.; Fouassier, C.; Hagenmuller, P., COMPARATIVE-STUDY ON MAGNETIC-PROPERTIES OF LAMELLAR OXIDES ACRO2 (A-LI, NA, K) .1. STUDY WITH MOSSBAUER-EFFECT ON IRON DOPED LICRO2. *J. Phys. Chem. Solids* **1978,** *39* (1), 51-53.

60. Delmas, C.; Fouassier, C.; Hagenmuller, P., STRUCTURAL CLASSIFICATION AND PROPERTIES OF THE LAYERED OXIDES. *Physica B & C* **1980,** *99* (1-4), 81-85.

61. Caballero, A.; Hernan, L.; Morales, J.; Sanchez, L.; Pena, J. S.; Aranda, M. A. G., Synthesis and characterization of high-temperature hexagonal P2-Na0.6MnO2 and its electrochemical behaviour as cathode in sodium cells. *J. Mater. Chem.* **2002,** *12* (4), 1142-1147.

62. Hinuma, Y.; Meng, Y. S.; Ceder, G., Temperature-concentration phase diagram of P2-Na(x)CoO(2) from first-principles calculations. *Physical Review B* **2008,** *77* (22).

63. Stoyanova, R.; Carlier, D.; Sendova-Vassileva, M.; Yoncheva, M.; Zhecheva, E.; Nihtianova, D.; Delmas, C., Stabilization of over-stoichiometric Mn4+ in layered Na2/3MnO2. *J. Solid State Chem.* **2010,** *183* (6), 1372-1379.

64. Hamani, D.; Ati, M.; Tarascon, J.-M.; Rozier, P., NaxVO2 as possible electrode for Na-ion batteries. *Electrochem. Commun.* **2011,** *13* (9), 938-941.

65. Berthelot, R.; Carlier, D.; Delmas, C., Electrochemical investigation of the P2-NaxCoO2 phase diagram. *Nat. Mater.* **2011,** *10* (1), 74-U3.

66. Yabuuchi, N.; Kajiyama, M.; Iwatate, J.; Nishikawa, H.; Hitomi, S.; Okuyama, R.; Usui, R.; Yamada, Y.; Komaba, S., P2-type Na-x Fe1/2Mn1/2 O-2 made from earth-abundant elements for rechargeable Na batteries. *Nat. Mater.* **2012,** *11* (6), 512-517.

67. Guignard, M.; Didier, C.; Darriet, J.; Bordet, P.; Elkaim, E.; Delmas, C., P2-NaxVO2 system as electrodes for batteries and electron-correlated materials. *Nat. Mater.* **2013,** *12* (1), 74-80.

68. Lee, D. H.; Xu, J.; Meng, Y. S., An advanced cathode for Na-ion batteries with high rate and excellent structural stability. *Phys. Chem. Chem. Phys.* **2013,** *15* (9), 3304-3312.

69. Singh, G.; Acebedo, B.; Casas Cabanas, M.; Shanmukaraj, D.; Armand, M.; Rojo, T., An approach to overcome first cycle irreversible capacity in P2-Na-2/3 Fe1/2Mn1/2 O-2. *Electrochem. Commun.* **2013,** *37*, 61-63.

70. Yoshida, H.; Yabuuchi, N.; Kubota, K.; Ikeuchi, I.; Garsuch, A.; Schulz-Dobrick, M.; Komaba, S., P2-type Na2/3Ni1/3Mn2/3-xTixO2 as a new positive electrode for higher energy Na-ion batteries. *Chem. Commun.* **2014,** *50* (28), 3677-3680.

71. Tabuchi, M.; Masquelier, C.; Takeuchi, T.; Ado, K.; Matsubara, I.; Shirane, T.; Kanno, R.; Tsutsui, S.; Nasu, S.; Sakaebe, H.; Nakamura, O., Li+/Na+ exchange from alpha-NaFeO2 using hydrothermal reaction. *Solid State Ion.* **1996,** *90* (1-4), 129-132.

72. Ma, X. H.; Chen, H. L.; Ceder, G., Electrochemical Properties of Monoclinic NaMnO2. *J. Electrochem. Soc.* **2011,** *158* (12), A1307-A1312.

73. Vassilaras, P.; Ma, X. H.; Li, X.; Ceder, G., Electrochemical Properties of Monoclinic NaNiO2. *J. Electrochem. Soc.* **2013,** *160* (2), A207-A211.

74. Didier, C.; Guignard, M.; Denage, C.; Szajwaj, O.; Ito, S.; Saadoune, I.; Darriet, J.; Delmas, C., Electrochemical Na-Deintercalation from NaVO2. *Electrochem. Solid State Lett.* **2011,** *14* (5), A75-A78.

75. Braconnier, J. J.; Delmas, C.; Fouassier, C.; Hagenmuller, P., ELECTROCHEMICAL BEHAVIOR OF THE PHASES NAXCOO2. *Mater. Res. Bull.* **1980,** *15* (12), 1797-1804.

76. Komaba, S.; Yabuuchi, N.; Nakayama, T.; Ogata, A.; Ishikawa, T.; Nakai, I., Study on the Reversible Electrode Reaction of Na1-xNi0.5Mn0.5O2 for a Rechargeable Sodium-Ion Battery. *Inorg. Chem.* **2012,** *51* (11), 6211-6220.

77. Dahn, J. R.; Fuller, E. W.; Obrovac, M.; Vonsacken, U., THERMAL-STABILITY OF LIXCOO2, LIXNIO2 AND LAMBDA-MNO2 AND CONSEQUENCES FOR THE SAFETY OF LI-ION CELLS. *Solid State Ion.* **1994,** *69* (3-4), 265-270.

78. Padhi, A. K.; Nanjundaswamy, K. S.; Goodenough, J. B., Phospho-olivines as positive-electrode materials for rechargeable lithium batteries. *J. Electrochem. Soc.* **1997,** *144* (4), 1188-1194.

79. Li, J.; Yao, W.; Martin, S.; Vaknin, D., Lithium ion conductivity in single crystal LiFePO4. *Solid State Ion.* **2008,** *179* (35-36), 2016-2019.

80. Yamada, A.; Chung, S. C.; Hinokuma, K., Optimized LiFePO4 for lithium battery cathodes. *J. Electrochem. Soc.* **2001,** *148* (3), A224-A229.

81. Chung, S.-Y.; Bloking, J. T.; Chiang, Y.-M., Electronically conductive phospho-olivines as lithium storage electrodes. *Nat. Mater.* **2002,** *1* (2), 123-128.

82. Ong, S. P.; Chevrier, V. L.; Hautier, G.; Jain, A.; Moore, C.; Kim, S.; Ma, X.; Ceder, G., Voltage, stability and diffusion barrier differences between sodium-ion and lithium-ion intercalation materials. *Energy Environ. Sci.* **2011,** *4* (9), 3680-3688.

83. Zhu, Y.; Xu, Y.; Liu, Y.; Luo, C.; Wang, C., Comparison of electrochemical performances of olivine NaFePO4 in sodium-ion batteries and olivine LiFePO4 in lithium-ion batteries. *Nanoscale* **2013,** *5* (2), 780-787.

84. Lee, K. T.; Ramesh, T. N.; Nan, F.; Botton, G.; Nazar, L. F., Topochemical Synthesis of Sodium Metal Phosphate Olivines for Sodium-Ion Batteries. *Chem. Mater.* **2011,** *23* (16), 3593-3600.

85. Andersson, A. S.; Kalska, B.; Haggstrom, L.; Thomas, J. O., Lithium extraction/insertion in LiFePO4: an X-ray diffraction and Mossbauer spectroscopy study. *Solid State Ion.* **2000,** *130* (1-2), 41-52.

86. Huang, H.; Yin, S. C.; Nazar, L. F., Approaching theoretical capacity of LiFePO4 at room temperature at high rates. *Electrochem. Solid State Lett.* **2001,** *4* (10), A170-A172.

87. Ravet, N.; Chouinard, Y.; Magnan, J. F.; Besner, S.; Gauthier, M.; Armand, M., Electroactivity of natural and synthetic triphylite. *J. Power Sources* **2001,** *97-8*, 503-507.

88. Yamada, A.; Koizumi, H.; Nishimura, S.-i.; Sonoyama, N.; Kanno, R.; Yonemura, M.; Nakamura, T.; Kobayashi, Y., Room-temperature miscibility gap in LixFePO4. *Nat. Mater.* **2006,** *5* (5), 357-360.

89. Kobayashi, G.; Nishimura, S.-i.; Park, M.-S.; Kanno, R.; Yashima, M.; Ida, T.; Yamada, A., Isolation of Solid Solution Phases in Size-Controlled LixFePO4 at Room Temperature. *Adv. Funct. Mater.* **2009,** *19* (3), 395-403.

90. Nishimura, S.; Nakamura, M.; Natsui, R.; Yamada, A., New Lithium Iron Pyrophosphate as 3.5 V Class Cathode Material for Lithium Ion Battery. *J. Am. Chem. Soc.* **2010,** *132* (39), 13596-13597.

91. Zhou, H.; Upreti, S.; Chernova, N. A.; Hautier, G.; Ceder, G.; Whittingham, M. S., Iron and Manganese Pyrophosphates as Cathodes for Lithium-Ion Batteries. *Chem. Mater.* **2011,** *23* (2), 293-300.

92. Kim, H.; Lee, S.; Park, Y.-U.; Kim, H.; Kim, J.; Jeon, S.; Kang, K., Neutron and X-ray Diffraction Study of Pyrophosphate-Based Li2-xMP2O7 (M = Fe, Co) for Lithium Rechargeable Battery Electrodes. *Chem. Mater.* **2011,** *23* (17), 3930-3937.

93. Tamaru, M.; Barpanda, P.; Yamada, Y.; Nishimura, S.-i.; Yamada, A., Observation of the highest Mn3+/Mn2+ redox potential of 4.45 V in a Li2MnP2O7 pyrophosphate cathode. *J. Mater. Chem.* **2012,** *22* (47), 24526-24529.

94. Furuta, N.; Nishimura, S.; Barpanda, P.; Yamada, A., Fe3+/Fe2+ Redox Couple Approaching 4 V in Li2-x(Fe1-yMny)P2O7 Pyrophosphate Cathodes. *Chem. Mater.* **2012,** *24* (6), 1055-1061.

95. Ha, K.-H.; Woo, S. H.; Mok, D.; Choi, N.-S.; Park, Y.; Oh, S. M.; Kim, Y.; Kim, J.; Lee, J.; Nazar, L. F.; Lee, K. T., Na4-M2+/2(P2O7)2 (2/3 7/8, M = Fe, Fe0.5Mn0.5, Mn): A Promising Sodium Ion Cathode for Na-ion Batteries. *Adv. Energy Mater.* **2013,** *3* (6), 770-776.

96. Barpanda, P.; Avdeev, M.; Ling, C. D.; Lu, J. C.; Yamada, A., Magnetic Structure and Properties of the Na2CoP2O7 Pyrophosphate Cathode for Sodium-Ion Batteries: A Supersuperexchange-Driven Non-Collinear Antiferromagnet. *Inorg. Chem.* **2013,** *52* (1), 395-401.

97. Barpanda, P.; Lu, J. C.; Ye, T.; Kajiyama, M.; Chung, S. C.; Yabuuchi, N.; Komaba, S.; Yamada, A., A layer-structured Na2CoP2O7 pyrophosphate cathode for sodium-ion batteries. *RSC Adv.* **2013,** *3* (12), 3857-3860.

98. Barpanda, P.; Ye, T.; Avdeev, M.; Chung, S. C.; Yamada, A., A new polymorph of Na2MnP2O7 as a 3.6 V cathode material for sodium-ion batteries. *J. Mater. Chem. A* **2013,** *1* (13), 4194-4197.

99. Park, C. S.; Kim, H.; Shakoor, R. A.; Yang, E.; Lim, S. Y.; Kahraman, R.; Jung, Y.; Choi, J. W., Anomalous Manganese Activation of a Pyrophosphate Cathode in Sodium Ion Batteries: A Combined Experimental and Theoretical Study. *J. Am. Chem. Soc.* **2013,** *135* (7), 2787-2792.

100. Kim, H.; Shakoor, R. A.; Park, C.; Lim, S. Y.; Kim, J. S.; Jo, Y. N.; Cho, W.; Miyasaka, K.; Kahraman, R.; Jung, Y.; Choi, J. W., Na2FeP2O7 as a Promising Iron-Based Pyrophosphate Cathode for Sodium Rechargeable Batteries: A Combined Experimental and Theoretical Study. *Adv. Funct. Mater.* **2013,** *23* (9), 1147-1155.

101. Barpanda, P.; Liu, G.; Ling, C. D.; Tamaru, M.; Avdeev, M.; Chung, S.-C.; Yamada, Y.; Yamada, A., Na2FeP2O7: A Safe Cathode for Rechargeable Sodium-ion Batteries. *Chem. Mater.* **2013,** *25* (17), 3480-3487.

102. Clark, J. M.; Barpanda, P.; Yamada, A.; Islam, M. S., Sodium-ion battery cathodes Na2FeP2O7 and Na2MnP2O7: diffusion behaviour for high rate performance. *J. Mater. Chem. A* **2014,** *2* (30), 11807-11812.

103. Barpanda, P.; Liu, G.; Avdeev, M.; Yamada, A., t-Na2(VO)P2O7: A 3.8 V Pyrophosphate Insertion Material for Sodium-ion Batteries. *ChemElectroChem* **2014**.

104. Song, Y.-M.; Han, J.-G.; Park, S.; Lee, K. T.; Choi, N.-S., A multifunctional phosphite-containing electrolyte for 5 V-class LiNi0.5Mn1.5O4 cathodes with superior electrochemical performance. *J. Mater. Chem. A* **2014,** *2* (25), 9506-9513.

105. Angenault, J.; Couturier, J. C.; Quarton, M.; Robert, F., STRUCTURE OF NA3.12FE2.44(P2O7)(2). *Eur. J. Solid State Inorg. Chem.* **1995,** *32* (4), 335-343.

106. Majling, J.; Hanic, F., The phase equilibria study in the system Na4P2O7 □ Mg2P2O7. *J. Solid State Chem.* **1973,** *7* (4), 370-373.

107. Hanic, F.; Zak, Z., CRYSTAL-STRUCTURE OF NA7MG4.5(P2O7)4. *J. Solid State Chem.* **1974,** *10* (1), 12-19.

108. Appapillai, A. T.; Mansour, A. N.; Cho, J.; Shao-Horn, Y., Microstructure of LiCoO2 with and without "AIPO(4)" nanoparticle coating: Combined STEM and XPS studies. *Chem. Mater.* **2007,** *19* (23), 5748-5757.

109. Ellis, B. L.; Makahnouk, W. R. M.; Makimura, Y.; Toghill, K.; Nazar, L. F., A multifunctional 3.5 V iron-based phosphate cathode for rechargeable batteries. *Nat. Mater.* **2007,** *6* (10), 749-753.

110. Muraliganth, T.; Manthiram, A., Understanding the Shifts in the Redox Potentials of Olivine LiM1-yMyPO4 (M = Fe, Mn, Co, and Mg) Solid Solution Cathodes. *J. Phy. Chem. C* **2010,** *114* (36), 15530-15540.

111. Xu, J.; Chen, G.; Li, H.-J.; Lv, Z.-S., Direct-hydrothermal synthesis of LiFe1-x Mn (x) PO4 cathode materials. *J. Appl. Electrochem.* **2010,** *40* (3), 575-580.

112. Erragh, F.; Boukhari, A.; Elouadi, B.; Holt, E. M., CRYSTAL-STRUCTURES OF 2 ALLOTROPIC FORMS OF NA2COP2O7. *J. Crystallogr. Spectrosc. Res.* **1991,** *21* (3), 321-326.

113. Ura, H.; Nishina, T.; Uchida, I., ELECTROCHEMICAL MEASUREMENTS OF SINGLE PARTICLES OF PD AND LANI5 WITH A MICROELECTRODE TECHNIQUE. *J. Electroanal. Chem.* **1995,** *396* (1-2), 169-173.

114. Bang, H. J.; Donepudi, V. S.; Prakash, J., Preparation and characterization of partially substituted LiMyMn2-yO4 (M = Ni, Co, Fe) spinel cathodes for Li-ion batteries. *Electrochim. Acta* **2002,** *48* (4), 443-451.